UNIVERSITE BRETAGNE LOIRE

université angers

Thèse de Doctorat

Daniel KÜN-DARBOIS

Mémoire présenté en vue de l'obtention du
grade de Docteur de l'Université d'Angers
sous le sceau de l'Université Bretagne Loire

École doctorale : Biologie Santé

Discipline : Physiologie, physiopathologie humaine

Unité de recherche : GEROM (Groupe d'Etudes Remodelage Osseux et bioMatériaux)

Soutenue le *13 novembre 2017*

Thèse N° :

Remodelage osseux et pathologies oro-faciales

JURY

Rapporteurs :	**Pascal GUGGENBUHL**,	Professeur des Universités-Praticien Hospitalier, Université de Rennes I
	Christian VACHER,	Professeur des Universités-Praticien Hospitalier, Université Paris VII
Examinateurs :	**Éric AGUADO**,	Maître de Conférences des Universités, ONIRIS Nantes
	Pierre CORRE,	Professeur des Universités-Praticien Hospitalier, Université de Nantes
	Boris LAURE,	Professeur des Universités-Praticien Hospitalier, Université de Tours
	Philippe MERCIER,	Professeur des Universités-Praticien Hospitalier, Université d'Angers
	Arnaud PICARD,	Professeur des Universités-Praticien Hospitalier, Université Paris V
Directeur de Thèse :	**Daniel CHAPPARD**,	Professeur des Universités-Praticien Hospitalier, Université d'Angers

L'auteur du présent document vous autorise à le partager, reproduire, distribuer et communiquer selon les conditions suivantes :



- Vous devez le citer en l'attribuant de la manière indiquée par l'auteur (mais pas d'une manière qui suggérerait qu'il approuve votre utilisation de l'œuvre).
- Vous n'avez pas le droit d'utiliser ce document à des fins commerciales.
- Vous n'avez pas le droit de le modifier, de le transformer ou de l'adapter.

Consulter la licence creative commons complète en français :
http://creativecommons.org/licences/by-nc-nd/2.0/fr/

Ces conditions d'utilisation (attribution, pas d'utilisation commerciale, pas de modification) sont symbolisées par les icônes positionnées en pied de page.



REMERCIEMENTS

A Monsieur le Professeur Daniel Chappard,
Je ne saurai jamais assez vous exprimer toute ma reconnaissance pour votre enseignement si complet et votre soutien si attentif. Recevez ici mes remerciements les plus profonds ainsi que l'expression de ma grande admiration.

A Monsieur le Professeur Dominique Goga,
Etre un de vos élèves est une chance et un honneur. Vous m'avez montré, par votre enseignement exigeant, la voie de l'excellence chirurgicale. Votre soutien attentionné et constant ainsi que la confiance que vous me témoignez me sont très précieux. Veuillez trouver ici l'expression de mes plus vifs remerciements et de ma grande admiration.

A Monsieur le Professeur Pierre Corre,
Auprès de qui j'ai tant appris et qui est pour moi un modèle de chirurgien et d'universitaire. Merci de ton aide attentionnée et de tout ce que tu fais pour m'aider dans mon parcours, sans compter ton temps. Merci d'avoir si gentiment accepté de faire partie de ce jury. Trouve ici l'expression de ma profonde reconnaissance et de ma non moins profonde admiration.

A Monsieur le Professeur Boris Laure,
Dont l'exemple chirurgical et scientifique de si haut niveau a été déterminant dans ma formation. Merci d'avoir accepté de faire partie de ce jury.

A Monsieur le Professeur Philippe Mercier,
Que je remercie de l'aide qu'il m'a apporté dans le déroulement de ces travaux et d'avoir accepté de faire partie de ce jury.

A Monsieur le Professeur Christian Vacher,
Que je remercie chaleureusement pour son enseignement de l'anatomie (depuis ma première année de médecine) ainsi que d'avoir accepté de faire partie de ce jury et d'en être rapporteur.

A Monsieur le Professeur Pascal Guggenbuhl,
Que je remercie chaleureusement d'avoir accepté de faire partie du jury et d'en être rapporteur.

A Monsieur le Professeur Arnaud Picard,
Que je remercie d'avoir si spontanément accepté de faire partie du jury de cette thèse alors qu'il ne me connaissait pas.

A Monsieur le Docteur Eric Aguado,
Que je remercie chaleureusement de son aide, de sa disponibilité et de son acceptation de faire partie de ce jury.

A Madame Hélène Libouban,
Que je remercie chaleureusement de son enseignement, de son aide et de sa disponibilité qui ont été indispensables à l'avancée de ces travaux.

A toute l'équipe du GEROM et du SCIAM,
Madame Laurence Lechat, Madame Florence Pascaretti, Monsieur Romain Mallet, Monsieur Guillaume Mabilleau, Monsieur Baptiste Arbez, Madame Alexandre Mieczkowska
Merci de votre si bon accueil au sein de votre équipe (depuis quelques années déjà) et pour la bonne ambiance qui y règne.

A toute l'équipe de l'animalerie de la faculté de médecine d'Angers,
Dont l'aide m'a été indispensable pour mener ces travaux à bien.

A toute l'équipe du service de chirurgie maxillo-faciale du CHU d'Angers,
le Professeur Laurent Laccourreye,
le Docteur Michel Khouri,
le Docteur Smaïl Badja dont la disponibilité et la compétence ont été indispensables à la poursuite de mes travaux
le Docteur Alexandre Gueutier,
Mesdames Karine Robin, Carole Boudet, Annie Trémoureux, Véronique Touzard, etc ... (je ne peux citer tout le monde)

~

A ma famille,
en particulier à ma femme, Agathe, et à mes filles Eugénie, Jeanne et Victoire

TABLE DES MATIERES

TABLE DES MATIERES **1**
LISTE DES ABREVIATIONS **2**
TABLE DES ILLUSTRATIONS **4**
TABLE DES TABLEAUX **6**
INTRODUCTION **7**
1. Anatomie comparative rat/Homme **8**
1.1. Ostéologie mandibulaire et dents 8
1.2. Vascularisation mandibulaire 10
1.3. Muscles masticateurs 13
1.4. Physiologie de la mastication 16
2. Le remodelage osseux **18**
2.1. Le remodelage osseux normal 18
2.2. Particularités du remodelage osseux mandibulaire 20
TRAVAUX PERSONNELS **22**
ARTICLE 1 ..... **23**
1. Travail préparatoire **25**
2. Protocole expérimental **25**
3. Résultats **27**
4. Conclusion **30**
ARTICLE 2 ..... **31**
1. Résultats **32**
2. Travail préparatoire **32**
3. Protocole expérimental **33**
4. Conclusion **33**
ARTICLE 3 ..... **34**
1. Protocole expérimental **36**
2. Résultats **37**
3. Conclusion **38**
ARTICLE 4 ..... **39**
1. Travail préparatoire **41**
2. Protocole expérimental **43**
3. Résultats **44**
4. Conclusion **47**
CONCLUSION GENERALE ET PERSPECTIVES **50**
REFERENCES **53**

LISTE DES ABREVIATIONS

AcU	Acétate d'uranyle - Uranyl acetate
Al	Aluminium - Aluminum
ARONJ	Antiresorptive drugs related osteonecrosis of the jaws
BMD	Bone mineral density
BMDD	Bone mineral density distribution
BP	Bisphosphonate
BRONJ	Bisphosphonate related osteonecrosis of the jaws
BTX	Botulinum toxin - Toxine botulique
BV/TV	3D measured trabecular bone volume - Volume osseux trabéculaire 3D
B.Ar/T.Ar	2D measured trabecular bone volume - Volume osseux trabéculaire 2D
Ca.O.Th	Épaisseur canaux de Havers - Haversian canal osteoid thickness
Cart. Th	Épaisseur cartilagineuse - Cartilage thickness
Ct.O.Th	Cortical osteoid thickness
CTRL	Contrôle - Control
Ct.Th	Cortical bone thickness
Df	Dimension fractale - Fractal dimension
EDS	Energy dispersive X-ray spectroscopy
Fe	Fer - Iron
IKI	Iodine-potassium iodide- Iodure de potassium-iode
LCt.Th	Lingual cortical bone thickness
LUT	Look up table
MAR	Mineral apposition rate – vitesse de minéralisation
Mf	Muscular fibers
MicroCT	Microcomputed tomography – Microtomographie aux rayons X
ONM	Ostéochimionécrose maxillo-mandibulaire
PMA	Phosphomolybdic acid – acide phosphomolybdique
PTA	Phosphotungstic acid – acide phosphotungstique
qBEI	Quantitative backscattered electron imaging
ROI	Region of interest
SAS	Syndrome d'apnées du sommeil
SEM	Standard error of the mean
TM	Torus mandibularis
TMax	Torus maxillaris

TP	Torus palatinus
TRAcP	Tartrate resistant acid phosphatase
UA	Uranyl acetate - acétate d'uranyle
UI	Unité Internationale
VCt.Th	Vestibular cortical bone thickness
VV/TV_{ALV}	3D Vascular volume of alveolar bone
ZA	Acide zolédronique – Zoledronic acid

TABLE DES ILLUSTRATIONS

Figure 1 : Mandibule humaine adulte, vue antérolatérale montrant le processus coronoïde et le processus condylien.

Figure 2 : Mandibule de rat adulte en vue latérale montrant le processus coronoïde, le processus condylaire et le processus angulaire. On remarque également les incisives et les molaires.

Figure 3 : Mandibule humaine montrant le foramen mandibulaire et le foramen mentonnier.

Figure 4 : Mandibule de rat montrant le foramen mandibulaire et le foramen mentonnier.

Figure 5 : Vascularisation mandibulaire osseuse et dentaire, vue schématique de l'artère dentaire inférieure et de ses branches terminales.

Figure 6 : Apport vasculaire extra-osseux de la vascularisation mandibulaire.

Figure 7 : Schématisation de l'origine de la vascularisation mandibulaire en secteur molaire.

Figure 8 : Schématisation de l'origine de la vascularisation mandibulaire en secteur symphysaire.

Figure 9 : Vascularisation mandibulaire chez le rat provenant de l'artère alvéolaire inférieure et de l'artère maxillaire externe.

Figure 10 : Vue latérale des muscles masticateurs chez l'Homme.

Figure 11 : Vue des muscles digastriques et du plancher buccal chez l'Homme.

Figure 12 : Vue latérale du muscle temporal chez le rat.

Figure 13 : Vue latérale du muscle masséter chez le rat.

Figure 14 : Vue inférieure montrant le muscle digastrique chez le rat.

Figure 15 : Le remodelage osseux : schématisation du « Basic Multicellular Unit »

Figure 16 : Appareils utilisé pour la microtomographie aux rayons X (Skyscan 1172, Bruker).

Figure 17 : Points d'injection dans le muscle temporal (n=2) et le muscle masséter (n=3).

Figure 18 : Injection intra musculaire de bleu de méthylène.

Figure 19 : Zones d'analyse osseuse sur les mandibules de rats en vue sur os sec et vue schématique.

Figure 20 : Positionnement des plans de coupe sur les images de reconstruction 3D pour obtention des images 2D condyliennes et alvéolaires toujours comparables.

Figure 21 : Analyse vectorielle de la porosité d'un volume, vue supérieure et vue du plan frontal.

Figure 22 : Résultats de la mesure du volume osseux trabéculaire condylien montrant une perte osseuse du côté injecté de 35%.

Figure 23 : Résultats de la mesure du volume osseux trabéculaire alvéolaire montrant une perte osseuse du côté injecté de 20%.

Figure 24 : Vue 3D de la face linguale de l'os alvéolaire d'un rat BTX montrant une prolifération de l'enthèse d'insertion du muscle digastrique.

Figure 25 : Résultats de l'analyse de la porosité osseuse alvéolaire par analyse vectorielle montrant une porosité accrue du côté injecté.

Figure 26 : Vue d'un torus mandibularis.

Figure 27 : Vue peropératoire d'un torus mandibularis après décollement sous périosté.

Figure 28 : Vue peropératoire d'un torus mandibularis après exérèse monobloc.

Figure 29 : Vue clinique d'exposition osseuse mandibulaire typique de l'ostéonécrose aux bisphosphonates.

Figure 30 : Images radiologiques d'ostéonécrose : séquestres osseux, zones déminéralisées.

Figure 31 : Utilisation d'instruments spécifiques pour avulsion dentaire chez le rongeur (ici : « Pas d'Ane », écarteur de joue et syndesmotome).

Figure 32 : Injection intracarotidienne par cathétérisme sous microscope opératoire.

Figure 33 : Image radiologique d'une tête de rat en vue latérale après injection de produit de contraste.

Figure 34 : Vue opératoire après avulsion des trois molaires mandibulaires droites chez un rat.

Figure 35 : Image d'exposition osseuse alvéolaire après sacrifice chez un rat ZA.

Figure 36 : Exemple d'image de tissu osseux alvéolaire utilisée pour l'analyse qBEI.

Figure 37 : Artère alvéolaire inférieure et microvascularisation alvéolaire visibles. La densité vasculaire est augmentée après avulsion dentaire (CTRL droit) et diminuée après avulsion dentaire (ZA droit).

Figure 38 : Volume vasculaire de l'os alvéolaire mesuré en 3D. Montrant un volume plus élevé à droite qu'à gauche dans le groupe CTRL et moins élevé à droite dans le groupe ZA par rapport au même coté dans le groupe CTRL.

TABLE DES TABLEAUX

Tableau 1 : Caractéristiques histologiques des tori de l'étude.

INTRODUCTION

 CC BY NC ND

INTRODUCTION

Découverte au milieu du XVIII^{ème} par l'anatomiste John Hunter (1), qui observait des mandibules animales et humaines, la notion de remodelage osseux était apparue dans la littérature comme le fait « que de l'os nouveau est déposé, s'il y a eu au préalable réabsorption ou destruction d'os ». Cette notion s'est considérablement affinée avec la description du couplage formation/résorption osseuse. Des anomalies du remodelage osseux peuvent être retrouvées dans diverses pathologies oro-faciales chez l'Homme. Nous avons choisi d'étudier les conséquences mandibulaires des injections de toxine botulique (BTX), sujet largement inexploré à l'heure actuelle bien que concernant un nombre de patients très élevé en pratique clinique. Nous nous sommes intéressés aux hypertrophies osseuses maxillaires et mandibulaires appelées tori et qui sont présentes dans 10 à 30% de la population générale sans que l'on en connaisse à l'heure actuelle la physiopathologie ni même les éventuelles caractéristiques spécifiques de ces lésions. Nous avons également étudié l'ostéonécrose mandibulaire aux bisphosphonates (BP) et sa physiopathologie par la mise au point d'un modèle animal. Il a été nécessaire d'étudier les principales différences entre le rat et l'Homme afin d'analyser au mieux les résultats des études animales effectuées dans le présent travail.

1. Anatomie comparative rat/Homme

1.1. Ostéologie mandibulaire et dents

Chez l'Homme, la mandibule est un os impair et médian d'ossification membraneuse. Elle est constituée d'un corps mandibulaire médian et de deux branches montantes latérales. En partie supérieure du corps mandibulaire se trouve le processus alvéolaire constitué par l'os alvéolaire qui supporte les dents mandibulaires. On retrouve sur chaque branche montante le processus coronoïde, sur lequel s'insère le muscle temporal, et le processus condylaire, qui s'articule avec l'os temporal pour former l'articulation temporo-mandibulaire (Fig. 1).

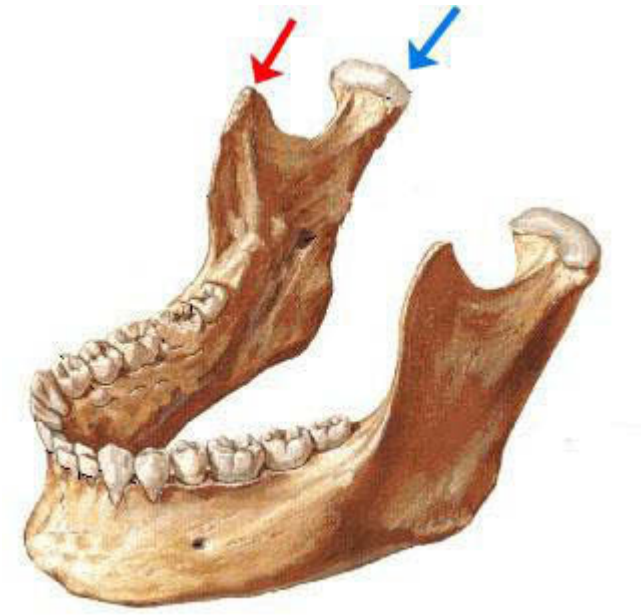


Figure 1 : Mandibule humaine adulte, vue antérolatérale montrant le processus coronoïde (flèche rouge) et le processus condylien (flèche bleue) (*Netter*, Masson)

Chez le rat, la mandibule est constituée de deux hémi-mandibules reliées par une symphyse médiane. On retrouve les processus condylaires et coronoïdes, comme chez l'Homme. Un processus angulaire est également présent. Chaque hémi-mandibule comprend une incisive à croissance continue (dont la racine s'étend très loin jusqu'à la troisième molaire), et trois molaires (Fig. 2). Il existe un diastème de taille importante entre l'incisive et le secteur molaire.

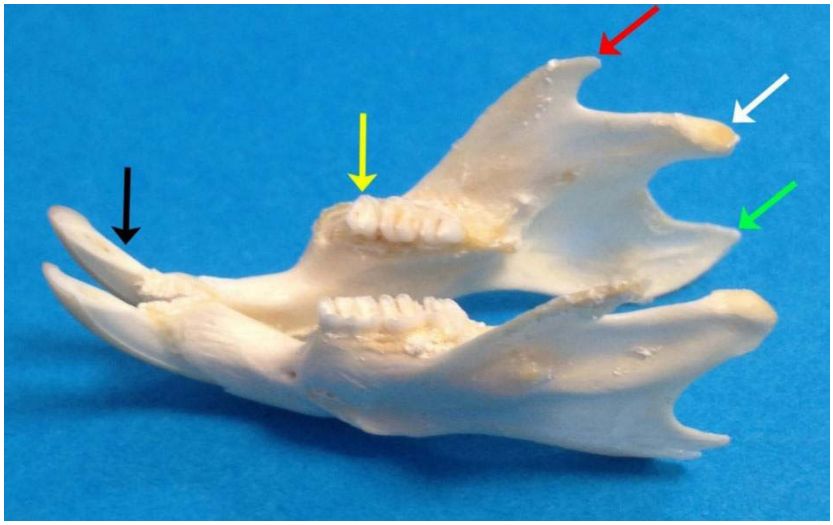


Figure 2 : Mandibule de rat adulte en vue latérale montrant le processus coronoïde (flèche rouge), le processus condylaire (flèche blanche) et le processus angulaire (flèche verte). On remarque également les incisives (flèche noire) et les molaires (flèche jaune).

Chez l'Homme comme chez le rat, le pédicule alvéolaire inférieur a un trajet intra-osseux mandibulaire dans le canal dentaire inférieur. L'orifice d'entrée est le foramen mandibulaire situé à la face interne de la branche montante. L'orifice de sortie est le foramen mentonnier. Ce dernier est situé à la face vestibulaire antérolatérale du corps mandibulaire en regard des apex des prémolaires chez l'Homme tandis que chez le rat il se trouve en avant de la première molaire (Figures 3 et 4).

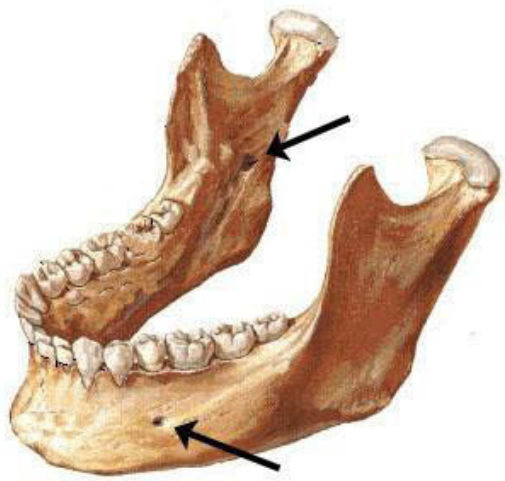


Figure 3 : Mandibule humaine montrant le foramen mandibulaire et le foramen mentonnier (flèches) (*Netter*, Masson)

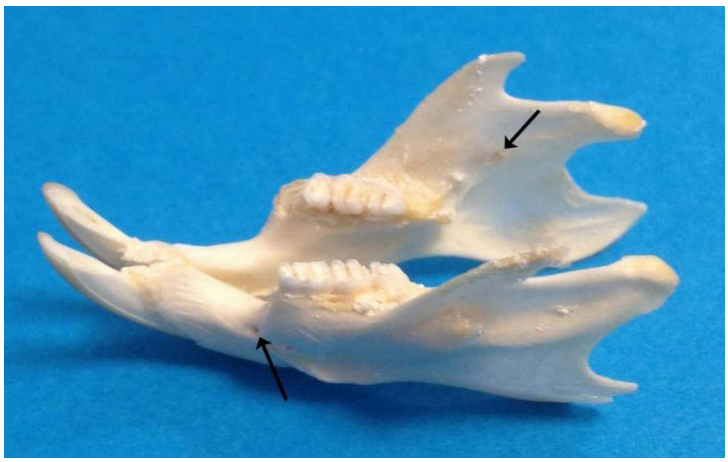


Figure 4 : Mandibule de rat montrant le foramen mandibulaire et le foramen mentonnier (flèches)

1.2. Vascularisation mandibulaire

Chez l'Homme, la vascularisation mandibulaire alvéolaire et dentaire est assurée principalement par l'artère alvéolaire inférieure, issue de l'artère maxillaire, elle-même issue de l'artère carotide externe. L'artère alvéolaire inférieure se distribue en rameaux ascendants dentaires (artères pulpaires) et inter dentaires et en rameaux descendants (Figure 5). Elle donne naissance aux artères mentonnière et incisive qui vascularisent le secteur antérieur. L'artère alvéolaire inférieure chemine dans le canal alvéolaire inférieur (ou canal mandibulaire) au contact du nerf alvéolaire inférieur. Son trajet intra mandibulaire a été beaucoup étudié (2).

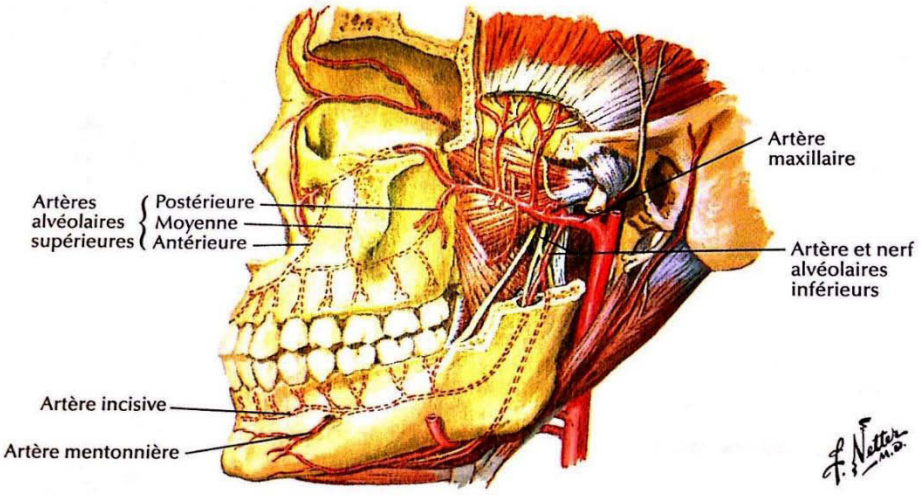
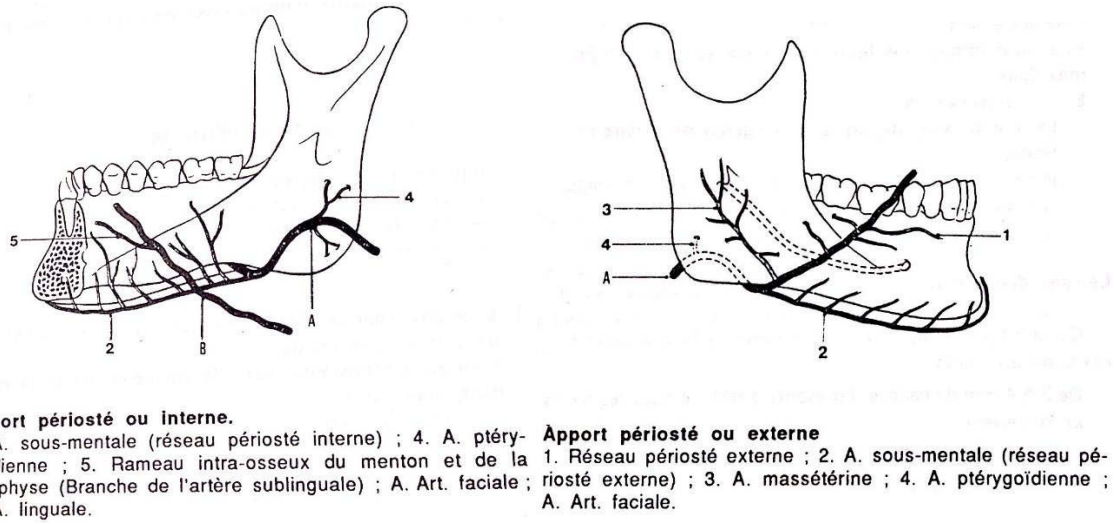


Figure 5 : Vascularisation mandibulaire osseuse et dentaire, vue schématique de l'artère dentaire inférieure et de ses branches terminales (*Netter*, Masson)

Un apport vasculaire externe provenant de l'artère faciale joue également un rôle dans la vascularisation de la mandibule chez l'Homme (Figure 6). Ce réseau est constitué par des branches de l'artère faciale (artère ptérygoïdienne, artère sous mentale, artère masséterine) et donne le réseau vasculaire périosté. Selon la localisation mandibulaire ces réseaux vasculaires ont une prépondérance

différente : dans la région molaire et rétro-molaire, l'essentiel de la vascularisation provient du réseau alvéolaire inférieur et seule la corticale linguale est vascularisée par le réseau artériel facial (Figure 7). En revanche, en région symphysaire, seul l'os trabéculaire est vascularisé par le réseau alvéolaire inférieur (Figure 8) (3) .



Apport périosté ou interne.
2. A. sous-mentale (réseau périosté interne) ; 4. A. ptérygoïdienne ; 5. Rameau intra-osseux du menton et de la symphyse (Branche de l'artère sublinguale) ; A. Art. faciale ; B. A. linguale.

Apport périosté ou externe
1. Réseau périosté externe ; 2. A. sous-mentale (réseau périosté externe) ; 3. A. massétérine ; 4. A. ptérygoïdienne ; A. Art. faciale.

Figure 6 : Apport vasculaire extra-osseux de la vascularisation mandibulaire (*Couly*, Editions cdp)

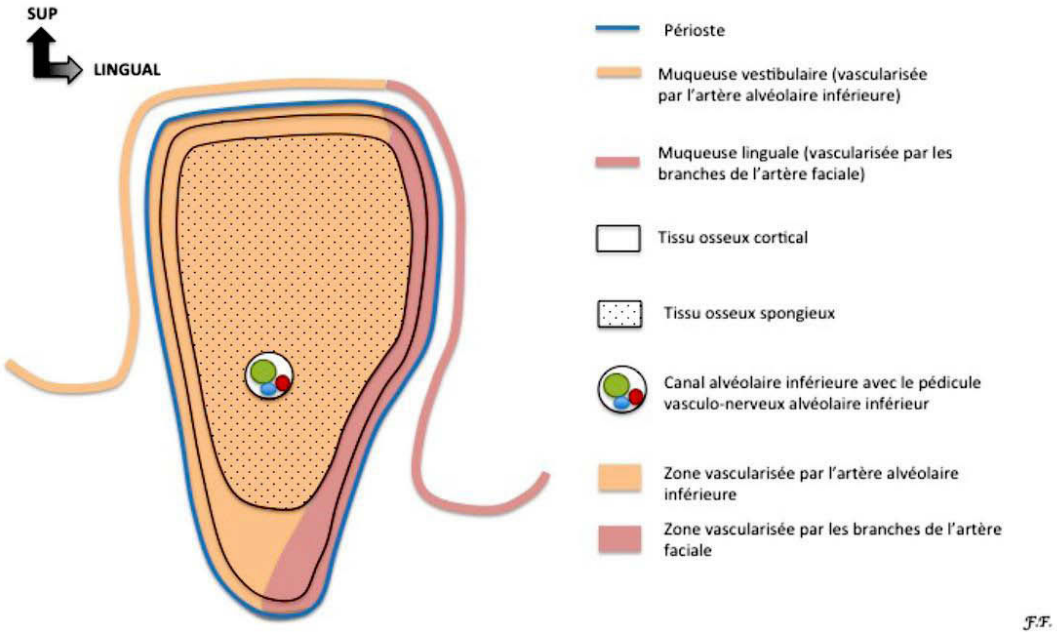


Figure 7 : Schématisation de l'origine de la vascularisation mandibulaire en secteur molaire (thèse Fauvel)

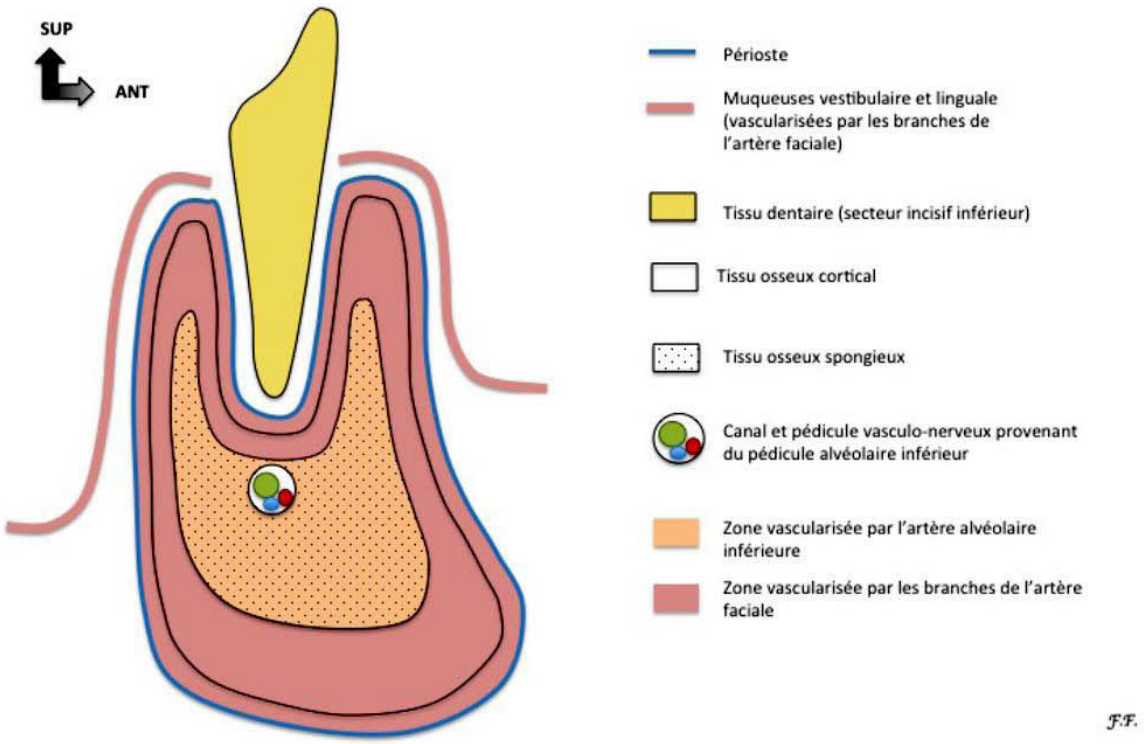


Figure 8 : Schématisation de l'origine de la vascularisation mandibulaire en secteur symphysaire (Thèse Fauvel)

Chez le rat, la vascularisation mandibulaire est organisée de la même façon avec un apport endo-osseux provenant de l'artère alvéolaire inférieure et un apport extra-osseux provenant de l'artère maxillaire externe (cette artère correspond à l'artère faciale chez l'Homme) (Fig. 9).

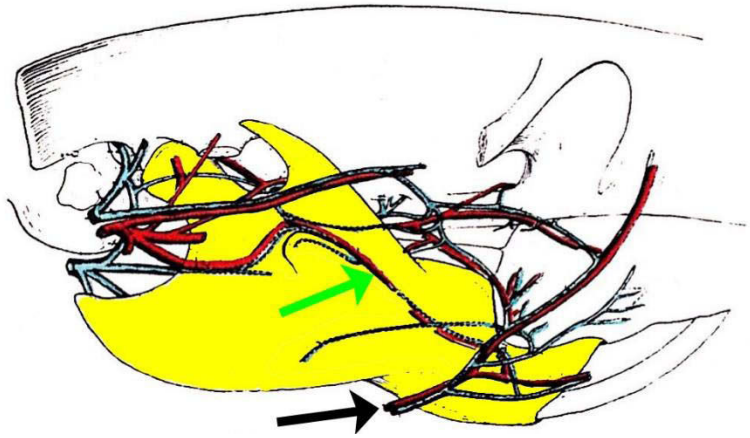


Figure 9 : Vascularisation mandibulaire chez le rat provenant de l'artère alvéolaire inférieure (flèche verte) et de l'artère maxillaire externe (flèche noire)

1.3. Muscles masticateurs

Chez l'Homme les muscles masticateurs principaux sont les muscles masséters, temporaux, ptérygoïdiens médiaux et ptérygoïdiens latéraux (Fig. 10). L'action principale des muscles masséters, temporaux et ptérygoïdiens médiaux est l'élévation de la mandibule. Les muscles du plancher buccal, principalement les muscles digastriques, génio-hyoïdiens et mylo-hyoïdiens sont considérés comme des muscles masticateurs accessoires dont l'action est antagoniste aux muscles masticateurs principaux (abaissement de la mandibule) (Fig. 11).

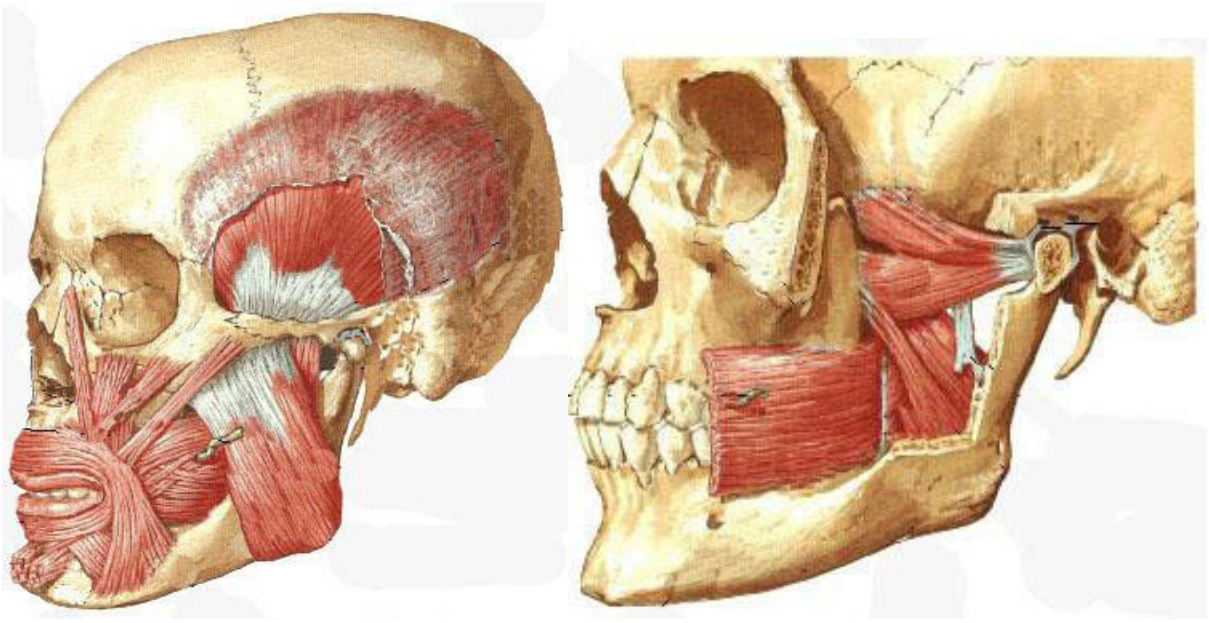


Figure 10 : Vue latérale des muscles masticateurs chez l'Homme

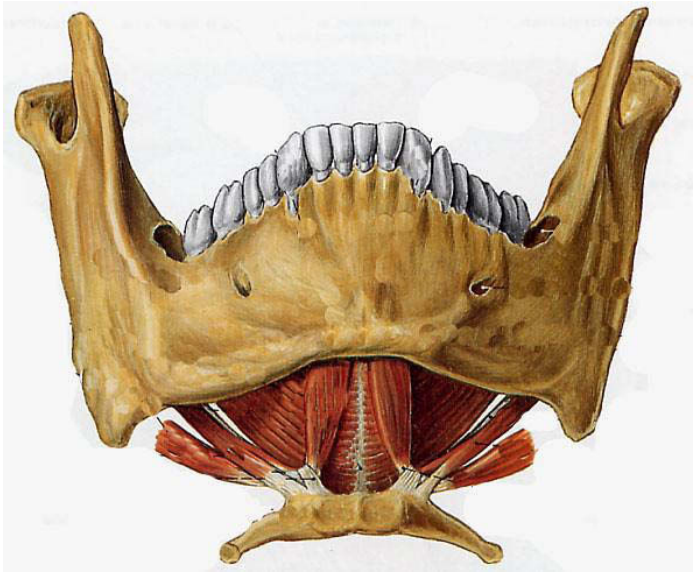


Figure 11 : Vue des muscles digastriques et du plancher buccal chez l'Homme

Chez le rat les muscles masticateurs principaux (masséters, temporaux, ptérygoïdiens latéraux et ptérygoïdiens médiaux sont également présents (Fig. 12 et 13).

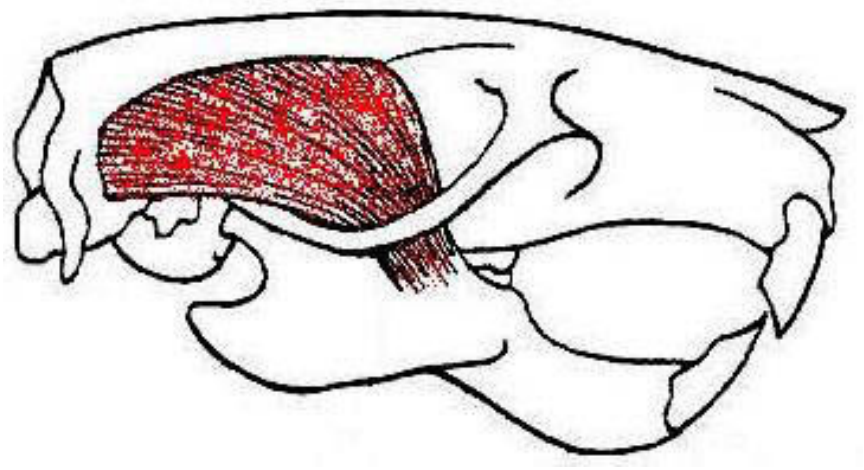


Figure 12 : Vue latérale du muscle temporal chez le rat

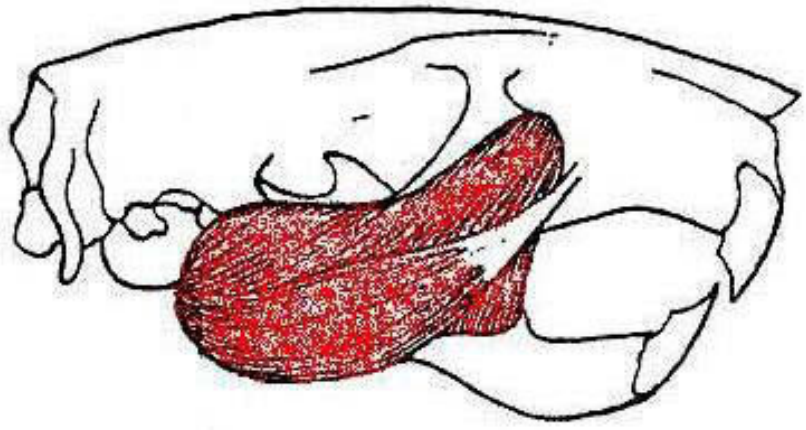


Figure 13 : Vue latérale du muscle masséter chez le rat

Chez le rat, le muscle masséter est proportionnellement plus important et plus développé et est constitué de quatre chefs (antérieur superficiel, postérieur superficiel, antérieur profond et postérieur profond) alors que chez l'Homme il n'est constitué que de deux chefs (superficiel et profond). Le muscle digastrique présente, chez l'Homme comme chez le rat, un tendon intermédiaire en regard de l'os hyoïde et une insertion antérieure à la face linguale de la mandibule (Fig. 11 et 14).

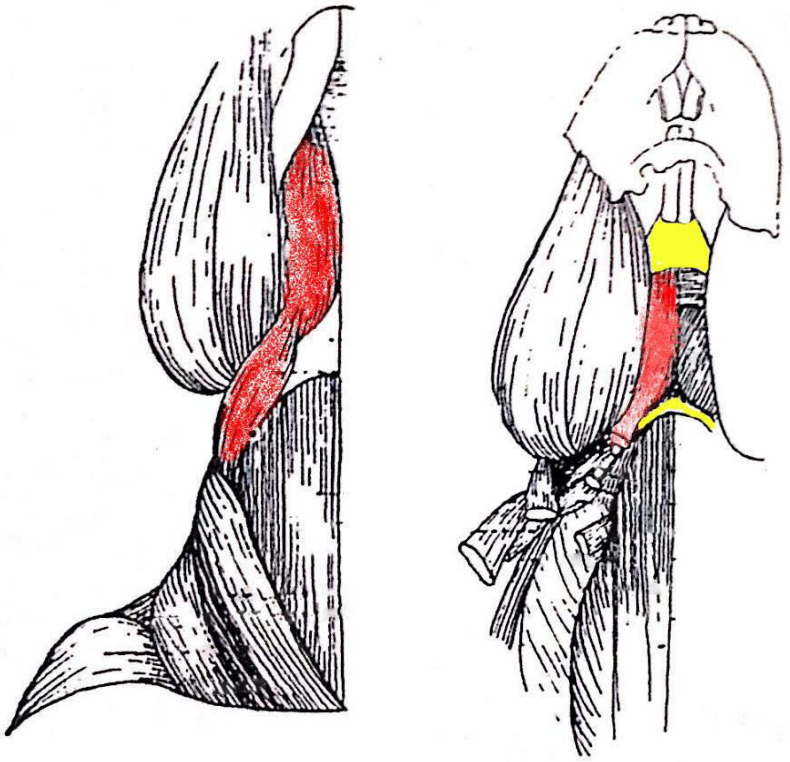


Figure 14 : Vue inférieure montrant le muscle digastrique chez le rat

1.4. Physiologie de la mastication

La mastication est la première étape de la digestion. Elle associe d'abord la préhension des aliments, leur incision, leur transport endo-buccal puis leur fragmentation avant la déglutition.

Chez l'Homme la mastication s'effectue par des mouvements mandibulaires rythmiques dans les trois plans de l'espace. Elle est le plus souvent unilatérale alternée c'est-à-dire que les aliments sont écrasés en alternance d'un côté puis de l'autre avec alternance selon les cycles masticatoires (4). L'Homme peut présenter une ou plusieurs déglutition(s) par séquence masticatoire mais les mouvements mandibulaires ne peuvent être concomitants à la déglutition (5). Les articulations temporo-mandibulaires sont sollicitées durant la mastication avec des déplacements d'amplitude importante. La charge s'y exerçant est fonction de la dureté de l'aliment concerné par les mouvements de mastication (6, 7). Le muscle digastrique intervient en tant qu'abaisseur de la mandibule pour l'ouverture buccale (8).

Chez le rat, on sépare l'alimentation en trois phases : l'ingestion, la mastication et la déglutition (9). L'ingestion implique le fait de « ronger » c'est-à-dire de progressivement couper les aliments en éclats de petite taille avec les incisives avant de les accumuler dans la cavité orale pour la mastication. Cela correspond à l'action des incisives, située en antérieur, avec des forces masticatrices s'exerçant horizontalement (10). Puis a lieu la mastication proprement dite et enfin la déglutition quand un volume suffisant est atteint par le bol alimentaire. Les articulations temporo-mandibulaires ne sont sollicitées fortement que lors des mouvements incisifs et non lors de la mastication par les molaires (10). La mastication n'est pas interrompue par la déglutition. Le muscle digastrique intervient pour abaisser la mandibule à l'ouverture buccale et également pour stabiliser l'articulation temporo-mandibulaire lors de la fermeture buccale à l'instar du muscle ptérygoïdien latéral chez l'Homme (11). Les muscles temporaux et masséters interviennent pour la fermeture buccale.

Les principales différences entre l'Homme et le rat concernant la mastication sont donc de plusieurs ordres. Tout d'abord de fortes disparités alimentaires et comportementales peuvent être observées chez l'Homme contrairement au rongeur. En outre les rongeurs utilisent leur incisives quotidiennement beaucoup plus longtemps que l'Homme car il s'agit d'incisives à croissance continue. La mastication unilatérale alternée et la déglutition après la mastication sont des spécificités humaines. Les articulations temporo-mandibulaires sont sollicitées de manière différente : principalement lors des mouvements des incisives chez le rongeur et principalement lors du broyage

des aliments par les molaires chez l'Homme. En mettant à part ces différences, la physiologie musculaire de la mastication reste assez comparable chez l'Homme et le rongeur et nombre d'auteurs considèrent que le rat constitue un modèle animal de qualité pour l'étude des phénomènes liés à la mastication (9).

2. Le remodelage osseux

2.1. Le remodelage osseux normal

Le remodelage osseux assure l'entretien et l'adaptation du squelette préalablement constitué par le modelage osseux (12). Il s'agit d'un processus adaptatif complexe impliquant des cellules qui résorbent le tissu osseux (ostéoclastes) et des cellules ostéoformatrices (ostéoblastes) et de nombreuses cytokines et facteurs de croissance. Elle fait intervenir un ensemble de cellules variées et de différentes origines, le BMU (« Basic Multicellular Unit ») (Fig. 15). Chez l'adulte le remodelage osseux aboutit normalement à la constitution d'un tissu osseux de type lamellaire.

Le tissu osseux est en constant remaniement par le remodelage osseux. Ce remodelage osseux résulte d'une double activité : ostéo-résorption des portions de matrice osseuse ancienne, qui ne sont plus adaptées d'un point de vue mécanique ou métabolique, et ostéo-formation de nouvelles unités de structures (*Bone Structure Units* (BSU)). Les ostéoclastes et les ostéoblastes agissent donc de façon coordonnée et en association étroite dans le temps et l'espace.

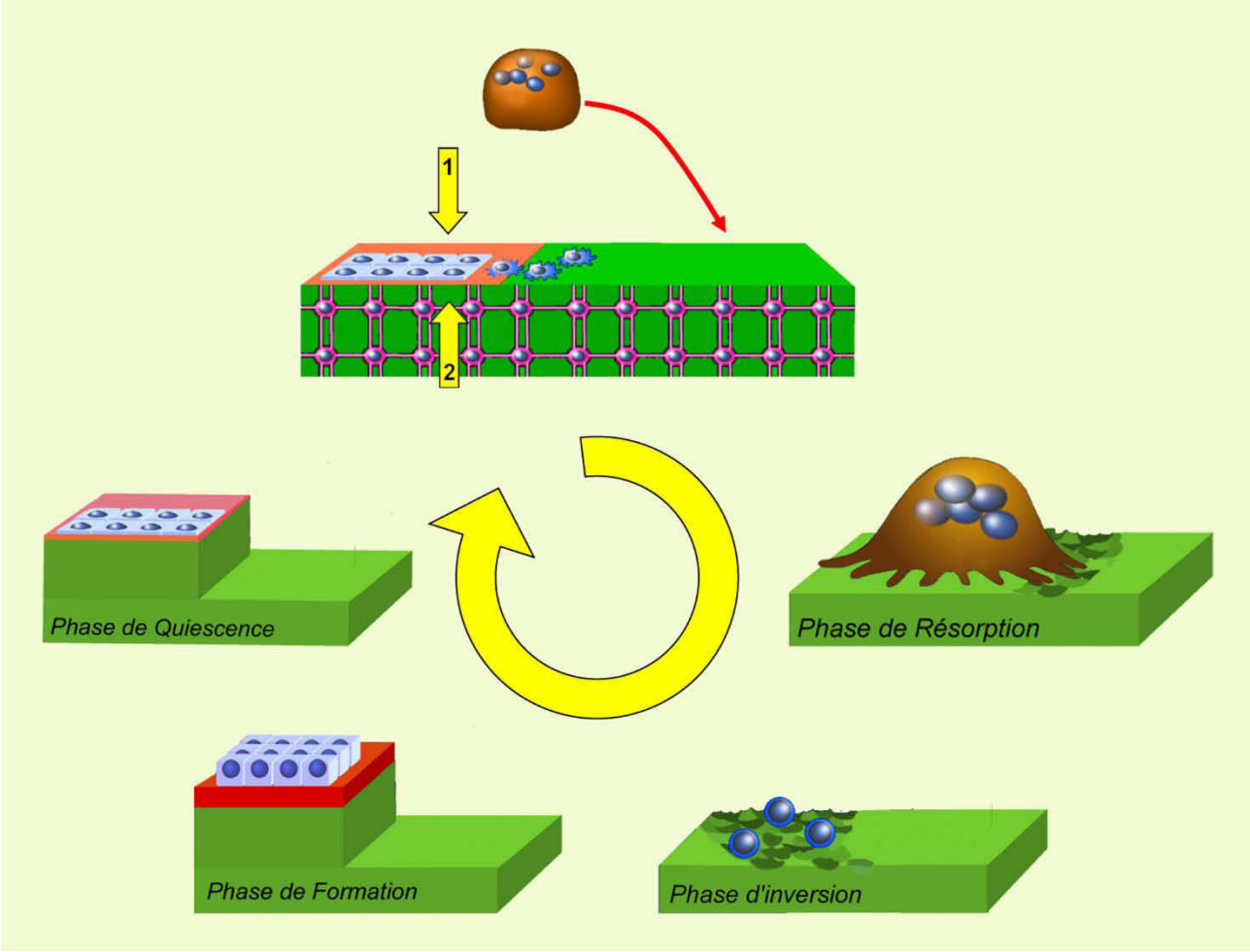


Figure 15 : Le remodelage osseux : schématisation du « Basic Multicellular Unit »

Les ostéoclastes sont les cellules chargées de résorber le tissu osseux. Elles proviennent de la fusion de précurseurs sanguins de la lignée monocyte/macrophage. L'ostéoclastogenèse est sous la dépendance de plusieurs molécules dont RANKL. Ces cellules sont volumineuses (jusqu'à 150 µm de diamètre) et plurinucléées (contenant jusqu'à dix noyaux). Leur taille dépend de l'espèce et du taux d'hormone parathyroïdienne. Elles sont également caractérisées par la présence de nombreuses mitochondries dans le cytoplasme. La membrane cellulaire au contact du tissu osseux est faite de nombreuses ondulations, avec des zones d'ancrage latérales. Cela délimite ainsi une chambre de résorption, lieu dans lequel s'effectue la résorption de la matrice osseuse.

La résorption de la matrice osseuse minéralisée s'effectue en deux phases. La première phase est une phase de décalcification par libération d'ions H^+ entrainant la formation d'acide chlorhydrique dans la chambre de résorption. Cela s'effectue grâce à la présence d'une anhydrase carbonique et d'un canal chlore. Il en résulte une dissolution des cristaux d'hydroxyapatite. La deuxième phase est une phase de dégradation du collagène. Elle s'effectue grâce à la libération de métalloprotéases des lysosomes des ostéoclastes. Les produits de dégradation du collagène sont ensuite phagocytés par l'ostéoclaste puis dégradés en intra-cellulaire grâce à la phosphatase acide tartrate résistante (TRAcP). Il se forme ainsi sous chaque ostéoclaste actif une zone de résorption appelée lacune de Howship.

Les ostéoblastes sont les cellules chargées de synthétiser et minéraliser le tissu osseux. Elles proviennent d'une cellule souche d'origine mésenchymateuse, la cellule stromale. Leur différenciation est sous la dépendance de facteurs de croissance (tels que TGF-β et IGFs). Ce sont des cellules mononucléées. Elles peuvent ensuite se transformer en ostéocytes et en cellules bordantes ou disparaitre par apoptose. Ce sont des cellules de forme cubique disposées en tapis cellulaires, pseudo-épithéliaux, à la surface des travées osseuses et des canaux de Havers. Elles contiennent un appareil de Golgi très développé témoignant d'une forte activité de sécrétion et de synthèse protéique. Les ostéoblastes sont couplés par des jonctions de type gap de manière à harmoniser la synthèse des fibrilles de collagène. Les ostéoblastes sont également couplés aux ostéocytes par des prolongements et des jonctions gap.

La formation de la matrice osseuse minéralisée s'effectue en deux phases. La première phase est une phase de synthèse de protéines collagéniques et non collagéniques. Ces protéines sont polymérisées dans l'espace extra-cellulaire. Elles sont caractérisées par une striation périodique de 67 nm en microscopie électronique. Cela aboutit à la formation d'une lamelle avec toutes les fibres qui ont une même orientation. L'orientation des fibres est ensuite modifiée pour la formation de la lamelle suivante. La couche de matrice osseuse non minéralisée ainsi obtenue s'appelle tissu ostéoïde. La

deuxième phase est une phase de minéralisation de cette matrice. Elle débute à la ligne cémentante puis se propage par nucléation secondaire à partir des cristaux préalablement formés. Le front de minéralisation est la limite entre tissu ostéoïde et tissu minéralisé.

Les ostéocytes sont les cellules présentes dans le tissu osseux minéralisé. Certains ostéoblastes vont se trouver progressivement emmurés dans une logette de la matrice osseuse minéralisée et devenir des ostéocytes. Ce sont des cellules mononucléées. Elles peuvent élaborer de la matrice osseuse et la minéraliser sur les parois des logettes dans lesquelles elles sont contenues. Elles restent en connexion avec les ostéocytes situés aux alentours par des prolongements dans des canalicules de la matrice osseuse.
Les ostéocytes ont un rôle trophique en agissant comme des mécanorecepteurs. Leur stimulation par des contraintes mécaniques entraine la transmission d'information vers la surface osseuse aux ostéoclastes et ostéoblastes.

Les cellules bordantes sont aplaties et tapissent la surface osseuse quand il n'y a ni ostéoblaste ni ostéoclaste. Ce sont des ostéoblastes qui ont arrêté leur activité d'ostéoformation mais restent à la surface osseuse. Elles peuvent être réactivées sous l'influence de divers activateurs (mécaniques, hormonaux, …) pour permettre aux ostéoclastes de se fixer et peuvent également se redifférencier en ostéoblastes.

2.2. Particularités du remodelage osseux mandibulaire

La portion alvéolaire de la mandibule est constituée d'un tissu osseux spécifique (dit os alvéolaire) car il contient les racines dentaires et est soumis à de fortes contraintes mécaniques durant la mastication. Il se résorbe de manière irréversible en cas de perte dentaire (13). Il est également caractérisé par un taux de remodelage osseux élevé (14).

2.3. Le remodelage osseux pathologique

Des anomalies du remodelage osseux peuvent être observées dans de nombreuses pathologies. Le plus souvent elles sont dues à un déséquilibre entre ostéo-formation et ostéo-résorption. Une ostéopétrose est due à un déficit d'ostéo-résorption par exemple du à l'absence d'anhydrase carbonique, de canaux chlore de la membrane ostéoclastique ou à l'absence d'ostéoclaste. A l'inverse,

une ostéoporose est due à un déséquilibre entre ostéoformation et ostéo-résorption. Des modifications des stimuli mécaniques sur les ostéocytes peuvent entrainer des troubles du remodelage osseux (vol spatial, diminution des forces musculaires exercées sur l'os).

 CC BY NC ND

TRAVAUX PERSONNELS

 CC BY NC ND

ARTICLE 1

Botulinum toxin in masticatory muscles of the adult rat induces bone loss at the condyle and alveolar regions of the mandible associated with a bone proliferation at a muscle enthesis

Jean-Daniel KÜN-DARBOIS, Hélène LIBOUBAN, Daniel CHAPPARD

Bone 77 : 75-82, 2015

Facteur d'impact 2015 : 3,736

La toxine botulique (BTX) provient d'une bactérie, le *Clostridium botulinum*. C'est une neurotoxine capable d'inhiber la transmission du signal nerveux en bloquant les vésicules présynaptiques d'acétylcholine. Elle entraine une paralysie musculaire réversible (15). L'injection de BTX dans certains muscles striés (*Mus Quadriceps femoris*) chez l'animal entraine une perte osseuse (tibia, fémur) due à la diminution des contraintes mécaniques exercées sur le tissu osseux (16, 17). En clinique humaine, la BTX est utilisée couramment en injections dans les muscles masticateurs pour le traitement de pathologies telles que trismus, bruxisme, dysfonctions temporo-mandibulaires et hypertrophie des muscles masticateurs (18, 19). La mandibule est un os particulier de par son ossification membranaire, sa localisation dans la sphère oro-faciale et sa stimulation par les muscles masticateurs. Elle est en outre constituée d'os basal et d'os alvéolaire. Ce dernier est caractérisé par un remodelage osseux intense.

Nos premiers travaux visaient à rechercher si une perte osseuse mandibulaire pouvait être observée après injection de BTX dans les muscles masticateurs chez l'animal. Des rats adultes ont reçu des injections intramusculaires de BTX dans les muscles temporaux et masséters droits. Ils ont été sacrifiés quatre semaines après. Une analyse osseuse des zones osseuses condyliennes et alvéolaires a été ensuite effectuée par microtomographie aux rayons X (microCT) (Fig. 15), analyse vectorielle de la porosité et histologie.



Figure 16 : Appareils utilisé pour la microtomographie aux rayons X (Skyscan 1172, Bruker)

1. Travail préparatoire

Ce dernier a consisté en la réalisation de plusieurs protocoles d'injections intramusculaires différents afin de déterminer lequel permettait d'obtenir la meilleure diffusion possible du produit dans les tissus musculaires. Le bleu de méthylène a été utilisé. Le schéma qui a été ainsi retenu a consisté en l'injection d'un volume de 0,2 ml en deux points d'injection dans le muscle temporal droit et trois points d'injection dans le muscle masséter droit (Fig. 16 et 17).

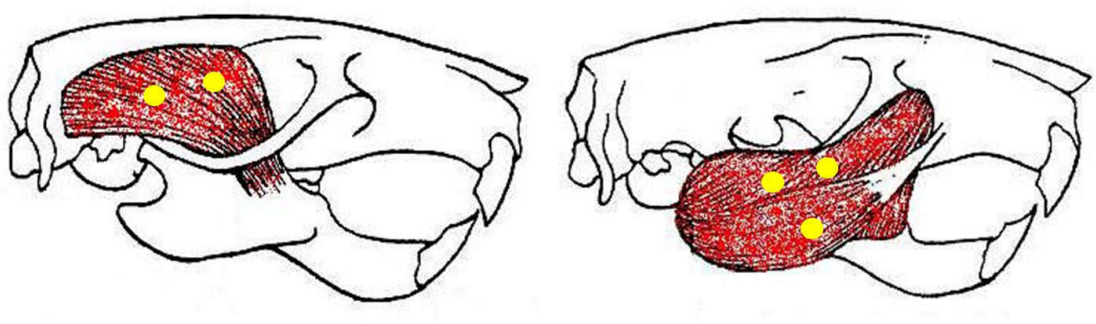


Figure 17 : Points d'injection dans le muscle temporal (n=2) et le muscle masséter (n=3)

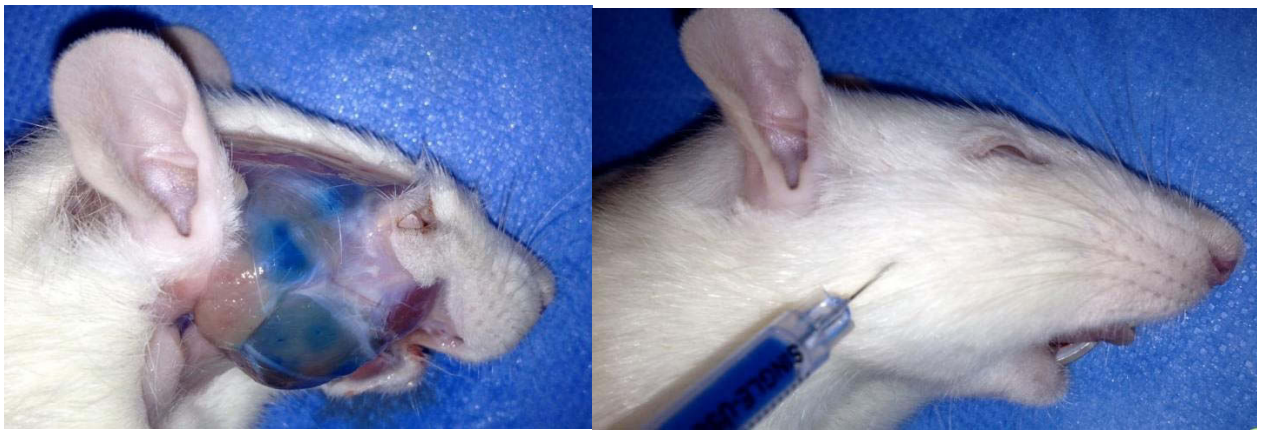


Figure 18 : Injection intra musculaire de bleu de méthylène

2. Protocole expérimental

Quinze rats mâles adultes ont été randomisés en deux groupes : groupe contrôle (CTRL) et groupe BTX. Les rats du groupe BTX ont reçu une injection unique de BTX : 1 UI par muscle comme ci-dessus, dans 0,2 ml de sérum physiologique dans les muscles masséters et temporaux droits. Les rats du groupe CTRL ont reçu des injections similaires de sérum physiologique. Les rats étaient sacrifiés 1 mois après. Une acquisition par microCT était ensuite réalisée pour chaque hémimandibule pour analyser l'os alvéolaire et l'os condylien (Fig. 18).

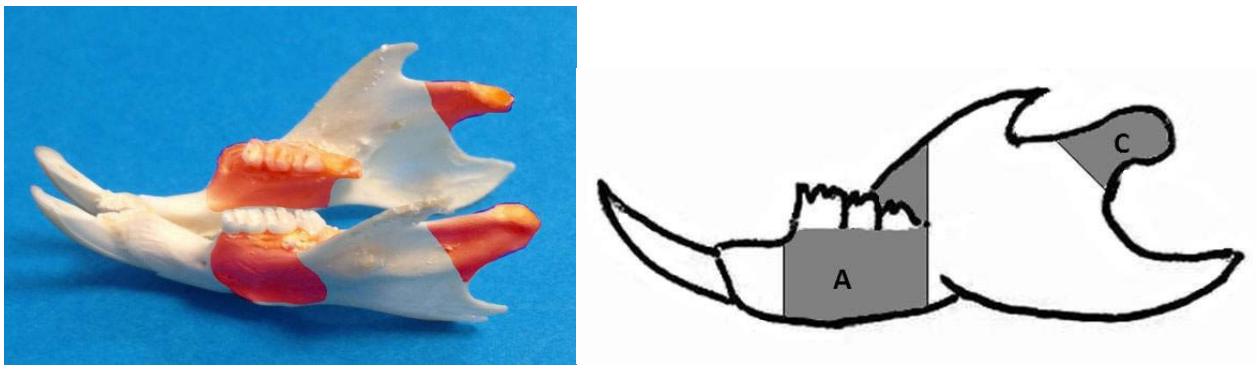


Figure 19 : Zones d'analyse osseuse sur les mandibules de rats en vue sur os sec (zones colorées) et vue schématique (C : os condylien, A : os alvéolaire)

Afin d'obtenir des coupes bidimensionnelles qui soient comparables, un plan de coupe sur les images 3D obtenues était positionné de façon stéréotypée pour chaque échantillon (Fig. 19). La surface occupée par l'os trabéculaire était ensuite calculée sur coupes 2D (10 coupes frontales pour l'os condylien, 5 coupes frontales et 1 coupe sagittale pour l'os alvéolaire) afin de mesurer le volume osseux trabéculaire (BV/TV). La mesure de l'épaisseur corticale était également mesurée sur coupe 2D.

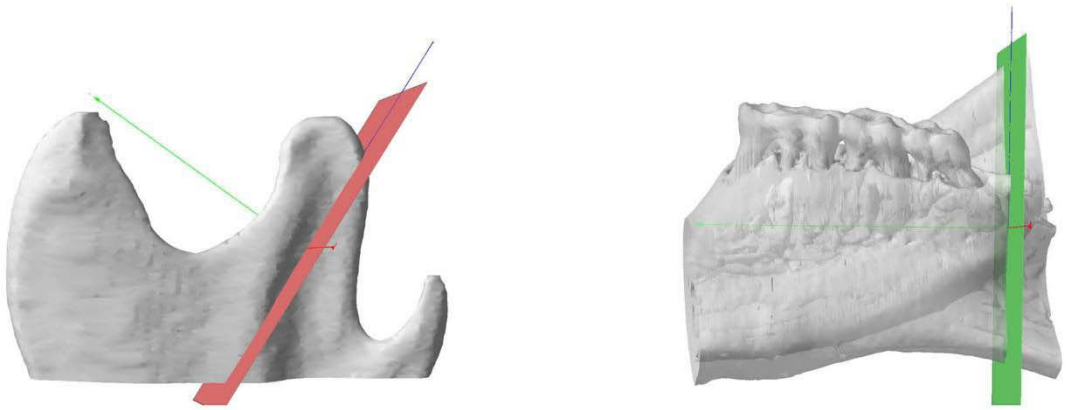


Figure 20 : Positionnement des plans de coupe sur les images de reconstruction 3D pour obtention des images 2D condyliennes et alvéolaires toujours comparables

L'analyse vectorielle tridimensionnelle de la porosité de l'os alvéolaire a été ensuite réalisée (Fig. 20). Celle-ci consiste en la binarisation des piles d'images microCT puis en l'utilisation d'un algorithme de projection vectorielle. Chaque vecteur traversant ainsi virtuellement l'objet étudié se voit attribué une pseudocouleur correspondant à la quantité de pixels traversés. La projection de l'ensemble des vecteurs traversant l'objet sur un plan frontal permet d'obtenir une image bidimensionnelle de la porosité tridimensionnelle de l'objet (plan fractal) (20).

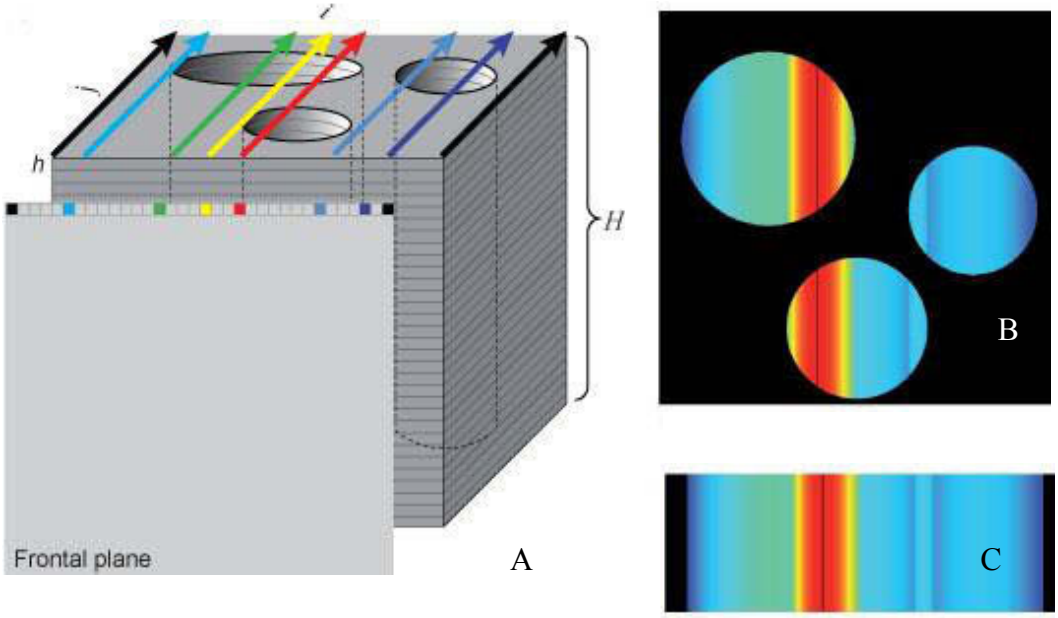


Figure 21 : Analyse vectorielle de la porosité d'un volume (A), vue supérieure (B) et vue du plan frontal (C)

3. Résultats

Une diminution de 35% du volume osseux trabéculaire condylien droit chez les rats BTX a été retrouvée (Fig. 21) par rapport au côté gauche des rats BTX et aux côtés droit et gauche des rats CTRL. Une diminution de 20% du volume osseux trabéculaire alvéolaire droit chez les rats BTX a été retrouvée (Fig. 22) par rapport au côté gauche des rats BTX et aux côtés droit et gauche des rats CTRL.

De manière inattendue, une hypertrophie osseuse de l'enthèse d'insertion du ventre antérieur du muscle digastrique droit a été retrouvée chez tous les rats du groupe BTX et aucun rat CTRL (Fig. 23). Une porosité significativement plus élevée de l'os alvéolaire du côté injecté a été retrouvée chez tous les rats BTX par analyse de porosité (Fig. 24).

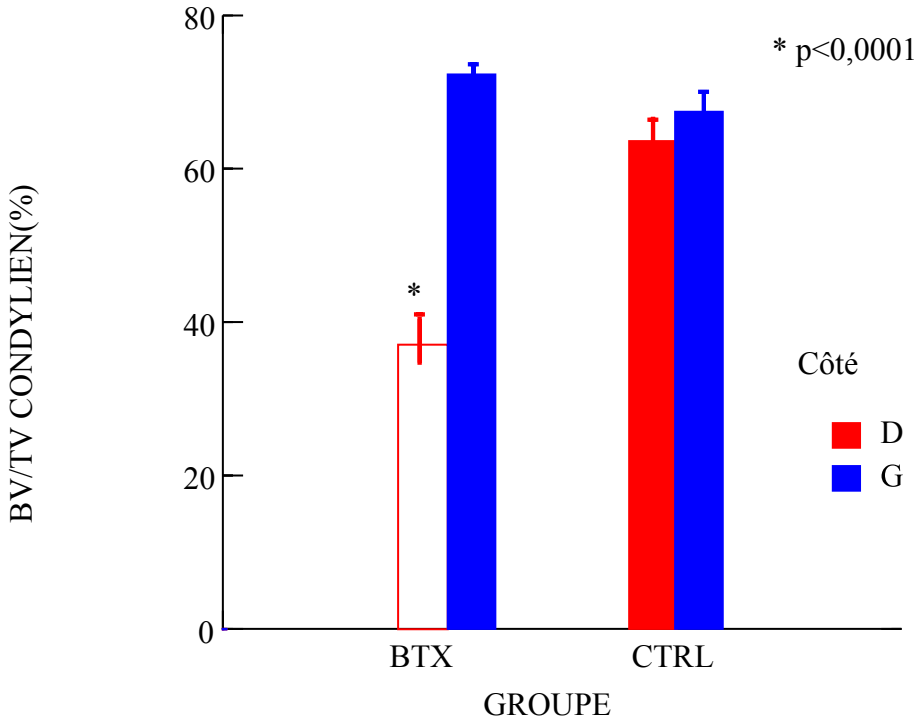


Figure 22 : Résultats de la mesure du volume osseux trabéculaire condylien montrant une perte osseuse du côté injecté de 35%

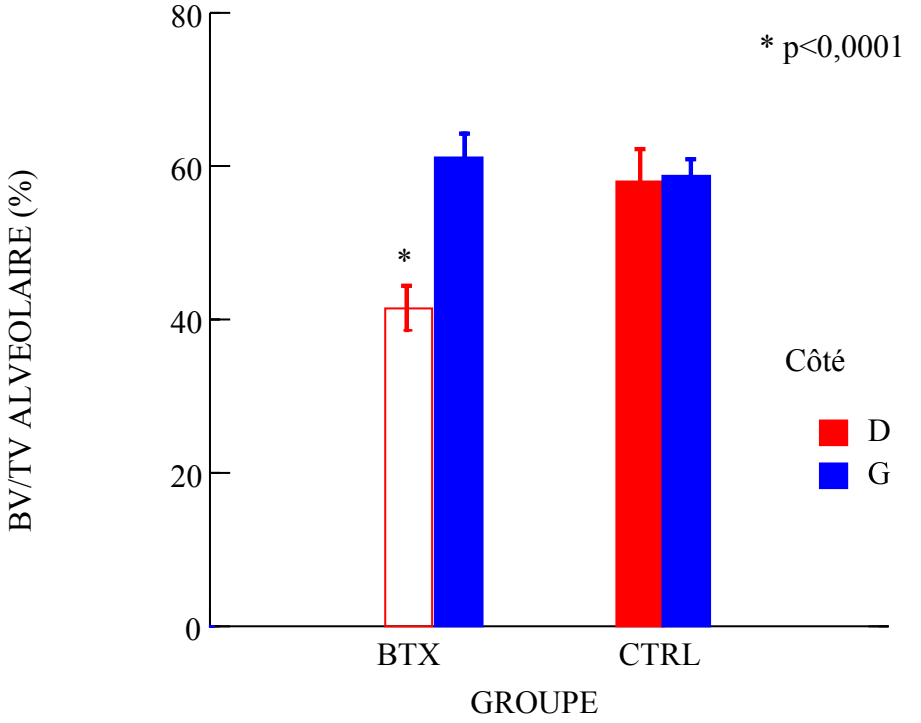


Figure 23 : Résultats de la mesure du volume osseux trabéculaire alvéolaire montrant une perte osseuse du côté injecté de 20%

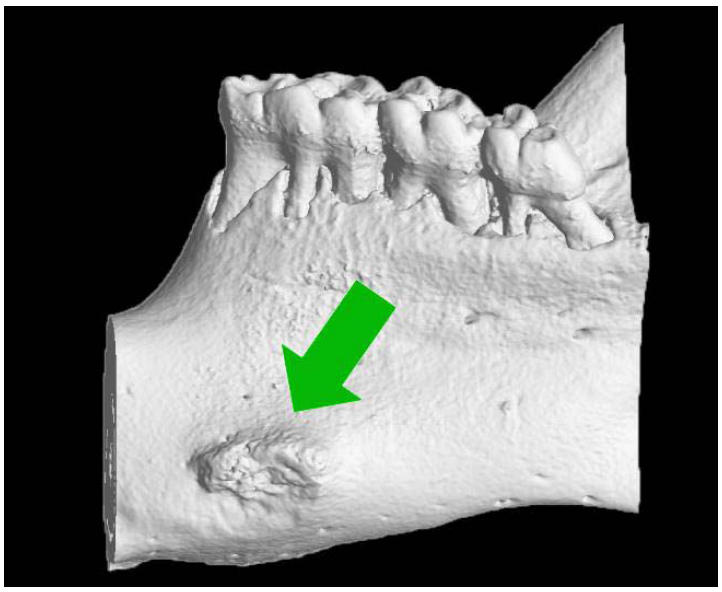


Figure 24 : Vue 3D de la face linguale de l'os alvéolaire d'un rat BTX montrant une prolifération de l'enthèse d'insertion du muscle digastrique (flèche)

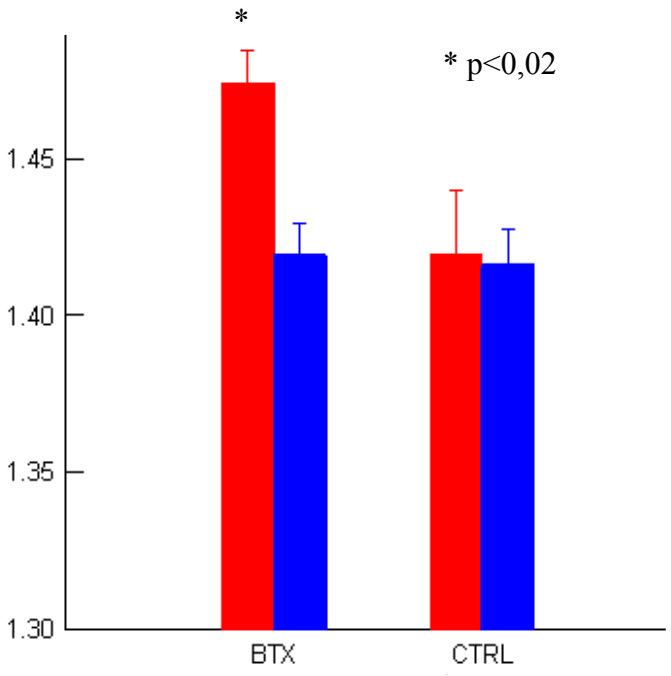


Figure 25 : Résultats de l'analyse de la porosité osseuse alvéolaire par analyse vectorielle montrant une porosité accrue du côté injecté

4. Conclusion

Nous avons donc pu montrer par ce travail que l'injection de BTX dans les muscles masticateurs chez le rat adulte entrainait une perte osseuse mandibulaire alvéolaire et condylienne ainsi que l'apparition d'une hypertrophie osseuse mandibulaire de l'enthèse d'insertion du muscle digastrique sur la mandibule.

Une nouvelle technique d'analyse de la porosité osseuse a été utilisée ici (analyse vectorielle) et a montré sa fiabilité pour l'analyse osseuse de la mandibule de rat qui est un os complexe à analyser (os fin, présence de racines dentaires, forme complexe).

La recherche d'une perte osseuse mandibulaire similaire après injection de BTX chez l'Homme en pratique courante apparait donc comme une perspective d'étude intéressante. L'apparition d'une hypertrophie osseuse semble être réactionnelle à un déséquilibre occlusal des forces musculaires s'exerçant sur la mandibule. Un tel déséquilibre pourrait dès lors avoir un rôle dans la physiopathologie des tori mandibulaires qui sont des hypertrophies osseuses mandibulaires chez l'Homme.

ARTICLE 2

Contrast enhancement with uranyl acetate allows quantitative analysis of the articular cartilage by microCT: Application to mandibular condyles in the BTX rat model of disuse

Jean-Daniel KÜN-DARBOIS, Florence MANERO, Louis RONY, Daniel CHAPPARD

Micron 97 : 35-40, 2017

Facteur d'impact 2015 : 1,838

Nous avons montré que l'injection de toxine botulique dans les muscles masticateurs entrainait une perte osseuse mandibulaire condylienne mandibulaire chez le rat (cf. article 1). De telles injections de BTX pourraient également entrainer une atteinte du cartilage articulaire condylien mandibulaire par modification des contraintes exercées sur ce cartilage. En effet, le cartilage articulaire condylien est fortement dépendant des contraintes exercées sur l'articulation (21, 22). D'ailleurs une diminution de l'épaisseur cartilagineuse articulaire a été observée sur un modèle comparable avec des animaux en croissance (23). Mais la littérature est contradictoire et pauvre à ce sujet (21, 23).

L'étude du cartilage articulaire condylien chez le rat se heurte cependant à plusieurs difficultés. La mesure de l'épaisseur cartilagineuse n'est pas fiable sur des coupes histologiques du fait de l'altération des tissus causée par la préparation (déshydratation et contraction) et de l'obliquité des coupes histologiques entrainant des imprécisions de mesure. L'étude du cartilage articulaire par microCT permettrait de s'affranchir de tels biais mais elle se heurte bien évidemment à l'absence de radio-opacité du tissu cartilagineux. Le développement d'une technique d'imprégnation du cartilage articulaire par un produit de contraste est donc indispensable.

De nombreuses techniques ont été décrites avec l'emploi de produits de contraste variés (acide ioxaglique, iopromide, gadolinium, iodure de potassium-iode (IKI), acide phosphotungstique (PTA), acide phosphomolybdique, tetroxide d'osmium), mais aucune ne s'est avérée d'assez bonnes qualité et reproductibilité quand nous les avons testées (24-32).

L'objectif de ce travail était de rechercher une atteinte cartilagineuse articulaire condylienne dans le modèle de rat BTX et de décrire une procédure d'analyse du cartilage articulaire par microCT en utilisant un nouvel agent de contraste (l'acétate d'uranyle).

1. Résultats

Le cartilage articulaire était bien identifié en microCT dans toute son épaisseur grâce à l'utilisation d'AcU. Aucune différence significative d'épaisseur cartilagineuse n'a été mise en évidence entre les condyles du côté injecté et les autres condyles.

2. Travail préparatoire

L'imprégnation de têtes fémorales humaines par différents agents de contrastes a été réalisée afin de les comparer et de trouver celui qui fournirait la meilleure radio-opacité au cartilage articulaire. Les produits utilisés ont été : acétate d'uranyle, lanthanides, acide phosphotungstique, IKI et iopamidol.

L'acétate d'uranyle (AcU) a permis d'obtenir la meilleure radio opacité après acquisition en microCT. C'est donc l'AcU qui a été retenu pour étudier le cartilage condylien dans le modèle de rat BTX.

3. Protocole expérimental

Onze rats mâles adultes ont été randomisés en deux groupes : groupe contrôle (CTRL) et groupe BTX. Les rats du groupe BTX ont reçu une injection unique de BTX : 1 UI par muscle (en 2 ou 3 points d'injection) dans 0,2 ml de sérum physiologique dans les muscles masséter et temporal droits. Les rats du groupe CTRL ont reçu des injections similaires de sérum physiologique. Les rats étaient sacrifiés un mois après. Une acquisition par microCT était ensuite réalisée pour chaque hémimandibule. Les condyles mandibulaires étaient ensuite récupérés puis imprégnés dans l'AcU pendant 24h puis rincés à l'eau pendant 1h. Une acquisition microCT était ensuite réalisée. Les échantillons étaient ensuite préparés sans décalcification pour analyse histologique. L'épaisseur cartilagineuse articulaire (Cart.Th) était ensuite mesurée sur coupes 2D et une moyenne était obtenue (12 mesures par condyle).

4. Conclusion

Dans le modèle de rats BTX avec injection dans les muscles masticateurs, aucune atteinte du cartilage articulaire n'a été mise en évidence.

ARTICLE 3

Asymmetric bone remodeling in mandibular and maxillary tori

Jean-Daniel KÜN-DARBOIS, Bernard GUILLAUME, Daniel CHAPPARD

Clinical Oral Investigation, DOI 10.1007/s00784-017-2080-8, 2017

Facteur d'impact 2016 : 2,454

La présence d'une hypertrophie osseuse localisée à la corticale linguale en réaction à un déséquilibre des forces musculaires dans le modèle de rat BTX a été observée (cf. article 1). Cette hypertrophie ayant des caractéristiques proches en termes de forme et de localisation, des tori de la cavité buccale que l'on observe chez l'Homme dans une proportion non négligeable de la population, cela nous a fait nous interroger sur la physiopathologie de ce type de lésion.

Les tori de la cavité buccale sont des hypertrophies osseuses bénignes de la cavité buccale (Fig. 25). Ils peuvent être localisés à la mandibule (*torus mandibularis,* TM), au palais (*torus palatinus,* TP) ou au maxillaire (*torus maxillaris*, TMax) (33, 34). Leur prévalence est assez élevée dans la population générale ; elle est comprise entre 10 et 30% et varie selon l'âge, le sexe et le groupe ethnique (35, 36).

La physiopathologie de ces excroissances osseuses n'est pas connue à l'heure actuelle et plusieurs facteurs pourraient être en cause : génétiques, environnementaux et mécaniques (forces occlusales) (34, 37, 38).

Leurs caractéristiques histologiques habituellement décrites sont celles du tissu osseux normal sans spécificité : os cortical d'organisation normale lamellaire et os trabéculaire si la taille du torus est suffisamment importante (33, 39, 40).

L'objectif de ce travail était de décrire les caractéristiques morphologiques et histologiques des tori humains. Il était également de les comparer à l'hypertrophie osseuse trouvée dans le modèle de rat BTX et aux exostoses que l'on trouve sur les os longs chez l'Homme.



Figure 26 : Vue d'un torus mandibularis

1. Protocole expérimental

Il s'agit d'une étude clinique prospective et multicentrique. Les tori ont été obtenus après exérèse chirurgicale « monobloc » (Fig. 26 et 27).

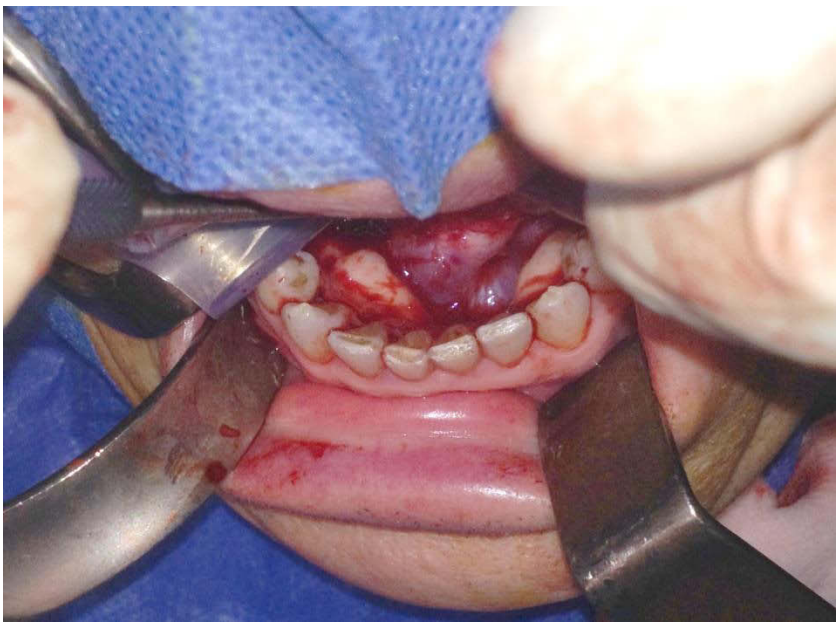


Figure 27 : Vue peropératoire d'un torus mandibularis après décollement sous périosté



Figure 28 : Vue peropératoire d'un torus mandibularis après exérèse monobloc

Une administration de tétracycline selon le protocole de double marquage classiquement utilisé en rhumatologie a été réalisée afin de permettre de mesurer la vitesse de minéralisation. Les tori étaient analysés par microCT et histologie sans décalcification.

2. Résultats

L'étude morphologique par microCT a permis l'identification d'une orientation aléatoire des canaux de Havers des tori.

L'étude histologique a montré que les tori étaient constitués de tissu osseux lamellaire dans la plupart des cas. Une bordure ostéoïde était visible à la surface de chaque torus et également dans les canaux de Havers. Une asymétrie du remodelage osseux a été mise en évidence dans les canaux de Havers : la bordure ostéoïde était toujours située du côté du bord libre de la tumeur alors que les lacunes de Howship et les ostéoclastes étaient toujours situés du côté opposé. Le remodelage osseux dans les tori se fait donc de façon asymétrique car l'ostéogenèse se fait du côté du bord libre et la résorption osseuse du côté opposé.

La vitesse de minéralisation a été trouvée plus élevée que la normale dans les canaux de Havers. Ceci témoigne d'une forte activité ostéogénique (Tableau 1).

Torus	Bordure ostéoïde	Os trabéculaire	Remodelage asymétrique	Texture osseuse	Ct.O.Th (µm)	Ca.O.Th (µm)	Ct.MAR (µm/j)	Ca.MAR (µm/j)	Ostéoclastes
1	Oui	Non	Oui	lamellaire	13,42	14,93	.	.	Oui
2	Oui	Non	Oui	lamellaire	17,70	13,23	.	.	Oui
3	Oui	Non	Oui	lamellaire	9,91	16,96	.	.	Non
4	Oui	Non	Oui	lamellaire	6,35	12,82	.	.	Non
5	Non	Oui	Non	Lamellaire + non lamellaire	.	.	.	.	Oui
6	Oui	Non	Oui	lamellaire	5,25	8,80	.	.	Non
7	Oui	Non	Oui	lamellaire	8,28	12,71	.	.	Oui
8	Oui	Non	Oui	lamellaire	9,36	12,81	.	.	Oui
9	Oui	Non	Non	lamellaire	11,28	.	0,71	.	Non
10	Oui	Non	Non	lamellaire	10,09	.	0,43	.	Non
11	Oui	Non	Oui	lamellaire	12,13	11,21	0,56	0,84	Oui
12	Oui	Non	Oui	lamellaire	10,23	12,31	0,46	0,66	Non
13	Oui	Non	Oui	lamellaire	12,01	13,34	1,05	1,03	Non
14	Oui	Non	Oui	lamellaire	9,16	17,90	0,39	0,96	Oui
15	Oui	Non	Oui	lamellaire	7,76	10,06	0,39	0,77	Oui
16	Oui	Non	Oui	lamellaire	13,11	12,44	.	.	Oui
17	Oui	Non	Oui	lamellaire	23,70	16,31	1,28	1,26	Oui
18	oui	Oui	Oui	Lamellaire + non lamellaire	25,09	18,14	.	.	Oui

Tableau 1 : Caractéristiques histologiques des tori de l'étude

3. Conclusion

Un remodelage osseux asymétrique avec une forte activité ostéogénique ont donc été mis en évidence sur les tori humains. Ceci semble expliquer la forme des tori et leur mode de croissance. Les analyses histochimiques du fer (coloration de Perls) et de l'aluminium (coloration au solochrome azurine) n'ont jamais décelé la présence de ces deux ions dans la matrice osseuse des tori alors qu'ils sont rencontrés dans les 2/3 des exostoses des os longs (41). Les tori apparaissent comme différents des exostoses des os longs et, de plus, ne comportent pas de coiffe cartilagineuse en raison de l'origine embryologique des os mandibulaires et maxillaire (os à modèle mésenchymateux).

ARTICLE 4

Bone mineralization and vascularization in bisphosphonate related osteonecrosis of the jaw: an experimental study in the rat

Jean-Daniel KÜN-DARBOIS, Hélène LIBOUBAN, Guillaume MABILLEAU, Florence PASCARETTI-GRIZON, Daniel CHAPPARD

Clinical Oral Investigation, accepté septembre 2017

Facteur d'impact 2016 : 2,454

L'ostéochimionécrose maxillo-mandibulaire (ONM) est une complication majeure redoutable des médicaments antirésorbeurs tels que les bisphosphonates (BP) et les anticorps monoclonaux (e.g. denosumab). La définition de cette maladie est précise et consensuelle : exposition osseuse clinique du maxillaire ou de la mandibule persistant au moins huit semaines après avoir été constatée une première fois par un médecin chez un patient ayant reçu des médicaments antirésorbeurs et n'ayant pas reçu de radiothérapie de la région cranio-faciale (Fig. 28 et 29) (42).

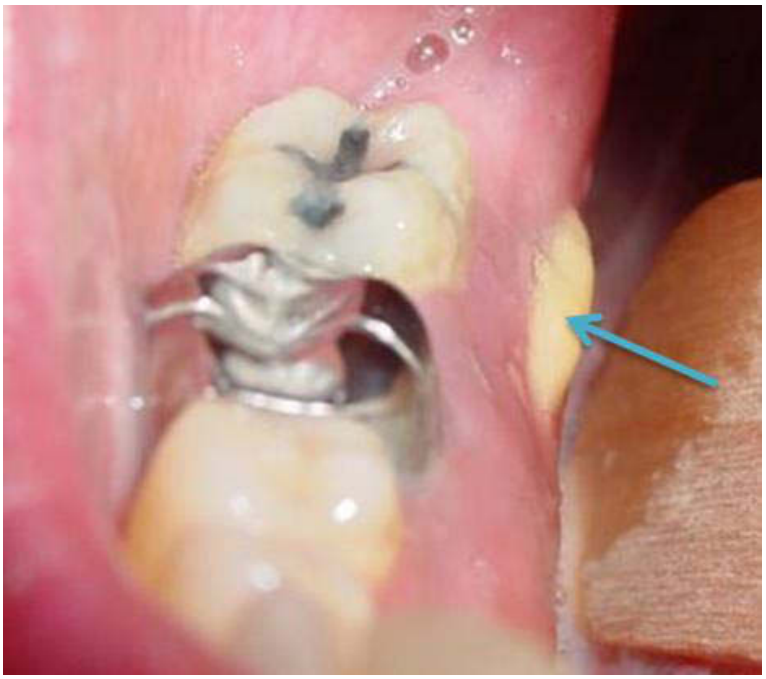


Figure 29 : Vue clinique d'exposition osseuse mandibulaire typique de l'ostéonécrose aux bisphosphonates (flèche)

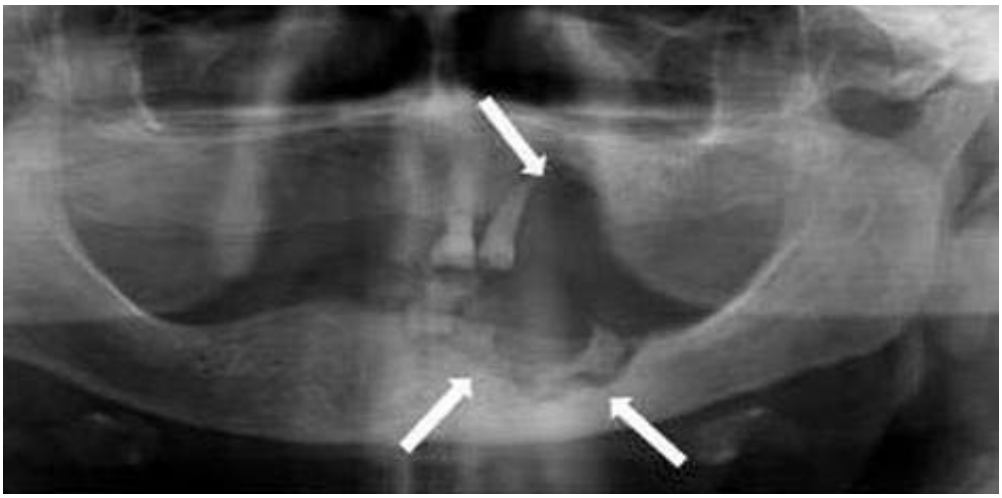


Figure 30 : Images radiologiques d'ostéonécrose : séquestres osseux, zones déminéralisées

La recherche sur le sujet en est encore à un stade précoce car la maladie n'a été décrite pour la première fois qu'en 2003 (43). Il s'agit d'un problème d'importance car l'incidence de cette maladie peut aller jusqu'à 13% dans certains cas de thérapie par BP par voie IV (44). De plus aucun traitement

n'a montré une efficacité réelle à ce jour car même une exérèse chirurgicale a souvent pour effet d'étendre la maladie. Cette maladie peut évoluer vers des complications à type d'extension de la nécrose, de surinfection, de douleurs et de fractures pathologiques.
La physiopathologie n'est pas élucidée à l'heure actuelle mais semble poly-factorielle. Les BP ayant un effet antiangiogénique *in vitro* et *in vivo*, l'hypothèse d'une origine vasculaire a été faite par plusieurs auteurs et pourrait consister en une altération du réseau micovasculaire osseux ce qui entrainerait des lésions ischémiques (45-48). D'autres hypothèses sont également étudiées. Une augmentation de la rigidité osseuse due à une perturbation du remodelage osseux rendant l'os hypodynamique pourrait favoriser l'apparition de micro altérations osseuses (49). Par ailleurs les BP ont une toxicité muqueuse directe par apoptose des cellules épithéliales et pourraient donc entrainer une altération de la couverture osseuse par la muqueuse buccale (50, 51). Ces facteurs pourraient également favoriser des lésions d'ostéomyélite chronique dues à la présence d'une flore buccale potentiellement pathogène (*Actynomyces*) (50, 52)
Cette maladie peut avoir une apparition spontanée ; un facteur déclenchant, le plus souvent une avulsion dentaire, est retrouvé dans environ 70% des cas (53, 54). De plus elle est localisée préférentiellement à la mandibule (70% des cas) (55).

Nos travaux visaient en premier lieu à créer un modèle animal d'ostéonécrose mandibulaire aux bisphosphonates chez le rat. Le second objectif était d'analyser la qualité ainsi que la micro vascularisation osseuses alvéolaires dans ce modèle afin de progresser dans la connaissance de la physiopathologie de cette maladie.

1. Travail préparatoire

Les caractéristiques de notre modèle animal ont été choisies afin de reproduire le plus fidèlement possible la maladie humaine et d'obtenir un taux élevé de lésions ostéonécrotiques. Il a été choisi d'administrer de l'acide zolédronique (ZA) à des doses très élevées qui sont équivalentes aux doses utilisées en clinique humaine chez les patients atteints de myélome et recevant des BP par voie IV (47, 56). C'est en effet dans cette configuration que l'incidence de la maladie est la plus élevée chez l'Homme (44, 57). Pour ces mêmes raisons il a été choisi de pratiquer des avulsions dentaires mandibulaires afin de reproduire le facteur déclenchant la maladie le plus communément.

Le premier travail préparatoire avait pour objectif de pratiquer des avulsions des trois molaires mandibulaires droites de manière stéréotypée et le moins traumatique possible. L'emploi d'une instrumentation spécifique adaptée aux rats a été indispensable (fig. 30).

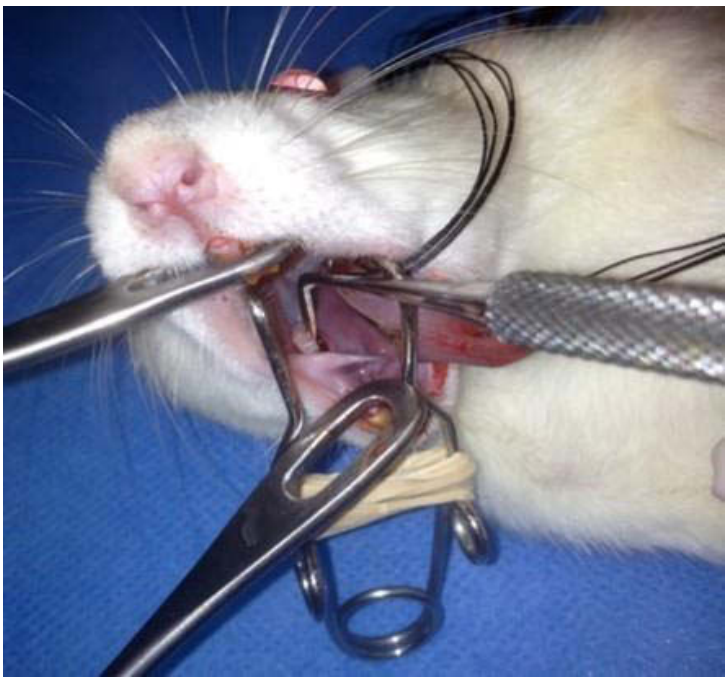


Figure 31 : Utilisation d'instruments spécifiques pour avulsion dentaire chez le rongeur (ici : « pas d'âne », écarteur de joue et syndesmotome)

Un second travail préparatoire a consisté en l'acquisition de la technique d'injection intraveineuse dans une veine caudale chez le rat.

Le dernier travail préparatoire a consisté en la mise au point d'une technique microchirurgicale sous microscope opératoire d'injection de produit de contraste en intra artériel pour opacification du réseau vasculaire mandibulaire. Ces injections ont été effectuées après cathétérisme dans l'artère carotide commune droite (Fig. 31 et 32). Le choix du produit de contraste utilisé a également nécessité plusieurs essais et, après comparaison des résultats obtenus un mélange gélatine et de baryte a été préféré au poly(méthylmétacrylate) initialement utilisé.

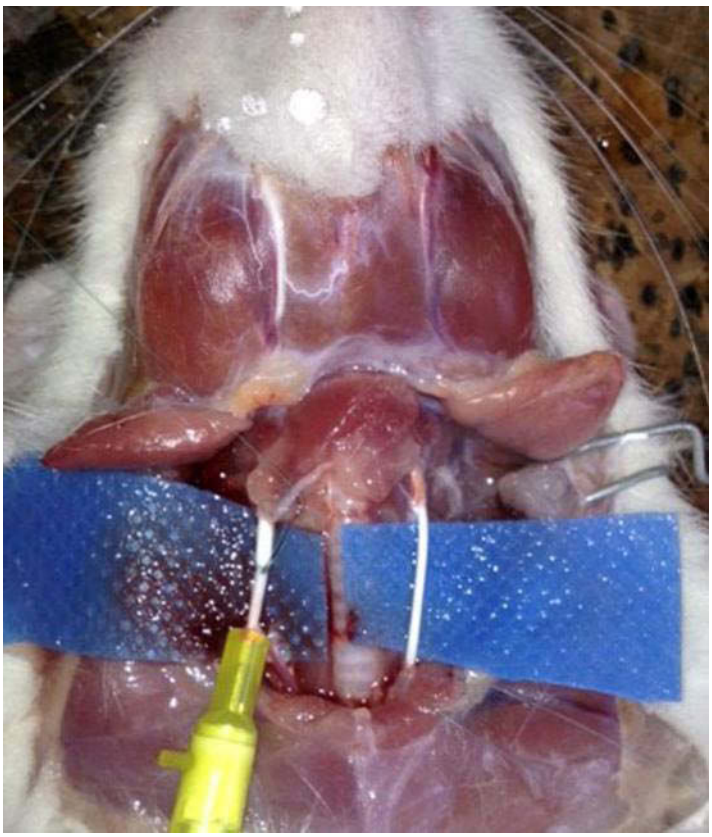


Figure 32 : Injection intracarotidienne par cathétérisme sous microscope opératoire



Figure 33 : Image radiologique d'une tête de rat en vue latérale après injection de produit de contraste

2. Protocole expérimental

Trente-huit rats mâles adultes ont été randomisés en deux groupes : groupe contrôle (CTRL) et groupe ZA. Les rats du groupe ZA ont reçu 10 injections hebdomadaires de ZA (100µg/kg). Les rats du groupe CTRL ont reçu dix injections hebdomadaires équivalentes en volume de sérum physiologique. Tous les rats ont eu l'avulsion des trois molaires mandibulaires droites sous anesthésie générale à l'isoflurane six semaines après le début des injections de ZA (Fig. 33). Les animaux ont été sacrifiés

14 semaines après la première injection. Les animaux ont été séparés en deux groupes différents d'analyse : groupe A (analyse microCT, Raman et qBEI – quantitative backscattered imaging en microscopie électronique à balayage) et groupe B (analyse microCT et analyse vasculaire). Chez les rats du groupe B, une injection intra carotidienne de produit de contraste était réalisée immédiatement après sacrifice.

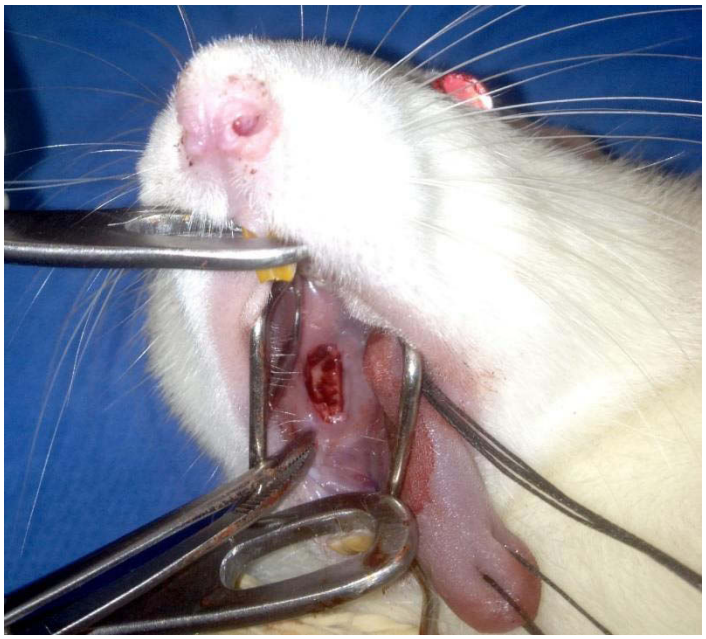


Figure 34 : Vue opératoire après avulsion des trois molaires mandibulaires droites chez un rat

3. Résultats

Une exposition osseuse alvéolaire a été observée au moment du sacrifice chez 55% des rats ZA (Fig. 34). Tous les rats CTRL présentaient en revanche une cicatrisation muqueuse gingivale de bonne qualité sans exposition osseuse.

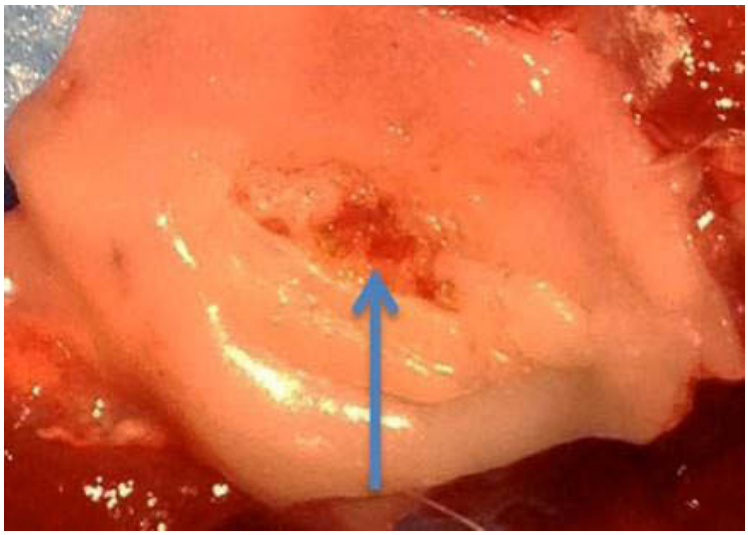


Figure 35 : Image d'exposition osseuse alvéolaire après sacrifice chez un rat ZA

De nombreux éléments radiologiques de l'ONM étaient retrouvés après analyse microCT : lyse corticale, réaction périostée et séquestres osseux de l'os alvéolaire mandibulaire droit des rats ZA. Aucun de ces signes radiologiques n'était retrouvé du côté gauche chez les rats ZA ni chez les rats CTRL.

Les spectres Raman moyens de l'os CTRL, l'os imprégné en ZA et du ZA ont été obtenus. Aucune différence n'a été retrouvée entre les spectres de l'os CTRL ou imprégné de ZA. L'os imprégné en ZA avait un rapport de minéralisation significativement plus élevé que l'os CTRL. En revanche l'analyse qBEI n'a pas montré de différence entre les groupes (Figure 35).

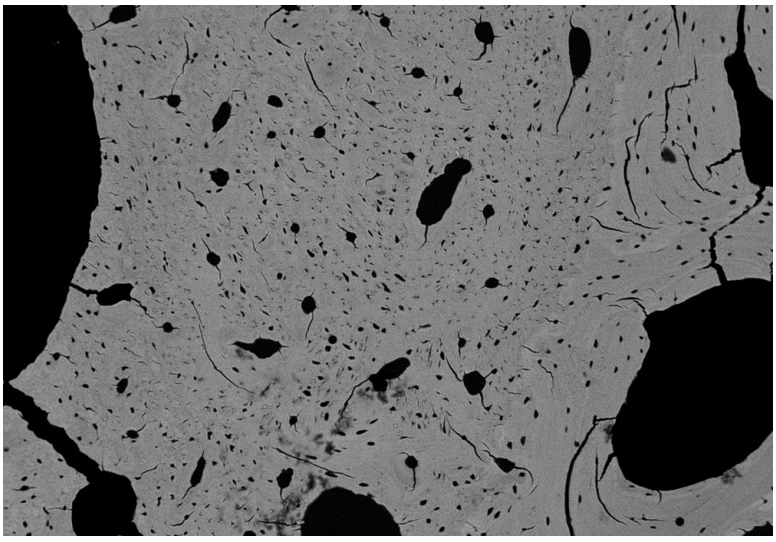


Figure 36 : Exemple d'image de tissu osseux alvéolaire utilisée pour l'analyse qBEI

L'analyse de la micro vascularisation osseuse alvéolaire a permis d'obtenir des images précises du réseau vasculaire et d'y analyser la densité vasculaire et le volume vasculaire total (Fig. 36 et 37). L'artère du pédicule mandibulaire inférieur était bien identifiable et les vaisseaux alvéolaires, très fins, également. La densité vasculaire observée du côté droit (après avulsion dentaire) paraissait augmentée chez les rats CTRL et non chez les rats ZA. Le volume vasculaire alvéolaire total était retrouvé significativement plus élevé du côté droit par rapport au côté gauche dans le groupe CTRL. Il était également significativement plus élevé du côté droit dans le groupe CTRL par rapport au côté droit du groupe ZA.

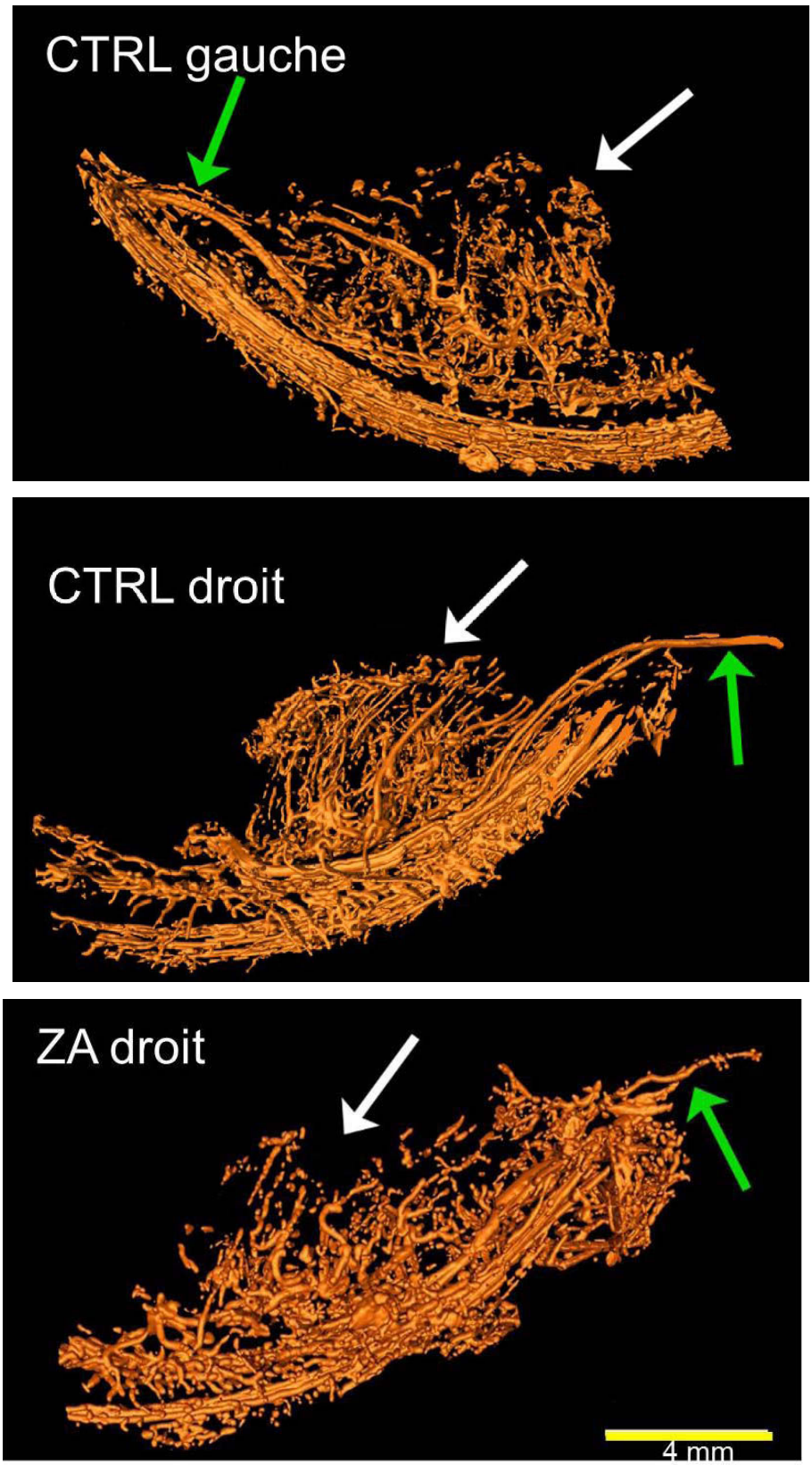


Figure 37 : Artère alvéolaire inférieure (flèches vertes) et microvascularisation alvéolaire (flèches blanches) visibles. La densité vasculaire est augmentée après avulsion dentaire (CTRL droit) et diminuée après avulsion dentaire (ZA droit).

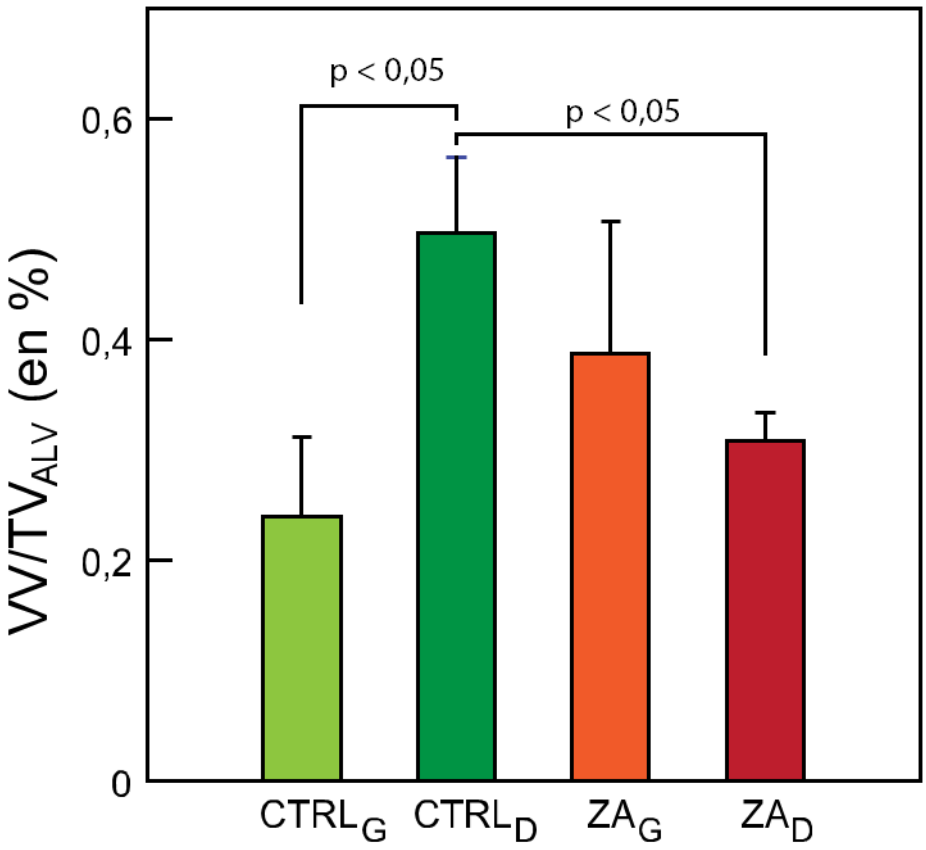


Figure 38 : Volume vasculaire de l'os alvéolaire mesuré en 3D. Montrant un volume plus élevé à droite qu'à gauche dans le groupe CTRL et moins élevé à droite dans le groupe ZA par rapport au même coté dans le groupe CTRL.

4. Conclusion

Le premier objectif de ce travail a été atteint car notre modèle animal reproduisait les éléments caractéristiques de l'ONM humaine chez le rat. De plus ce travail a permis de montrer qu'une imprégnation osseuse en ZA augmentait le degré de minéralisation de la matrice osseuse, rendant celle-ci probablement plus rigide. L'analyse vasculaire a permis de montrer une augmentation de la densité vasculaire réactionnelle à une extraction dentaire dans l'os normal. Cette augmentation de vascularisation n'est pas retrouvée dans un os imprégné en BP. En revanche l'imprégnation en BP n'entraine pas, à elle seule sans facteur déclenchant, de diminution de la densité vasculaire de l'os alvéolaire.

Le rôle de l'effet anti-angiogénique des BP dans la physiopathologie de l'ONM se trouve donc renforcée mais elle ne peut expliquer à elle seule la survenue d'ONM. Dans l'ensemble de causes physiopathologiques de l'ONM, l'effet antiangiogénique des BP semble donc jouer un rôle spécialement en cas de facteur déclenchant tel qu'une extraction dentaire.

De: "Matthias Hannig" <em@editorialmanager.com>
À: "daniel Chappard" <daniel.chappard@univ-angers.fr>
Envoyé: Jeudi 28 Septembre 2017 15:59:12
Objet: CLOI: Your manuscript entitled Bone mineralization and vascularization in bisphosphonate related osteonecrosis of the jaw: an experimental study in the rat

Ref.: Ms. No. CLOI-D-17-00415
Bone mineralization and vascularization in bisphosphonate related osteonecrosis of the jaw: an experimental study in the rat
Clinical Oral Investigations

Dear Prof Chappard,

Meanwhile the comments on your manuscript ID CLOI-D-17-00415 entitled "Bone mineralization and vascularization in bisphosphonate related osteonecrosis of the jaw: an experimental study in the rat" have been submitted. The reviewers' comments can be found at the end of this email or can be accessed by following the provided link.

A number of concerns has been expressed by the reviewers. Please, revise the manuscript accordingly. Please submit together with the revised version a cover letter stating in detail, where and how you have changed the manuscript. Additionally, please highlight in the revised version, where you have made the changes.

This cover letter must have the following format, otherwise the manuscript cannot be further processed:

Reply to reviewer # ....
1. Concern of the reviewer: ......
Our response: ....
Revised text: ..... (if no revised text is regarded to necessary, write: not applicable).
2. concern of the reviewer: ......
Our response: ....
Revised text: ....
3. etc.
Reply to reviewer # ....
1. Concern of the reviewer: ......
etc.

To submit a revision, go to http://cloi.edmgr.com/ and log in as an Author. You will see a menu item called 'Submissions Needing Revision'. You will find your submission record there.

This is your login information:

Your username is: daniel.chappard@univ-angers.fr
If you forgot your password, you can click the 'Send Login Details' link on the EM Login page at http://cloi.edmgr.com/.

You will be unable to make your revisions on the originally submitted version of the manuscript. Instead, revise your manuscript using a word processing program and save it on your computer. Please also highlight the changes to your manuscript within the document by using the track changes
mode in MS Word or by using bold or colored text.

Once the revised manuscript is prepared, you can upload it and submit it through your Author Center.

Please make sure to submit your editable source files (i. e. Word, TeX)

When submitting your revised manuscript, you will be able to respond to the comments made by the reviewer(s) in the space provided. You can use this space to document any changes you make to the original manuscript. In order to expedite the processing of the revised manuscript, please be as specific as possible in your response to the reviewer(s).

IMPORTANT: Your original files are available to you when you upload your revised manuscript. Please delete any redundant files before completing the submission.

Because we are trying to facilitate timely publication of manuscripts submitted to Clinical Oral Investigations, your revised manuscript should be uploaded as soon as possible. If it is not possible for you to submit your revision in two months' time, we may have to consider your paper as a new submission.

Once again, thank you for submitting your manuscript to Clinical Oral Investigations and I look forward to receiving your revision.

Yours sincerely

Matthias Hannig, Univ.-Prof. Dr.
Editor-in-Chief
Clinical Oral Investigations

Reviewers' comments:

Reviewer #1: It is a very well designed and elaborated animal study worth conducting. The methods used are precise and adequate. Unfortunately the results mostly reflect the already known facts on BRONJ. The study focusses on the role of bone remodeling in BRONJ, that do not fully explain the mechanisms of the etiopathogenesis of this disease. Some more aspects of other hypotheses could have been discussed. The animal model is worth to be reported but there are some more models producing reliable BRONJ lesions in rodents.

Figures 2 and 4 can be omitted.

In Figure 8 the selection of statistical significant correlations is unclear. In 4 groups the corresponding groups or the intra-animal groups should be correlated.

Abbreviations should be explained when used the first time (even in the abstract)

CONCLUSION GENERALE ET PERSPECTIVES

 CC BY NC ND

CONCLUSION GENERALE ET PERSPECTIVES

1) Nous avons montré que la toxine botulique injectée dans les muscles masticateurs entrainait une perte osseuse mandibulaire chez le rat sans atteinte de l'épaisseur cartilagineuse condylienne. Elle entraine également l'apparition d'une prolifération osseuse mandibulaire à la corticale linguale.

Une étude clinique est actuellement en cours afin de rechercher si le même phénomène de perte osseuse est également observé chez l'Homme. Le protocole consiste à étudier la texture osseuse mandibulaire alvéolaire avant et après injections de toxine botulique. Les injections sont réalisées en pratique courante pour des indications telles que le bruxisme.

Une diminution de l'épaisseur cartilagineuse condylienne a été cependant décrite dans la littérature chez des animaux en croissance après injection de BTX. La recherche d'une atteinte cartilagineuse condylienne chez l'Homme adulte ou en croissance pourrait faire l'objet de futurs travaux.

La recherche d'un autre type d'atteinte cartilagineuse condylienne chez le rat est également une piste à explorer car nous n'avons ici recherché que des modifications de l'épaisseur du cartilage.

Nous avons décrit au cours de ce travail une nouvelle technique d'analyse vectorielle de la porosité d'un os de forme complexe. Nous avons décrit également une technique nouvelle d'observation du cartilage par microCT grâce à l'utilisation d'acétate d'uranyle comme produit de contraste.

2) Nous avons pu montrer des caractéristiques spécifiques inédites des tori mandibulaires chez l'Homme avec l'observation d'un remodelage osseux asymétrique.

L'hypothèse physiopathologique mécanique de l'origine des tori se trouve confortée par notre travail. Il n'y a cependant, à l'évidence, pas de lien direct entre hyperactivité de muscle digastrique et apparition de tori mandibulaires car la fossette digastrique est située au niveau du rebord basilaire alors que les tori mandibulaires sont situés au niveau de l'os alvéolaire. Les tori pourraient être cependant liés à une augmentation de l'activité musculaire de certains muscles crânio-faciaux. Cette hypothèse est également retrouvée dans la littérature ou la présence de tori est associée à une activité musculaire cranio-faciale augmentée. Elle résulterait en une augmentation de la résistance de la portion d'os mandibulaire concernée. Une relation inversement proportionnelle entre la taille des tori mandibulaires et la gravité de la maladie chez des patients atteints de syndrome d'apnée du sommeil

(SAS) a été décrite. Elle pourrait résulter d'une plus grande activité musculaire des muscles pharyngés et hyoïdiens (58).
Un travail ultérieur pourrait consister en une étude prospective sur une cohorte de patients atteints de SAS afin d'observer la prévalence des tori dans diverses sous populations de ces patients.

3) Nous avons pu décrire un modèle animal pour reproduire l'ostéonécrose mandibulaire aux bisphosphonates.

Nous avons pu montrer que l'effet antiangiogénique *in vitro* des BP pouvait exister *in vivo* et pourrait avoir un rôle dans la physiopathologie de l'ONM en cas d'avulsion dentaire.

Des travaux ultérieurs viseront à réutiliser ce modèle animal d'ONM pour étudier d'autres aspects de la maladie ou effectuer des essais thérapeutiques. Une piste de recherche thérapeutique se trouve ouverte par l'observation de ce rôle anti-angiogénique in vivo des bisphosphonates. Des thérapeutiques pro-angiogéniques pourraient être testées (NO, sildénafil, VEGF, caisson hyperbare).

Nous avons utilisé au cours de ces travaux une nouvelle technique d'analyse microvasculaire par l'utilisation de la gélatine associée à la baryte. Cette technique semble prometteuse pour l'analyse microvasculaire.

REFERENCES

 CC BY NC ND

REFERENCES

1. Evans CH. John Hunter and the origins of modern orthopaedic research. J Orthop Res. 2007;25(4):556-60.
2. Drikes S, Delcampe P, Sabin P, Lavis JF, Cordier G, Vacher C, et al. [Computed tomography study of the lower alveolar intra-mandibular nerve path]. Rev Stomatol Chir Maxillofac. 2008;109(6):358-62.
3. Bras J, de Jonge HK, van Merkesteyn JP. Osteoradionecrosis of the mandible: pathogenesis. Am J Otolaryngol. 1990;11(4):244-50.
4. Bourdiol P, Mioche L. Correlations between functional and occlusal tooth-surface areas and food texture during natural chewing sequences in humans. Arch Oral Biol. 2000;45(8):691-9.
5. Hiiemae K, Heath MR, Heath G, Kazazoglu E, Murray J, Sapper D, et al. Natural bites, food consistency and feeding behaviour in man. Arch Oral Biol. 1996;41(2):175-89.
6. Gibbs CH, Suit SR, Benz ST. Masticatory movements of the jaw measured at angles of approach to the occlusal plane. J Prosthet Dent. 1973;30(3):283-8.
7. Komiyama O, Asano T, Suzuki H, Kawara M, Wada M, Kobayashi K, et al. Mandibular condyle movement during mastication of foods. J Oral Rehabil. 2003;30(6):592-600.
8. Yamada Y, Yamamura K, Inoue M. Coordination of cranial motoneurons during mastication. Respir Physiol Neurobiol. 2005;147(2-3):177-89.
9. Krekeler BN, Connor NP. Age-related changes in mastication are not improved by tongue exercise in a rat model. Laryngoscope. 2017;127(1):E29-E34.
10. Weijs WA, Dantuma R. Electromyography and mechanics of mastication in the albino rat. J Morphol. 1975;146(1):1-33.
11. Thomas NR, Peyton SC. An electromyographic study of mastication in the freely-moving rat. Arch Oral Biol. 1983;28(10):939-45.
12. Chappard D. [Bone modeling and remodeling during osseointegration]. Rev Stomatol Chir Maxillofac Chir Orale. 2013;114(3):159-65.
13. Bodic F, Hamel L, Lerouxel E, Baslé MF, Chappard D. Bone loss and teeth. Joint Bone Spine. 2005;72(3):215-21.
14. Vignery A, Baron R. Dynamic histomorphometry of alveolar bone remodeling in the adult rat. The Anatomical Record. 1980;196(2):191-200.
15. Tighe AP, Schiavo G. Botulinum neurotoxins: mechanism of action. Toxicon. 2013;67:87-93.
16. Bouvard B, Mabilleau G, Legrand E, Audran M, Chappard D. Micro and macroarchitectural changes at the tibia after botulinum toxin injection in the growing rat. Bone. 2012;50(4):858-64.
17. Chappard D, Chennebault A, Moreau M, Legrand E, Audran M, Baslé MF. Texture analysis of X-ray radiographs is a more reliable descriptor of bone loss than mineral content in a rat model of localized disuse induced by the Clostridium botulinum toxin. Bone. 2001;28(1):72-9.
18. Batifol D, de Boutray M, Goudot P, Lorenzo S. Contribution of botulinum toxin to maxillo-facial surgery. Rev Stomatol Chir Maxillofac Chir Orale. 2013;114(2):72-8.
19. Persaud R, Garas G, Silva S, Stamatoglou C, Chatrath P, Patel K. An evidence-based review of botulinum toxin (Botox) applications in non-cosmetic head and neck conditions. JRSM Short Rep. 2013;4(2):10.
20. Chappard D, Stancu IC. Porosity imaged by a vector projection algorithm correlates with fractal dimension measured on 3D models obtained by microCT. J Microsc. 2014;# JMI-2014-0104.
21. Matthys T, Ho Dang HA, Rafferty KL, Herring SW. Bone and cartilage changes in rabbit mandibular condyles after 1 injection of botulinum toxin. Am J Orthod Dentofacial Orthop. 2015;148(6):999-1009.
22. Matthys T, Ho Dang HA, Rafferty KL, Herring SW. Authors' response. Am J Orthod Dentofacial Orthop. 2016;149(4):443-5.
23. Kim JY, Kim ST, Cho SW, Jung HS, Park KT, Son HK. Growth effects of botulinum toxin type A injected into masseter muscle on a developing rat mandible. Oral Dis. 2008;14(7):626-32.

24. Cockman MD, Blanton CA, Chmielewski PA, Dong L, Dufresne TE, Hookfin EB, et al. Quantitative imaging of proteoglycan in cartilage using a gadolinium probe and microCT. Osteoarthritis Cartilage. 2006;14(3):210-4.
25. Das Neves Borges P, Forte AE, Vincent TL, Dini D, Marenzana M. Rapid, automated imaging of mouse articular cartilage by microCT for early detection of osteoarthritis and finite element modelling of joint mechanics. Osteoarthritis Cartilage. 2014;22(10):1419-28.
26. Kerckhofs G, Sainz J, Marechal M, Wevers M, Van de Putte T, Geris L, et al. Contrast-enhanced nanofocus X-ray computed tomography allows virtual three-dimensional histopathology and morphometric analysis of osteoarthritis in small animal models. . Cartilage. 2014;5(1):55-65.
27. Metscher BD. MicroCT for comparative morphology: simple staining methods allow high-contrast 3D imaging of diverse non-mineralized animal tissues. BMC Physiol. 2009;9:11.
28. Nieminen HJ, Ylitalo T, Karhula S, Suuronen JP, Kauppinen S, Serimaa R, et al. Determining collagen distribution in articular cartilage using contrast-enhanced micro-computed tomography. Osteoarthritis Cartilage. 2015;23(9):1613-21.
29. Pauwels E, Van Loo D, Cornillie P, Brabant L, Van Hoorebeke L. An exploratory study of contrast agents for soft tissue visualization by means of high resolution X-ray computed tomography imaging. J Microsc. 2013;250(1):21-31.
30. Renders GA, Mulder L, Lin AS, Langenbach GE, Koolstra JH, Guldberg RE, et al. Contrast-enhanced microCT (EPIC-muCT) ex vivo applied to the mouse and human jaw joint. Dentomaxillofac Radiol. 2014;43(2):20130098.
31. Xie L, Lin AS, Guldberg RE, Levenston ME. Nondestructive assessment of sGAG content and distribution in normal and degraded rat articular cartilage via EPIC-microCT. Osteoarthritis Cartilage. 2010;18(1):65-72.
32. Yoo HJ, Hong SH, Choi JY, Lee IJ, Kim SJ, Choi JA, et al. Contrast-enhanced CT of articular cartilage: experimental study for quantification of glycosaminoglycan content in articular cartilage. Radiology. 2011;261(3):805-12.
33. Garcia-Garcia AS, Martinez-Gonzalez JM, Gomez-Font R, Soto-Rivadeneira A, Oviedo-Roldan L. Current status of the torus palatinus and torus mandibularis. Med Oral Patol Oral Cir Bucal. 2010;15(2):e353-60.
34. Loukas M, Hulsberg P, Tubbs RS, Kapos T, Wartmann CT, Shaffer K, et al. The tori of the mouth and ear: a review. Clin Anat. 2013;26(8):953-60.
35. Ihunwo AO, Phukubye P. The frequency and anatomical features of torus mandibularis in a Black South African population. Homo. 2006;57(4):253-62.
36. Yoshinaka M, Ikebe K, Furuya-Yoshinaka M, Hazeyama T, Maeda Y. Prevalence of torus palatinus among a group of Japanese elderly. J Oral Rehabil. 2010;37(11):848-53.
37. Chossegros C, Foletti JM, Graillon N, Guyot L. [Oral Torus or Torii, why?]. Rev Stomatol Chir Maxillofac Chir Oral. 2016.
38. Yoshinaka M, Ikebe K, Furuya-Yoshinaka M, Maeda Y. Prevalence of torus mandibularis among a group of elderly Japanese and its relationship with occlusal force. Gerodontology. 2014;31(2):117-22.
39. Antoniades DZ, Belazi M, Papanayiotou P. Concurrence of torus palatinus with palatal and buccal exostoses: case report and review of the literature. Oral Surg Oral Med Oral Pathol Oral Radiol Endod. 1998;85(5):552-7.
40. Seah YH. Torus palatinus and torus mandibularis: a review of the literature. Aust Dent J. 1995;40(5):318-21.
41. Chappard D, Mabilleau G, Moukoko D, Henric N, Steiger V, Le Nay P, et al. Aluminum and iron can be deposited in the calcified matrix of bone exostoses. J Inorg Biochem. 2015;152:174-9.
42. Ruggiero SL, Dodson TB, Assael LA, Landesberg R, Marx RE, Mehrotra B, et al. American Association of Oral and Maxillofacial Surgeons position paper on bisphosphonate-related osteonecrosis of the jaws--2009 update. J Oral Maxillofac Surg. 2009;67(5 Suppl):2-12.
43. Marx RE. Pamidronate (Aredia) and zoledronate (Zometa) induced avascular necrosis of the jaws: a growing epidemic. J Oral Maxillofac Surg. 2003;61(9):1115-7.
44. Walter C, Al-Nawas B, Frickhofen N, Gamm H, Beck J, Reinsch L, et al. Prevalence of bisphosphonate associated osteonecrosis of the jaws in multiple myeloma patients. Head Face Med. 2010;6:11.
45. Pabst AM, Ziebart T, Ackermann M, Konerding MA, Walter C. Bisphosphonates' antiangiogenic potency in the development of bisphosphonate-associated osteonecrosis of

the jaws: influence on microvessel sprouting in an in vivo 3D Matrigel assay. Clin Oral Invest. 2013.
46. Petcu EB, Ivanovski S, Wright RG, Slevin M, Miroiu RI, Brinzaniuc K. Bisphosphonate-related osteonecrosis of jaw (BRONJ): an anti-angiogenic side-effect? Diagnos Pathol. 2012;7:78.
47. Sharma D, Hamlet S, Petcu E, Ivanovski S. Animal models for bisphosphonate-related osteonecrosis of the jaws--an appraisal. Oral Dis. 2013;19(8):747-54.
48. Stresing V, Fournier PG, Bellahcene A, Benzaid I, Monkkonen H, Colombel M, et al. Nitrogen-containing bisphosphonates can inhibit angiogenesis in vivo without the involvement of farnesyl pyrophosphate synthase. Bone. 2011;48(2):259-66.
49. Im G-I, Jeong S-H. Pathogenesis, management and prevention of atypical femoral fractures. J Bone Metab. 2015;22(1):1-8.
50. Rasmusson L, Abtahi J. Bisphosphonate associated osteonecrosis of the jaw: an update on pathophysiology, risk factors, and treatment. Int J Dent. 2014;2014:471035.
51. Reid IR, Bolland MJ, Grey AB. Is bisphosphonate-associated osteonecrosis of the jaw caused by soft tissue toxicity? Bone. 2007;41(3):318-20.
52. Russmueller G, Seemann R, Weiss K, Stadler V, Speiss M, Perisanidis C, et al. The association of medication-related osteonecrosis of the jaw with Actinomyces spp. infection. Sci Rep. 2016;6:31604.
53. Marx RE, Cillo JE, Jr., Ulloa JJ. Oral bisphosphonate-induced osteonecrosis: risk factors, prediction of risk using serum CTX testing, prevention, and treatment. J Oral Maxillofac Surg. 2007;65(12):2397-410.
54. Ruggiero SL, Carlson ER, Assael LA. Comprehensive review of bisphosphonate therapy: implications for the oral and maxillofacial surgery patient. J Oral Maxillofac Surg. 2009;67(5 Suppl):1.
55. Woo SB, Hellstein JW, Kalmar JR. Narrative [corrected] review: bisphosphonates and osteonecrosis of the jaws. Ann Intern Med. 2006;144(10):753-61.
56. Biasotto M, Chiandussi S, Zacchigna S, Moimas S, Dore F, Pozzato G, et al. A novel animal model to study non-spontaneous bisphosphonates osteonecrosis of jaw. J Oral Pathol Med. 2010;39(5):390-6.
57. Bouvard B, Gallois Y, Legrand E, Audran M, Chappard D. Glucocorticoids reduce alveolar and trabecular bone in mice. Joint Bone Spine. 2013;80(1):77-81.
58. Palm E, Franklin KA, Marklund M. Mandibular tori size is related to obstructive sleep apnea and treatment success with an oral appliance. Sleep Breath. 2014;18(2):431-8.

Les schémas anatomiques concernant les rongeurs sont reproduits à partir du livre *Anatomy of the rat* d'Eunice Chace Greene, American Philosophical Society Philadelphia, 1935, Hafner Press.

Les schémas anatomiques concernant l'Homme sont reproduits à partir des livres :

- *Sobotta – Atlas d'anatomie humaine* de R. Putz et R. Pabst, 2000, Editions Médicales Internationales.
- *Précis d'anatomie Clinique de la tête et du cou* de Neil S. Norton , Frank H. Netter et Fabrice Duparc, 2009, Masson.
- *Anatomie Maxillo-faciale*, de G. Couly, 1989, Editions CDP

RÉSUMÉ

Un 1er travail a étudié les effets osseux mandibulaires de l'injection unilatérale dans les muscles masticateurs de toxine botulique (BTX) chez le rat adulte. Ceci entraine une perte osseuse mandibulaire condylienne et alvéolaire homolatérale importante. Une hypertrophie osseuse de l'enthèse d'insertion mandibulaire du muscle digastrique a été observée et pourrait correspondre à une étiologie pour les tori.
Les effets de la BTX sur le cartilage articulaire condylien mandibulaire dans le même modèle animal ont été recherchés par analyse microtomographique du cartilage articulaire après augmentation de contraste à l'acétate d'uranyle. Aucune différence d'épaisseur cartilagineuse n'a été mise en évidence entre les groupes contrôles et BTX.
Le 3ème travail a consisté en l'étude histologique et microtomographique des tori mandibulaires chez l'homme. Les tori sont différents des exostoses des os longs par plusieurs caractéristiques (dont l'absence de Fe et Al dans la matrice osseuse) et une asymétrie du remodelage osseux a été mise en évidence.
La 4ème partie a consisté en l'étude de la qualité osseuse et de la microvascularisation alvéolaire dans un modèle animal d'ostéonécrose mandibulaire (ONM) aux bisphosphonates (BP). Des signes cliniques et microtomographiques d'ONM ont été observés dans la majorité des cas. La minéralisation osseuse était plus élevée après imprégnation en BP. La microvascularisation osseuse alvéolaire apparaissait augmentée après avulsion dentaire chez les animaux contrôles mais pas chez les animaux ayant reçu des BP témoignant ainsi d'un effet antiangiogénique in vivo des BP qui pourrait jouer un rôle dans la physiopathologie de l'ONM.

mots-clés : Remodelage osseux, Toxine botulique, Torus mandibularis, Remodelage asymétrique, Microtomographie, Bisphosphonates, Ostéonécrose, Microvascularisation.

ABSTRACT

First, bone changes at the mandible were studied after a unilateral botulinum toxin (BTX) injection in masticatory muscles in adult rats. A major alveolar and condylar bone loss was evidenced. The occurrence of a hypertrophic bone metaplasia at the digastric muscle enthesis was evidenced as well. This could constitute an etiological factor for tori.
Then, condylar articular cartilage changes at the mandible were studied in the same BTX animal model, using microtomography after contrast enhancement of cartilage with uranyl acetate. Cartilage thickness measurement showed no difference when comparing control and BTX groups.
A third work studied mandibular tori in human using histologic and microtomographic techniques. Tori appeared different from long bone exostoses by several characteristics (absence of Fe and Al in the bone matrix) and a specific asymmetric bone remodeling was evidenced.
The fourth part consisted in the study of alveolar mandibular vascularization and quality of the bone matrix in an animal model of osteonecrosis of the jaws (ONJ) after bisphosphonates (BP) injections. Clinical and microtomographic signs of ONJ were found in most of the cases. An increased mineralization of the alveolar bone was observed after BP impregnation. Microvascularization was increased after tooth extraction in the alveolar bone of control animals but it was impaired in ZA treated rats. Such an in vivo antiangiogenic effect of BPs could play a role in the pathophysiology of ONJ.

keywords : Bone remodeling, Botulinum toxin, Torus mandibularis, Asymmetric bone remodeling, Microtomography, Bisphosphonates, Osteonecrosis, Microvascularization

Présidence de l'université
40 rue de rennes – BP 73532
49035 Angers cedex
Tél. 02 41 96 23 23 | Fax 02 41 96 23 00

ENGAGEMENT DE NON PLAGIAT

Je, soussigné(e)
déclare être pleinement conscient(e) que le plagiat de documents ou d'une partie d'un document publiée sur toutes formes de support, y compris l'internet, constitue une violation des droits d'auteur ainsi qu'une fraude caractérisée.
En conséquence, je m'engage à citer toutes les sources que j'ai utilisées pour écrire ce rapport ou mémoire.

signé par l'étudiant(e) le …….23/10/2017……..



Cet engagement de non plagiat doit être signé et joint à tous les rapports, dossiers, mémoires.

Présidence de l'université
40 rue de rennes – BP 73532
49035 Angers cedex

Bone 77 (2015) 75–82

Contents lists available at ScienceDirect

Bone

journal homepage: www.elsevier.com/locate/bone

Original Full Length Article

Botulinum toxin in masticatory muscles of the adult rat induces bone loss at the condyle and alveolar regions of the mandible associated with a bone proliferation at a muscle enthesis

Jean-Daniel Kün-Darbois [a,b], Hélène Libouban [a], Daniel Chappard [a,*]

[a] GEROM Groupe d'Etude Remodelage Osseux et bioMatériaux, LHEA, IRIS-IBS Institut de Biologie en Santé, LUNAM Université, CHU d'Angers, 4, rue Larrey, 49933 Angers Cedex, France
[b] Service de chirurgie maxillo-faciale et stomatologie, CHU d'Angers, 4, rue Larrey, 49933 Angers Cedex, France

ARTICLE INFO

Article history:
Received 23 November 2014
Revised 29 March 2015
Accepted 31 March 2015
Available online 7 April 2015

Edited by David Fyhrie

Keywords:
Botulinum toxin
Mandible
Disuse osteoporosis
Masticatory muscles
Torus mandibularis

ABSTRACT

In man, botulinum toxin type A (BTX) is injected in masticatory muscles for several indications such as trismus, bruxism, or masseter hypertrophy. Bone changes in the mandible following BTX injections in adult animal have therefore became a subject of interest. The aim of this study was to analyze condylar and alveolar bone changes following BTX unilateral injections in masseter and temporal muscles in adult rats. Mature male rats ($n = 15$) were randomized into 2 groups: control (CTRL; $n = 6$) and BTX group ($n = 9$). Rats of the BTX group received a single injection of BTX into right masseter and temporal muscles. Rats of the CTRL group were similarly injected with saline solution. Rats were sacrificed 4 weeks after injections. Masticatory muscles examination and microcomputed tomography (microCT) were performed. A significant difference of weight was found between the 2 groups at weeks 2, 3 and 4 ($p < 0.05$). Atrophy of the right masseter and temporal muscles was observed in all BTX rats. MicroCT analysis showed significant bone loss in the right alveolar and condylar areas in BTX rats. Decrease in bone volume reached −20% for right alveolar bone and −35% for right condylar bone. A hypertrophic bone metaplasia at the digastric muscle enthesis was found on every right hemimandible in the BTX group and none in the CTRL group. BTX injection in masticatory muscles leads to a significant and major mandible bone loss. These alterations can represent a risk factor for fractures in human. The occurrence of a hypertrophic bone metaplasia at the *Mus Digastricus* enthesis may constitute an etiological factor for tori.

© 2015 Elsevier Inc. All rights reserved.

Introduction

Type A botulinum toxin (BTX) is a bacterial metalloprotease produced by *Clostridium botulinum*. It is a neurotoxin that causes specific inhibition of the neurotransmitter release in cholinergic nerve terminals. Acetylcholine vesicles are blocked at the presynaptic membrane of neuromuscular junctions because BTX degrades the SNAP-25 protein required for vesicle fusion and release of acetylcholine at the axon end [1]. This leads to a transient muscle paralysis which is fully reversible in a few months [1–3]. BTX injection in the *Mus Quadriceps femoris* of rodents is now well-known to create a model of tibial and femoral bone loss by immobilization which is easily quantified by reduction of the trabecular bone volume and cortical thickness [4–6].

In human, BTX injections are used in masticatory muscles (*Mus Masseter* and/or *Mus Temporalis*) for several indications such as trismus, bruxism, masticatory myalgia, temporomandibular joint disorders or masseter hypertrophy [7–10]. It is also used in facial injections (subcutaneous, intraglandular or intramuscular); the main indications being sialorrhoea, blepharospasm, hemifacial spasm and aesthetic use [7,8,11]. There are level 1 or 2 evidences supporting the efficacy of BTX in many of those treatments [7,12]. Repeated injections are needed in many indications. Side effects are rare and reversible: non-desirable focal facial muscle paralysis by toxin diffusion and complications at the injection site (bruising, pain, and edema) [13–16].

The mandible is a non-weight bearing bone which is stimulated by masticatory muscles. It is composed of alveolar and basal bone. Teeth roots are anchored into alveolar bone by the periodontal ligament. Alveolar bone has a high plasticity and is remodeled at a high rate. Its mechanical stimulation during mastication is essential in keeping the teeth and underlying bone healthy. Loss of teeth leads to an irreversible alveolar bone resorption [17,18]. Alveolar bone loss is also found in several metabolic bone diseases or due to glucocorticoid treatment [19–21]. However, trabecular bone is also present in other parts of the mandible such as the condylar process. Fractures of this area are also observed in clinical practice and may occur in osteoporosis [22,23].

The aim of the present study was to evaluate bone changes following a unilateral BTX injection in the right masseter and temporalis muscles in adult rats. Two areas were selected and analyzed by microcomputed tomography (condylar and alveolar bone) 4 weeks after injection.

* Corresponding author at: GEROM-LHEA, IRIS-IBS, CHU d'Angers, 49933 Angers Cedex, France. Fax: + 33 244 68 84 51.
E-mail address: daniel.chappard@univ-angers.fr (D. Chappard).

http://dx.doi.org/10.1016/j.bone.2015.03.023
8756-3282/© 2015 Elsevier Inc. All rights reserved.

Material and methods

Animals and experimental procedure

Eighteen week-old male Sprague–Dawley rats (n = 15), weighing 595 ± 41 g, were used for the study (Janvier-Labs, Le Genest-Saint-Isle, France). They were acclimated for two weeks to the local vivarium conditions (24 °C and 12 h/12 h light dark cycle) where they were given standard laboratory food (UAR, Villemoison-sur-Orge, France) and water ad libitum. Rats were randomized into 2 groups: control group (CTRL, n = 6) and BTX-injected group (BTX, n = 9). Rats from the BTX group were anesthetized with isoflurane and injected intramuscularly with 2U of type A BTX: 1 U in 0.2 ml in the *Mus Masseter* and 1 U (in 0.2Ml) in the *Mus Temporalis* (Botox®, Allergan Inc., Irvine, CA, USA). Three points of injections for each *Mus Masseter* and two for each *Mus Temporalis* were necessary. Rats of the CTRL group were similarly injected with equivalent volume of saline solution. Rats were weighted weekly and were sacrificed 4 weeks after injection by CO_2 inhalation. Facial skin was carefully dissected and removed to perform visual examination of right and left masticatory muscles. Hemimandibles were then dissected, defleshed and fixed in formalin until use.

Animal care and experimental protocols were approved by the French Ministry of Research and were done in accordance with the institutional guidelines of the French Ethical Committee (protocol agreement number 01732.01) and under the supervision of authorized investigators.

Microcomputed tomography (microCT)

MicroCT of right and left hemimandibles was performed using a Skyscan 1172 X-ray computerized microtomograph (Bruker microCT, Kontich, Belgium) equipped with an X-ray tube working at 70 kV/100 μA. Bones were placed in plastic tubes filled with water to prevent desiccation. The tubes were fixed on a brass stub with plasticine. Analysis was done with a pixel size corresponding to 10.5 μm; the rotation step was fixed at 0.25° with a 0.5 mm aluminum filter. For each hemimandible, a stack of 2D-sections was obtained and reconstructed using NRecon software (Bruker) and analyzed with CTan software (Skyscan, release 1.13.11.0). Frontal and sagittal sections of alveolar regions and frontal sections of condylar regions were then obtained from 3D models to perform measurements.

Alveolar bone measurements

Because the amount of alveolar and condylar bone is very limited in rodents, measurement of the trabecular bone volume could not be done in 3D and its equivalent (fraction of the tissue area occupied by trabecular bone — B.Ar/T.Ar, expressed in %), was obtained on 2D sections as previously reported [19]. Measurement of B.Ar/T.Ar was done on sections of right and left hemimandibles using ImageJ 1.49c software. Condylar B.Ar/T.Ar was measured using 10 serial frontal sections obtained in the middle of the condylar head (Fig. 1A). Alveolar B.Ar/T.Ar was measured using 5 frontal sections and 1 sagittal section of alveolar region (Figs. 1B–C). Measurements were averaged for each bone.

Cortical bone measurements

Measurements of the mandibular cortical thickness were performed on 2D frontal sections of the right and left hemimandibles (taking the distal root of the first molar as a reference point) using CTan. Eight measures were done (4 for the lingual side and 4 for the vestibular side) and averaged to provide the lingual (LCt.Th, in μm) and vestibular (VCt.Th, in μm) cortical thickness (Fig. 1B).

Analysis of mandibular 3D porosity by a vector projection algorithm

Binarization of stacks of 2D sections was performed using CTan software (Skyscan) and transferred to a lab-made software written in Matlab (Math Works, Natick, MA) release 7.10. The algorithm has been extensively described elsewhere [24]. Briefly, on the binarized images, porosity was visible in white and bone in black. For each binarized image of the stack, the pores which belong to the same image column received the same pseudo-color according to a look up table (LUT). The same color was applied on the image boundary and on a frontal plane image which was constructed line by line from all images of the microCT stack. A 3D model was reconstructed from the subsequent colorized images with VG Studiomax (Volume Graphics GmbH, Heidelberg, Germany). The frontal plane image was saved with the colorized LUT and analyzed by the FracLab plug-in module developed for ImageJ, to obtain the box plot fractal dimension D_f (of the frontal plane image) [25,26].

Histology

Osteotomy of the hemimandibles was performed in order to isolate the molar area. Samples were then decalcified using Decalcifier II® (Surgipath®, Leica Biosystems, Richmond Inc., USA) during 8 days. The specimens were embedded in paraffin. Serial frontal sections were performed (6 μm in thickness) and stained with HPS (hematoxylin, phloxine saffron).

Statistical analysis

Statistical analysis was performed using the Systat statistical software release 13.0 (Systat Software Inc., San Jose, CA). All data were expressed as mean ± standard error of the mean (SEM). Differences among groups were analyzed by a non-parametric ANOVA (Kruskall–Wallis) and between groups by the Mann and Whitney's *U* test. Data

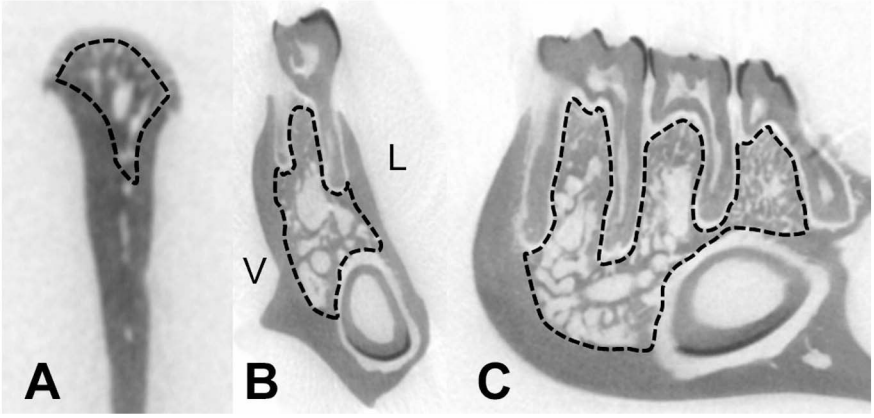


Fig. 1. Regions of interest (outlined areas) used to measure trabecular bone volume on 2D sections of the mandible obtained by microCT.

from right and left hemimandibles were compared using a paired *t*-test. Differences were considered significant when $p < 0.05$.

Results

Body weight and anatomic muscle examination

No significant difference in body weight was found within each group during the time course of the study. However, a significant difference was found between the 2 groups at weeks 2, 3 and 4 ($p < 0.05$) (Fig. 2). The weight loss was −15 ± 11.17 g (i.e. −2.5% of initial weight) in the BTX group. All rats of the BTX group presented a masseter and temporal amyotrophy at the injected side (Fig. 3). No differences were noticed in the CTRL group.

MicroCT analysis of bone effects of BTX injection

Bone loss was clearly seen on the right side of alveolar bone in the BTX group with less trabeculae and wider marrow cavity (Figs. 4A–B). No difference was noted when comparing both sides of the CTRL group. Trabecular bone loss was also clearly seen on the right side of condylar bone in the BTX group (Figs. 4C–D) with a reduced trabecular density. No differences were noted when comparing both sides of the CTRL group.

Of considerable interest was the occurrence of a hypertrophic bone proliferation at the enthesis of *Mus Digastricus* on the right hemimandible. This proliferation was observed in every rats of the BTX group but was not encountered on the non-paralyzed left side (Figs. 4B and 5B). No such proliferation occurred in the CTRL group. These bony proliferations appeared composed of thin trabeculae which evocated a bone metaplasia.

MicroCT measurements are summarized in Table 1. A marked decrease in alveolar B.Ar/T.Ar (reaching −20%) was observed at the right vs. left hemimandible ($p < 0.0001$) in the BTX group. Similarly, a −35% reduction in condylar B.Ar/T.Ar occurred at the right vs. left hemimandible ($p < 0.0001$). The BTX group had a significantly lower condylar B.Ar/T.Ar and alveolar B.Ar/T.Ar at the right side compared to the CTRL group ($p < 0.05$). There were no significant differences between left sides of the BTX group and both sides of the CTRL groups for all parameters.

Cortical bone thickness was not significantly reduced on the right side of the BTX group at both lingual and vestibular sites.

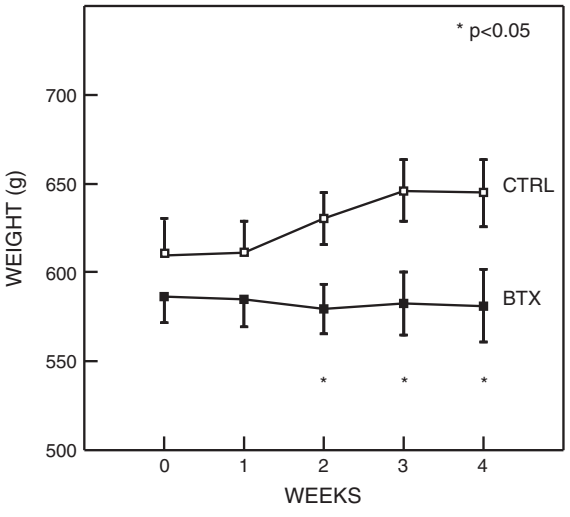


Fig. 2. Evolution of the body weight of rats showing significant differences between groups at weeks 2, 3 and 4.

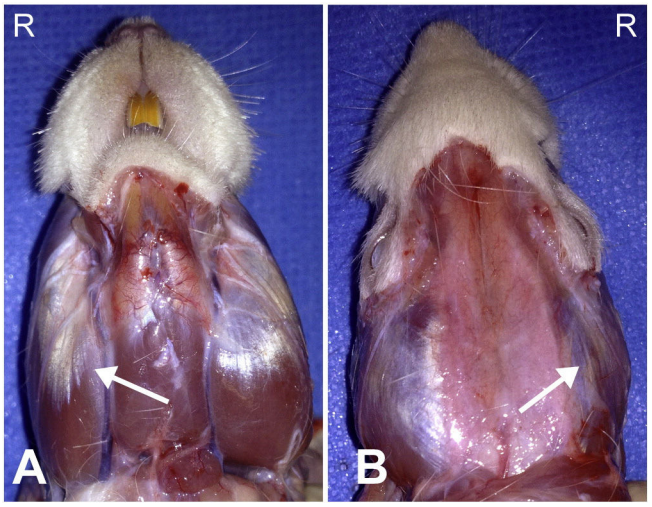


Fig. 3. Macroscopic aspect of muscles after BTX injections; A) in the right *Mus Masseter* (bottom view, arrow); B) in the right *Mus Temporalis* (upper view, arrow).

Analysis of mandibular porosity by vector analysis

Porosity could be well evidenced on the frontal plane and at the surface of the 3D models (Figs. 5C–D). The most porous areas appeared as red-orange and yellow areas (hot colors) while the blue areas indicate a low porosity according to the LUT selected. The area comprising the roots and the alveolar bone was selected by hand drawing of a ROI on the frontal plane images. The lower limit corresponded to the upper part of the incisor socket. No difference was noted morphological between the left and right side in the CTRL group. On the other hand, the amount of hot areas was increased on the right side of BTX group. Quantitative analysis confirmed that D_f was significantly increased in the BTX right side versus the left side and also versus the CTRL sides ($p < 0.02$) (Table 1).

Histological analysis

Study of the hypertrophic bone proliferation at the enthesis of Mus *Digastricus* evidenced bone metaplasia with woven bone in active remodeling. Numerous osteoblast alignments were seen together with large osteoclasts (Fig. 6). Fibers of the digastric muscle were seen anchored at the surface of this bony proliferation. The separation between normal cortical bone and woven bone was clearly identified. Cortical bone appeared made of lamellar bone in CTRL group. (See Fig. 7.)

Discussion

The present study was designed to determine the effect of motor denervation induced by *Clostridium botulinum* toxin serotype A on the mandibular bone of the rat. In our study, amyotrophy was anatomically evidenced by the naked eye and no attempt was done to quantify muscle loss after dissection. Amyotrophy after BTX injection has been reported in a large number of papers [4,27–31]. It is due to a complete motor denervation starting between 2 and 5 days after injection; paralysis is reversible in 4 to 6 weeks. BTX injection is known to reduce the thickness and weight of muscles [32]. It is likely that the failure to gain weight in BTX rats did not reflect the amyotrophy of *Mus Masseter* and *Mus Temporalis* but was provoked by a slightly reduced food intake due to difficulty in chewing.

Condylar and molar areas of the injected side are under-loaded after BTX injections [27]. Although the gain (or loss) of body weight was not significant in each group, the weight loss reached −2.5% of initial weight in the BTX group and differences with the CTRL group became significant after 2 weeks. This indicates that animals did not suffer

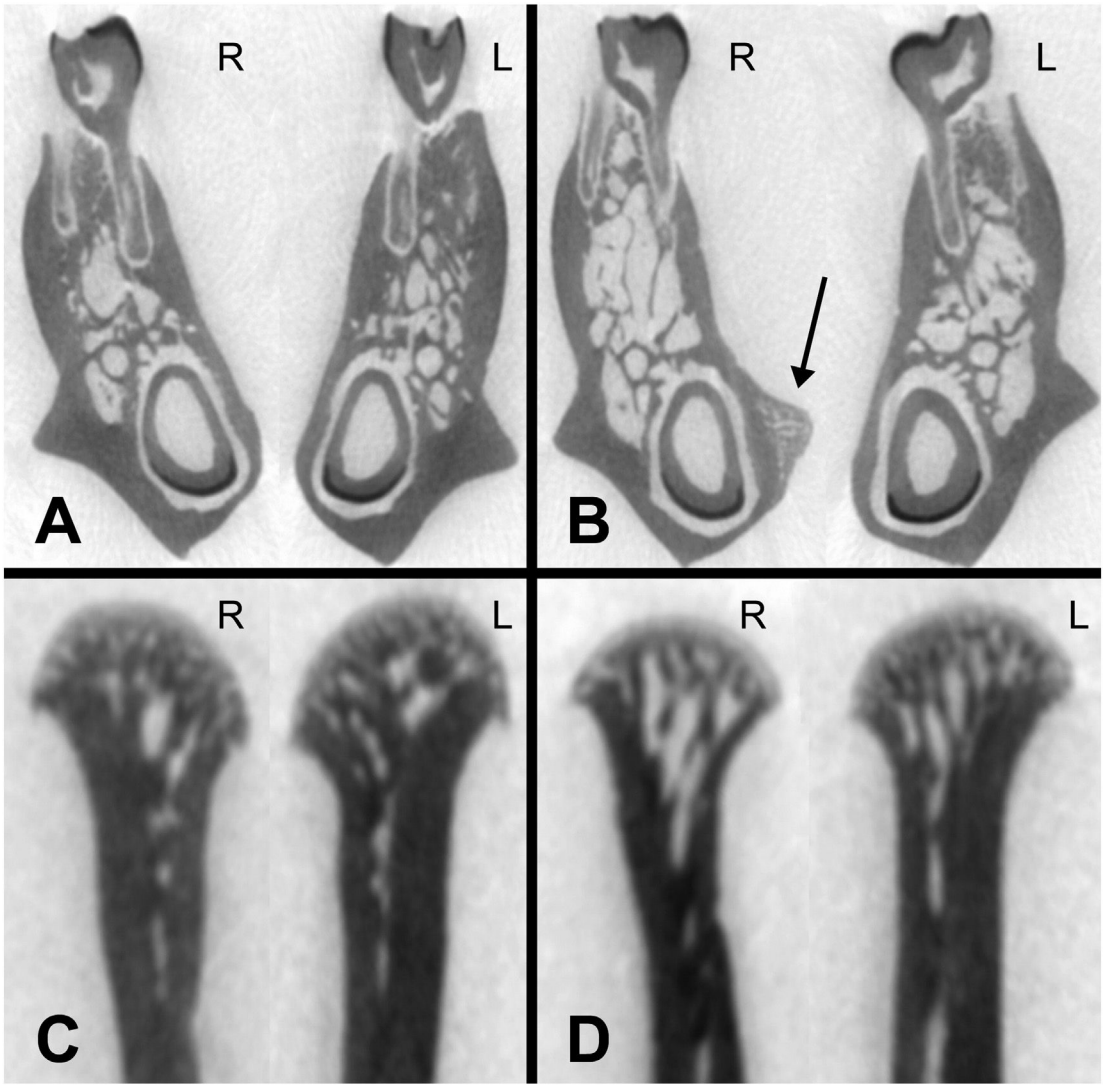


Fig. 4. MicroCT analysis of bone loss as seen on 2D sections: A) Frontal sections of right (R) and left (L) hemimandibles in a rat of the CTRL group showing no difference at the alveolar bone and at the right *Mus Digastricus* enthesis. B) Frontal sections of right (R) and left (L) hemimandibles in a rat of the BTX group. Note the alveolar bone loss on the right side and the occurrence of a hypertrophic bone proliferation at the *Mus Digastricus* enthesis (arrow). C) Frontal sections of the mandibular condylar heads in a rat of the CTRL group showing no difference between each side. D) Frontal sections of the mandibular condylar heads in a rat of the BTX group showing a marked trabecular bone loss. For each image R and L identify respectively the right, and the left side.

from food starvation after BTX injection. Surprisingly, weight loss has not been reported in other studies with unilateral or even bilateral BTX injections in *Mus Masseter* and/or *Mus Temporalis* in growing or adult animals (rats or rabbits) [27–31,33]. Rabbits are reported to keep chewing at an unaltered rate despite a significant functional deficit of injected muscles [27]. Injection of BTX in other types of muscle (such as the *Mus Quadriceps femoris*) did not affect the body weight [6,34], so the effect noted in the present study appears specific to the site of injection. In rabbits with BTX injections in right *Mus Masseter*, the muscle was found significantly 15–18% lighter than the contralateral muscle and *Mus Pterygoideus medialis* of the non-injected side was found significantly 25% heavier than contralateral muscles, this tends to indicate a compensatory mechanism [27,29]. In growing rats with bilateral BTX injections and muscle volume measurements by plethysmometry, the injected masseter volume was found 31% lower if injected alone and 47% lower if *Mus Temporalis* was injected at the same time [28]. In human, it has been shown that *Mus Masseter* loses 30% of its volume 3 months after a BTX injection [35].

In the present study, 1 U of BTX was injected in the 2 main masticatory muscles on the right side. We chose to use 3 points of injection in the *Mus Masseter* and 2 points of injection in the *Mus Temporalis* to ensure complete diffusion in the entire muscle; this is similar to BTX injection in humans for clinical purposes. We chose an injection volume of 0.2 ml for 1 U of BTX. In human, the dilution of BTX is 5 U in 0.2 ml of saline and usually 30 to 50 U are injected per each masticatory muscle. We chose to use 1 U of BTX per each muscle and a less concentrated solution because of the smaller muscle volume in rats compared to humans. One of the main interests of the BTX model is that the paralyzed side can be compared with the contralateral side; in other words, the animal is its own control [5,34]. In the literature, the doses used are comprised between 1 and 7.5 U per masticatory muscle in the rat, with comparable results [27–31,33].

In order to assess bone loss, microCT and subsequent image analysis treatments were used. Mandibular bone mineral density by dual energy X-ray densitometry was not measured in the present study because the method is not reliable and reproducible enough at the mandible with devices available for clinical purposes, even with the use of software for small animals [6,36]. In the present study, a major decrease of B.Ar/T.Ar was found at condylar and alveolar bone. However, due to the complexity of the alveolar region (presence of the molar roots, proximity of the incisor), it was not possible to determine a volume of interest in 3D with the technique offered by the software provided by

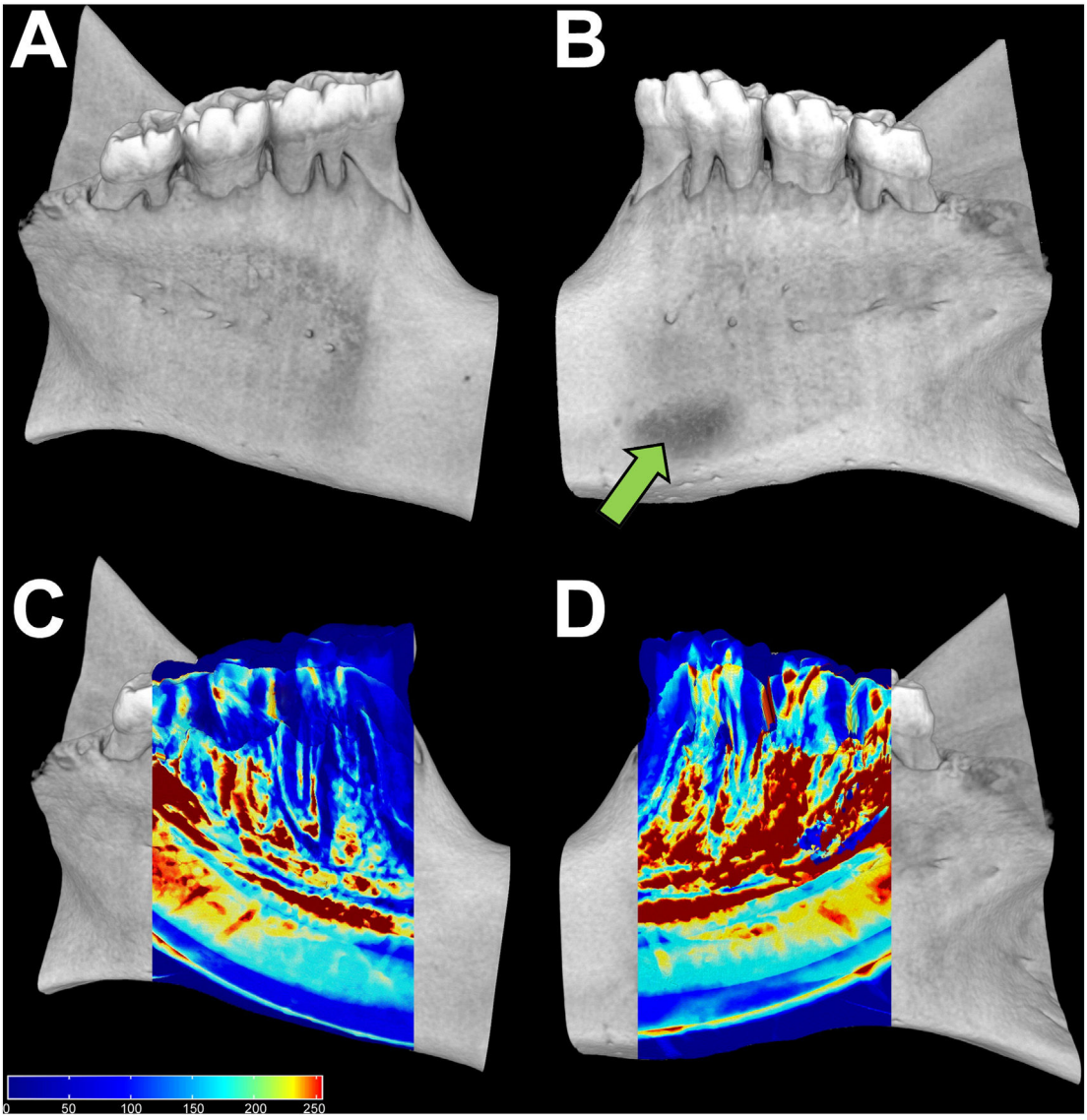


Fig. 5. MicroCT analysis of the hemimandibles of rat with BTX paralysis of *Mus Masseter* and *Mus Temporalis* on the right side. A) General view from the lingual side of the left hemimandible. B) Similar view of the right hemimandible. The green arrow identifies the hypertrophic bone proliferation at the *Mus Digastricus* enthesis. Analysis of porosity by vector analysis on microCT sections in the molar region of the same bones C) left hemimandible, D) right hemimandible. The red pseudo color of alveolar bone indicates higher bone porosity according to the LUT. Note the considerable increase in hot colors (red–orange–yellow in the alveolar area of the right side. (For interpretation of the references to color in this figure legend, the reader is referred to the web version of this article.)

the microCT manufacturer and the 2D measurements are favored in this location for rodents [19]. Our results fit in well with other studies using BTX injections in masticatory muscles of adult animals [27,31]. In the rabbit, the decrease in alveolar B.Ar/T.Ar reached −6% for the BTX-paralyzed side and −12% for condylar bone vs. control animals; however, the decrease was only −2% for alveolar bone and −9% for condylar bone when compared to the uninjected side [27]. In the present study, bone loss was higher (−20%) for alveolar bone and (−35%) for condylar bone, however, this might reflect differences in morphometric evaluation. A similar decreased B.Ar/T.Ar was reported in an adult rat model with mandibular hypofunction due to a soft diet [37]. The vector projection algorithm used here appeared interesting in the evaluation of the alveolar bone. The method allows evaluation of a complex volume of interest and provides quantitative measurements of the complexity of bone loss in the alveolar area; the roots had no influence on the measurements. We have previously reported that the

Table 1
Bone morphometric parameters.

	CTRL Left	CTRL Right	BTX Left	BTX Right
Alveolar B.Ar/T.Ar (%)	59.66 ± 1.87	58.92 ± 2.85	60.29 ± 1.96	40.27 ± 1.65 [a,b]
Condylar B.Ar/T.Ar (%)	67.32 ± 3.42	66.58 ± 3.81	69.62 ± 1.21	35.22 ± 2.49 [a,b]
LCt.Th (μm)	512 ± 13	494 ± 15	518 ± 19	483 ± 25
VCt.Th (μm)	506 ± 18	518 ± 11	504 ± 19	483 ± 22
D_f frontal plane	1.416 ± 0.010	1.420 ± 0.018	1.419 ± 0.009	1.474 ± 0.009 [a,b]

[a] Indicates a significant difference between the right vs. the left side.
[b] Indicates a significant difference vs. CTRL.

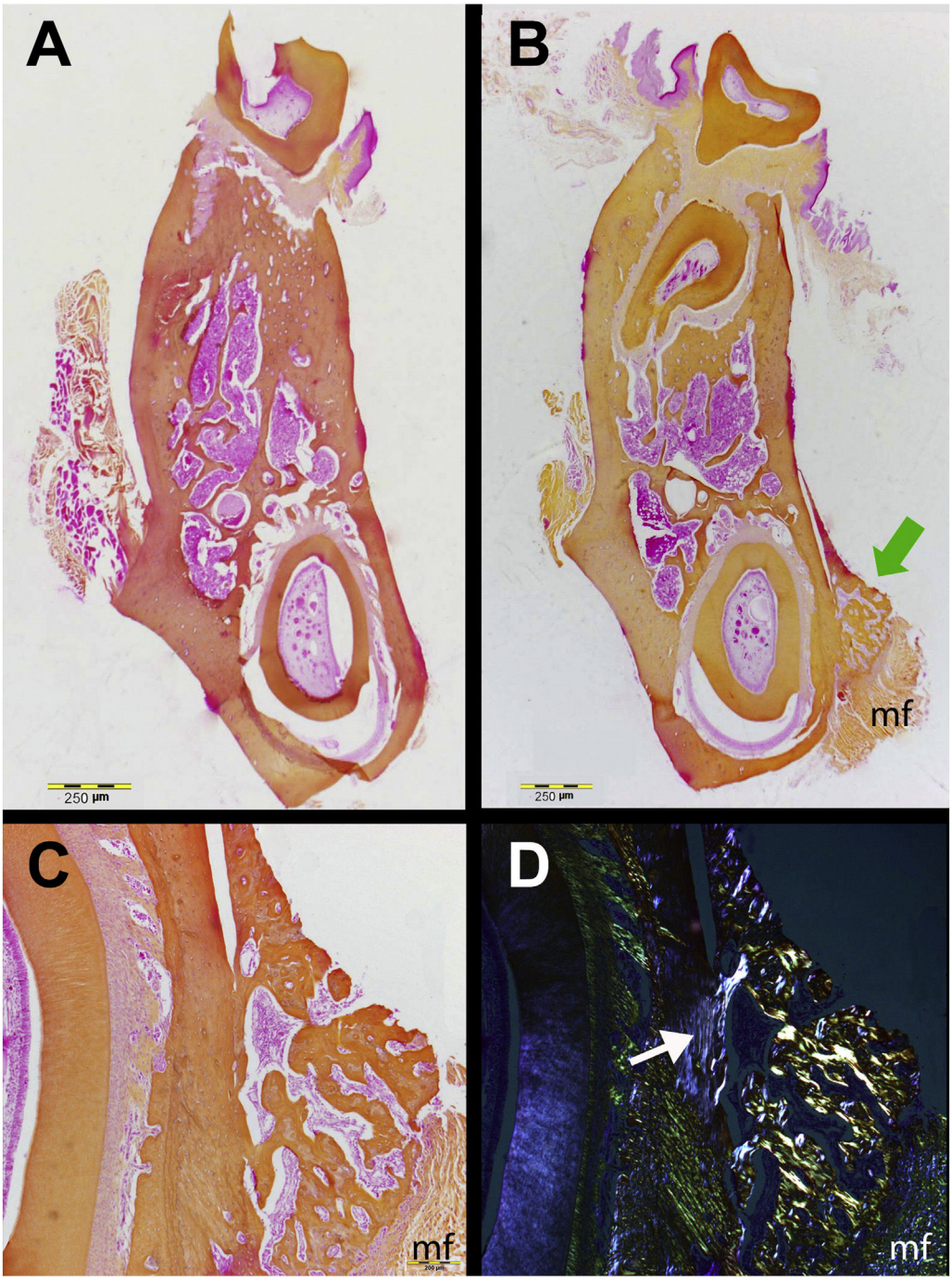


Fig. 6. Histological analysis: A) Frontal section of a right hemimandible from a rat of the CTRL group. B) Frontal section of a right hemimandible from a rat of the BTX group showing the hypertrophic bone proliferation made of metaplastic bone at the *Mus Digastricus* enthesis (green arrow). C) Higher magnification of the bone proliferation showing the woven bone. Fibers of *Mus Digastricus* (mf) are anchored at the surface of the bony proliferation. D) Same section seen in polarized microscopy showing normal cortical bone made of lamellar bone (arrow) while the proliferation is composed of woven bone. (For interpretation of the references to color in this figure legend, the reader is referred to the web version of this article.)

fractal dimension measured on the frontal plane was well correlated with the 3D porosity in an in vitro model [24]. In addition, the method allows a mapping of porosity at the surface of the mandibular bone and evidenced the differences between the right and left sides in these animals.

Masticatory function is significantly decreased in human after BTX injection into masticatory muscles; masticatory efficiency recovers completely after 12 weeks [38]. All these results show the importance of masticatory function on alveolar and condylar bone remodeling and architecture. It is noticeable that in our study, as in others, the percentages of bone loss were higher in condylar bone compared to alveolar bone. This fact seems consistently described. Cortical bone thickness was not significantly reduced in our study whereas it was significantly lower in similar models by others [27,28,31]. A possible explanation could be that this occurred only in growing animals. Another explanation could be differences with other studies in the localization and number of measuring sites of cortical bone. A last explanation is that a 4 weeks endpoint is insufficient to develop a cortical bone loss due to the lower remodeling rate in this bony envelope. Longer studies are necessary to evaluate the cortical bone loss which is an important parameter to assess since it is known that cortical changes increase fracture risk in humans [39].

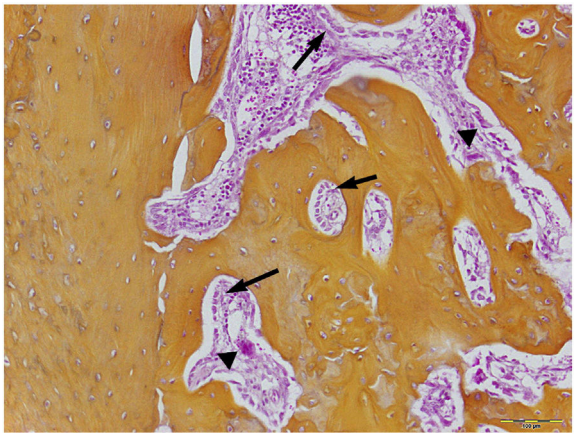


Fig. 7. Histological analysis, higher magnification of the bone proliferation exhibiting an active remodeling with numerous osteoblast alignments (arrows) and active osteoclasts (arrowheads).

A relevant finding was that hypertrophic bone proliferation made of metaplastic bone developed on the paralyzed side at the mandibular *Mus Digastricus* enthesis in every animal of the BTX group. *Mus Digastricus* is an accessory masticatory muscle and a jaw-opener [40]. An increased activity of *Mus Digastricus* on the paralyzed side probably leads to a local increase of mechanical strains at the mandible which compensates the loss of activity of the temporal and masseter muscles. An increased muscle activity is known to stimulate bone remodeling leading to an increased bone mass [41]. It has also been shown that it induces the development of woven bone [42]. In rabbits injected by BTX in *Mus masseter*, a compensating hypertrophy of *Mus Medial pterygoid* (another jaw-closer main masticatory muscle) has been reported [27]. However no such hypertrophic bone metaplasia was reported at the muscle enthesis (the *pterygoid fossa*, on the vestibular side of the mandible) and we also did not find bone changes in this location on our microCT sections. Such a hypertrophic metaplasia mimics a *torus mandibularis*. Although the pathophysiology of tori is not fully understood, a relationship between *tori* and a disequilibrium of occlusal forces is hypothesized [43].

Differences between our model and others of the literature (failure to gain weight in growing animals, more important percentages of bone loss, hypertrophic bone metaplasia) were found. Those bone alterations, if they happened equally in human, could constitute a major risk factor for fractures, especially in patients receiving repeated BTX injections in masticatory muscles. This remains to be studied in human since there are many differences between rat and human masticatory functions (masticatory apparatus, bone volume, dosage of BTX). One single study in the literature reports mandibular bone assessment (cortical thickness, mandibular thickness, and total mandibular volume) following BTX unilateral single injections in masseter in human with no significant change [35]. Furthermore, future works shall aim at assessing bone loss in human receiving those treatments and at assessing minimal periods of time between injections in human in order to avoid potential increased risk fracture.

Conflicts of interest

The authors declare that they have no conflicts of interest concerning this article.

Acknowledgments

Authors are greatly indebted to the SCAHU (Service commun d'animalerie hospitalo-universitaire) of Angers, especially to P. Legras and J. Roux for their help with the animal care. Our vector analysis software (VECTOPOR) is now licensed by the APP (Agence de Protection des Programmes) JDKD IDDN.FR.001.150014.000.S.P.2015.000.10000 received a scholarship from the ARS (Agence Régionale de Santé) "Pays de la Loire".

References

[1] Tighe AP, Schiavo G. Botulinum neurotoxins: mechanism of action. Toxicon 2013;67:87–93.
[2] Poulain B. Molecular mechanism of action of tetanus toxin and botulinum neurotoxins. Pathol Biol 1994;42:173–82.
[3] Rossetto O, Pirazzini M, Bolognese P, Rigoni M, Montecucco C. An update on the mechanism of action of tetanus and botulinum neurotoxins. Acta Chim Slov 2011;58:702–7.
[4] Marchand-Libouban H, Le Drevo MA, Chappard D. Disuse induced by botulinum toxin affects the bone marrow expression profile of bone genes leading to a rapid bone loss. J Musculoskelet Neuronal Interact 2013;13:27–36.
[5] Bouvard B, Mabilleau G, Legrand E, Audran M, Chappard D. Micro and macroarchitectural changes at the tibia after botulinum toxin injection in the growing rat. Bone 2012;50:858–64.
[6] Chappard D, Chennebault A, Moreau M, Legrand E, Audran M, Baslé MF. Texture analysis of X-ray radiographs is a more reliable descriptor of bone loss than mineral content in a rat model of localized disuse induced by the *Clostridium botulinum* toxin. Bone 2001;28:72–9.
[7] Persaud R, Garas G, Silva S, Stamatoglou C, Chatrath P, Patel K. An evidence-based review of botulinum toxin (Botox) applications in non-cosmetic head and neck conditions. JRSM Short Rep 2013;4:10.
[8] Batifol D, de Boutray M, Goudot P, Lorenzo S. Contribution of botulinum toxin to maxillo-facial surgery. Rev Stomatol Chir Maxillofac Chir Orale 2013;114:72–8.
[9] Shim YJ, Lee MK, Kato T, Park HU, Heo K, Kim ST. Effects of botulinum toxin on jaw motor events during sleep in sleep bruxism patients: a polysomnographic evaluation. J Clin Sleep Med 2014;10:291–8.
[10] Sinclair CF, Gurey LE, Blitzer A. Oromandibular dystonia: long-term management with botulinum toxin. Laryngoscope 2013;123:3078–83.
[11] Niamtu III J. Aesthetic uses of botulinum toxin A. J Oral Maxillofac Surg 1999;57:1228–33.
[12] Wheeler A, Smith HS. Botulinum toxins: mechanisms of action, antinociception and clinical applications. Toxicology 2013;306:124–46.
[13] Kim BW, Park G-H, Yun WJ, Rho NK, Jang KA, Won CH, et al. Adverse events associated with botulinum toxin injection: a multidepartment, retrospective study of 5310 treatments administered to 1819 patients. J Dermatolog Treat 2014;25:331–6.
[14] Cavallini M, Cirillo P, Fundaro SP, Quartucci S, Sciuto C, Sito G, et al. Safety of botulinum toxin a in aesthetic treatments: a systematic review of clinical studies. Dermatol Surg 2014;40:525–36.
[15] Cote TR, Mohan AK, Polder JA, Walton MK, Braun MM. Botulinum toxin type A injections: adverse events reported to the US Food and Drug Administration in therapeutic and cosmetic cases. J Am Acad Dermatol 2005;53:407–15.
[16] Wollina U, Konrad H. Managing adverse events associated with botulinum toxin type A: a focus on cosmetic procedures. Am J Clin Dermatol 2005;6:141–50.
[17] Mays S. Resorption of mandibular alveolar bone following loss of molar teeth and its relationship to age at death in a human skeletal population. Am J Phys Anthropol 2014;153:643–52.
[18] Bodic F, Hamel L, Lerouxel E, Baslé MF, Chappard D. Bone loss and teeth. Joint Bone Spine 2005;72:215–21.
[19] Bouvard B, Gallois Y, Legrand E, Audran M, Chappard D. Glucocorticoids reduce alveolar and trabecular bone in mice. Joint Bone Spine 2013;80:77–81.
[20] Barron MJ, McDonnell ST, Mackie I, Dixon MJ. Hereditary dentine disorders: dentinogenesis imperfecta and dentine dysplasia. Orphanet J Rare Dis 2008;3:31.
[21] Padbury Jr AD, Tozum TF, Taba Jr M, Ealba EL, West BT, Burney RE, et al. The impact of primary hyperparathyroidism on the oral cavity. J Clin Endocrinol Metab 2006;91:3439–45.
[22] de Los Aguilera-Barreiro A, Davalos-Vazquez KF, Jimenez-Mendez C, Jimenez-Mendoza D, Olivarez-Padron LA, Rodriguez-Garcia ME. The relationship of nutritional status, body and mandibular bone mineral density, tooth loss and fracture risk (FRAX) in pre- and postmenopausal women with periodontitis. Nutr Hosp 2014;29:1419–26.
[23] Glowacki J. Impact of postmenopausal osteoporosis on the oral and maxillofacial surgery patient. Oral Maxillofac Surg Clin North Am 2007;19:187–98.
[24] Chappard D, Stancu IC. Porosity imaged by a vector projection algorithm correlates with fractal dimension measured on 3D models obtained by microCT. J Microsc 2015;258:24–30.
[25] Karperien A FracLac for ImageJ. http://rsb.info.nih.gov/ij/plugins/fraclac/FLHelp/Introduction.htm Australia: Charles Sturt University; 1999-2013.
[26] Rasband WS ImageJhttp://imagej.nih.gov/ij/ , In: U. S. Ntl Inst. Health, editor. ; 1997-2014 [Bethesda, MA, USA].
[27] Rafferty KL, Liu ZJ, Ye W, Navarrete AL, Nguyen TT, Salamati A, et al. Botulinum toxin in masticatory muscles: short- and long-term effects on muscle, bone, and craniofacial function in adult rabbits. Bone 2012;50:651–62.
[28] Tsai CY, Shyr YM, Chiu WC, Lee CM. Bone changes in the mandible following botulinum neurotoxin injections. Eur J Orthod 2011;33:132–8.
[29] Matic DB, Yazdani A, Wells RG, Lee TY, Gan BS. The effects of masseter muscle paralysis on facial bone growth. J Surg Res 2007;139:243–52.
[30] Tsai CY, Chiu WC, Liao YH, Tsai CM. Effects on craniofacial growth and development of unilateral botulinum neurotoxin injection into the masseter muscle. Am J Orthod Dentofacial Orthop 2009;135:142e1–6 [discussion 42-3].

[31] Tsai CY, Huang RY, Lee CM, Hsiao WT, Yang LY. Morphologic and bony structural changes in the mandible after a unilateral injection of botulinum neurotoxin in adult rats. J Oral Maxillofac Surg 2010;68:1081–7.
[32] Filippi GM, Errico P, Santarelli R, Bagolini B, Manni E. Botulinum A toxin effects on rat jaw muscle spindles. Acta Otolaryngol 1993;113:400–4.
[33] Kim JY, Kim ST, Cho SW, Jung HS, Park KT, Son HK. Growth effects of botulinum toxin type A injected into masseter muscle on a developing rat mandible. Oral Dis 2008; 14:626–32.
[34] Blouin S, Gallois Y, Moreau MF, Baslé MF, Chappard D. Disuse and orchidectomy have additional effects on bone loss in the aged male rat. Osteoporos Int 2007;18: 85–92.
[35] Chang CS, Bergeron L, Yu CC, Chen PKT, Chen YR. Mandible changes evaluated by computed tomography following botulinum toxin A injections in square-faced patients. Aesthetic Plast Surg 2011;35:452–5.
[36] Lerouxel E, Libouban H, Moreau M-F, Baslé MF, Audran M, Chappard D. Mandibular bone loss in an animal model of male osteoporosis (orchidectomized rat): a radiographic and densitometric study. Osteoporos Int 2004;15:814–9.
[37] Mavropoulos A, Odman A, Ammann P, Kiliaridis S. Rehabilitation of masticatory function improves the alveolar bone architecture of the mandible in adult rats. Bone 2010;47:687–92.
[38] Park HU, Kim BI, Kang SM, Kim ST, Choi JH, Ahn HJ. Changes in masticatory function after injection of botulinum toxin type A to masticatory muscles. J Oral Rehabil 2013; 40:916–22.
[39] Jonasson G, Sundh V, Hakeberg M, Hassani-Nejad A, Lissner L, Ahlqwist M. Mandibular bone changes in 24 years and skeletal fracture prediction. Clin Oral Investig 2013;17:565–72.
[40] Norton NS muscles of mastication. Netter's Head and Neck Anatomy for Dentistry. Philadelphia: Elsevier-Saunders; 2012[pp. Chap. 8].
[41] Sugiyama T, Price JS, Lanyon LE. Functional adaptation to mechanical loading in both cortical and cancellous bone is controlled locally and is confined to the loaded bones. Bone 2010;46:314–21.
[42] Sugiyama T, Meakin LB, Browne WJ, Galea GL, Price JS, Lanyon LE. Bones' adaptive response to mechanical loading is essentially linear between the low strains associated with disuse and the high strains associated with the lamellar/woven bone transition. J Bone Miner Res 2012;27:1784–93.
[43] Yoshinaka M, Ikebe K, Furuya-Yoshinaka M, Maeda Y. Prevalence of torus mandibularis among a group of elderly Japanese and its relationship with occlusal force. Gerodontology 2014;31:117–22.

Micron 97 (2017) 35–40

Contents lists available at ScienceDirect

Micron

journal homepage: www.elsevier.com/locate/micron

Contrast enhancement with uranyl acetate allows quantitative analysis of the articular cartilage by microCT: Application to mandibular condyles in the BTX rat model of disuse

Jean-Daniel Kün-Darbois[a,b], Florence Manero[c], Louis Rony[a,d], Daniel Chappard[a,c,*]

[a] GEROM Groupe d'Etude Remodelage Osseux et bioMatériaux, IRIS-IBS Institut de Biologie en Santé, Université d'Angers, CHU d'Angers, 4 rue Larrey, 49933 ANGERS Cedex, France
[b] Service de chirurgie maxillo-faciale et stomatologie, CHU d'Angers, 4 rue Larrey, 49933 ANGERS Cedex, France
[c] SCIAM, Service Commun d'Imagerie et Analyses Microscopiques, IRIS-IBS Institut de Biologie en Santé, Université d'Angers, CHU d'Angers, 4 rue Larrey, 49933 ANGERS Cedex, France
[d] Service de chirurgie orthopédique et traumatologique, CHU d'Angers, 4 rue Larrey, 49933 ANGERS Cedex, France

ARTICLE INFO

Article history:
Received 17 January 2017
Received in revised form 15 March 2017
Accepted 15 March 2017

Keywords:
Botulinum toxin
Uranyl acetate
Soft tissue imaging
MicroCT
Cartilage
Contrast enhancement

ABSTRACT

Microcomputed tomography (microCT) is well adapted to quantitative analysis of calcified tissues but soft tissues (such as cartilage) are radiolucent and need a contrast enhancement procedure for microCT. We developed a "staining" method allowing microCT imaging of articular cartilage using uranyl acetate (UA). The method was used to see whether adult rats with a botulinum toxin (BTX) injection in masticatory muscles present a change at the condylar cartilage of the mandible in association with a localized trabecular bone loss.

Human femoral head samples were used to develop the enhanced contrast method using UA or lanthanides (recently proposed as a substitute for UA). The method was then applied to the condylar cartilage of rat mandibles. Mature male rats ($n = 11$) were randomized into 2 groups: control (CTRL; $n = 4$) and BTX group ($n = 7$). Rats of the BTX group received a single injection of BTX into the right *M. Masseter* and *M. Temporalis*. Rats of the CTRL group were similarly injected with saline. Rats were sacrificed 4 weeks after injection. Condyles were harvested, fixed in formalin and immersed in UA. MicroCT was performed for bone and cartilage measurements.

After UA impregnation, articular cartilage of human femoral head samples was clearly seen on its full thickness whereas lanthanides produced a much less pronounced contrast, with a faint labeling at the upper layer. In BTX rats, microCT analysis showed a significant bone loss at the right condyles. After UA, the whole thickness of articular cartilage was clearly evidenced. Cartilage thickness measurement showed no difference when comparing the right with the left sides of the BTX group nor between the two sides of the CTRL group.

Contrast enhancement with UA is a simple technique allowing quantitative analysis of cartilage by microCT.290 words.

© 2017 Elsevier Ltd. All rights reserved.

1. Introduction

Articular cartilage is a highly specialized connective tissue of synovial joints, it is supported by subchondral bone. Its main function is to provide a smooth articular surface in order to facilitate the transmission of loads with a low frictional coefficient (Sophia Fox et al., 2009). It is made of a dense extracellular matrix composed mainly of water, type II collagen and proteoglycans with specialized cells called chondrocytes. Histology is a commonly used method to analyze articular cartilage in pathologic conditions. The main limitation of the technique is that it is destructive and causes tissue alterations. Furthermore, sample positioning is difficult to reproduce, leading to a different section obliquity for each slide. Microcomputed tomography (microCT) allows high resolution 3D imaging making precise quantitative measurement possible (Ruegsegger, 1994; Sasov and Van Dyck, 1998). This technique is challenging for soft tissue imaging, such as cartilage, because X-ray attenuation of a non-mineralized soft tissue is very low (Naveh et al., 2014). Contrast enhancement using a "staining" procedure is therefore mandatory with the use of various metal salts (Metscher, 2009; Pauwels et al., 2013). Several contrasting

* Corresponding author at: GEROM LHEA, IRIS IBS, CHU d'Angers, 49933 ANGERS Cedex, France.
E-mail address: daniel.chappard@univ-angers.fr (D. Chappard).

http://dx.doi.org/10.1016/j.micron.2017.03.008
0968-4328/© 2017 Elsevier Ltd. All rights reserved.

methods allowing cartilage imaging have been described using iodinated contrasting agents for computed tomography or magnetic resonance imaging (such as ioxaglic acid (Hexabrix®) iopromide (Ultravist®) gadolinium), iodine-potassium iodide (IKI), phosphotungstic acid (PTA), phosphomolybdic acid (PMA), or osmium tetroxide (Cockman et al., 2006; Das Neves Borges et al., 2014; Kerckhofs et al., 2014; Metscher, 2009; Nieminen et al., 2015; Pauwels et al., 2013; Renders et al., 2014; Xie et al., 2010; Yoo et al., 2011). However, none of them were fully reproducible in our hands for contrast enhancement of cartilage imaging in 3D using microCT.

The aim of the present study was to describe a new contrast enhancement technique of cartilage for microCT based on electron microscopy procedures allowing a quantitative analysis of cartilage thickness. The technique was first elaborated on the human hip articular cartilage and then applied in an animal study. We have searched if changes in a thin articular cartilage (*e.g.*, the condylar articular cartilage of the mandible) occur in a pathologic condition. We chose to study the changes induced by botulinum toxin (BTX) injected in masticatory muscles. In animal models, BTX injections cause a muscle atrophy associated with a disuse bone loss (Chappard et al., 2001). Whether disuse also acts on this articular cartilage is largely unknown and a microCT method after contrast enhancement of the cartilage matrix is of great interest.

2. Materials and methods

2.1. Human femoral heads

Femoral heads from patients with a recent trans-cervical hip fracture were used in this study to develop the contrast enhancement technique for articular cartilage. The specimens were cut at the top of the head, in the area of the main compressive bundle of trabeculae. On a first femoral head, four samples were harvested and fixed in 10% formalin for 48 h (Merck KGaA, Darmstadt, Germany) (Carson and Hladik, 2009). The first specimen was included undecalcified in poly(methylmethacrylate) for routine histology. The second sample was imaged by microCT while in the fixative. The second sample was immersed for 48 h in uranyl acetate (UA). UA (Merck) was prepared as a 3% solution in 50° ethanol; the solution was filtered on a 0.2 μm syringe filter and stored at 4 °C in the dark. The "stained" specimen was rinsed during 1 h in running tap water, transferred to 10% formalin and scanned in the fixative. The fourth specimen was stained with a lanthanide solution (LFG Distribution, Lyon, France). It comprised 1% lanthanum acetate, 1% gadolinium acetate and 1% samarium acetate and was prepared in ethanol 50°. The specimen was immersed similarly during 48 h in the lanthanide salts solution, rinsed during one hour in tap water, placed in formalin and scanned as above. Additional trials were done with IKI (1% iodine, 2% potassium iodide), PTA (1.5% in water) and Iopamiron 300® (Bracco Imaging France), a contrasting agent for computed tomography containing 300 mg iodine/ml. These three additional reagents were used on pieces coming from another femoral head.

2.2. Animals and experimental procedure

Animal care and experimental protocols were approved by the French Ethical Committee (protocol agreement number 01732.01) and under the supervision of authorized investigators. Eighteen weeks-old male Sprague-Dawley rats ($n = 11$), weighing 587 ± 26 g, were used for the study (Janvier-Labs, Le Genest-Saint-Isle, France). They were acclimated for two weeks to the local vivarium conditions (24 °C and 12 h/12 h light dark cycle) where they were given standard laboratory food (UAR, Villemoison-sur-Orge, France) and water *ad libitum*. Rats were randomized into 2 groups: control group (CTRL, $n = 4$) and BTX-injected group (BTX, $n = 7$). Rats from the BTX group were anesthetized with isoflurane and injected intramuscularly with 2 U (0.4 ml) of type A BTX: 1 U in the *M. Masseter* and 1 U in the *M. Temporalis* (Botox®, Allergan Inc., Irvine, CA, USA) as previously described (Kün-Darbois et al., 2015). Three points of injection for each *M. Masseter* and two for each *M. Temporalis* were necessary. Rats of the CTRL group were similarly injected with equivalent volume of saline. Rats were weighed weekly and were sacrificed 4 weeks after injection by CO_2 inhalation. Hemimandibles were dissected, defleshed and fixed in 10% formalin until use (Carson and Hladik, 2009). Condylar processes were separated from the rest of each hemimandible and scanned in the fixative prior to immersion in UA (Fig. 1A and B). Because the rat condylar cartilage is thinner than the human hip cartilage, each sample was then immersed for 24 h in the UA solution, rinsed in tap water for one hour to remove unlabeled UA, transferred in 10% formalin and scanned as above. After microCT analysis, samples were embedded undecalcified as above for histological analysis.

2.3. Microcomputed tomography

MicroCT of human femoral samples and rat mandibular condyles were performed using a Skyscan 1172 X-ray computerized microtomograph (Bruker microCT, Kontich, Belgium) equipped with an X-ray tube working at 70 kV/100 μA. Bones were placed in plastic tubes filled with formalin. The tubes were fixed on a brass stub with plasticine. Analysis was done with a pixel size corresponding to 13 μm (human femoral heads) and 2.94 μm (rat condyles). The rotation step was fixed at 0.20° with a 0.5 mm aluminum filter. For each sample, a stack of 2D-sections was obtained and reconstructed using NRecon software (Bruker) and analyzed with the CTAn, DataViewer and CTvol softwares (Bruker). MicroCT acquisition parameters, reconstruction and rendering settings were strictly alike between all the concerned specimens and for all images. After microCT analysis, the condyles were embedded in poly(methylmethacrylate) for histological analysis.

2.4. Quantitative analysis of cartilage and bone effects of BTX injections

Cartilage thickness (Cart.Th) measurement of the condyles was performed on 2D sagittal and frontal sections obtained by using the cutting plane facility of the software. For each condyle, 12 measurement points were used in 3 serial frontal sections and 1 sagittal section (Fig. 1C). The measured width (in μm) was comprised between the tide-mark and the external surface of the articular cartilage.

Bone morphometric parameters were obtained from the first scan images obtained before immersion in UA. The absolute bone volume (C.BV/C.TV, expressed in % and representing the percentage of volume occupied by cortical and trabecular bone) was measured in 3D using the CTAn software for each condyle. Trabecular bone volume could only be accurately measured in 2D (B.Ar/T.Ar, expressed in %, representing the fractional area occupied by trabecular bone) as previously described because the delineation of the region of interest is difficult on such a small bone segment (Kün-Darbois et al., 2015).

2.5. Histology on undecalcified bones

Because we wanted to see if the UA location corresponded to specific histological areas, the bones were processed undecalcified. Samples were dehydrated in a mixture of acetone/xylene and embedded undecalcified in poly(methylmethacrylate) as previously described (Chappard, 2014). Sections (7 μm in thickness) were cut dry on a heavy-duty microtome equipped with 50° tung-

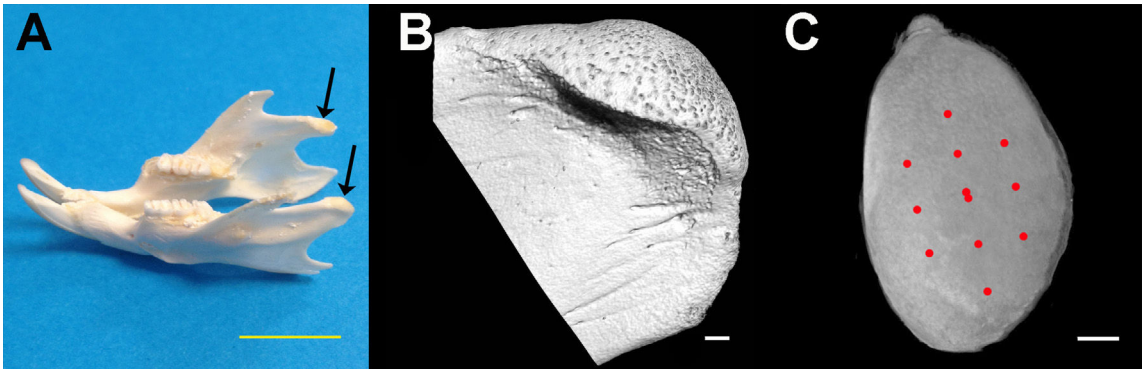


Fig. 1. (A) Lateral view of a rat mandible. Arrows indicate the right and left condylar processes (=articular processes) that have been analyzed in the present study. The scale bar stands for 1 cm. (B) Lateral view of a 3D reconstruction after microCT analysis of a right condylar process without metallic "staining". (C) Upper view of a condylar process showing the distribution of the 12 points used for cartilage thickness measurement. In all images (except image A) the scale bar stand for 500 μm.

sten carbide (Leica Polycut S, Rueil-Malmaison, France). Sections were stained by Goldner's trichrome for the differentiation of mineralized and osteoid tissues.

2.6. Statistical analysis

Statistical analysis was performed using the Systat statistical software release 13.0 (Systat Software Inc., San José, CA). All data were expressed as mean ± standard error of the mean (SEM). Differences among groups were analyzed by a non-parametric ANOVA (Kruskal–Wallis) and between groups by the Mann and Whitney's *U* test. Data from right and left hemimandibles were compared using a paired *t*-test. Differences were considered significant when $p < 0.05$.

3. Results

3.1. Femoral heads

The results of the 3 types of microCT analyses appear in Fig. 2. Routine histology revealed no signs of necrosis in the bone or marrow compartments. On the sample processed without metallic impregnation for microCT, the subchondral bone was evidenced as a rather smooth surface. The network of trabeculae was anchored at its endosteal surface and the marrow cavities were well delineated. The bone marrow was radiolucent as the articular cartilage that did not absorb X-rays. After UA impregnation, the articular cartilage was clearly seen on its full thickness. There was a line with an increased density above the subchondral bone which could correspond to the tide-mark separating the calcified/uncalcified layers of the articular cartilage. UA was also faintly deposited in the bone matrix and inside the marrow spaces making the difference between bone and marrow less obvious. When lanthanides were used, the articular cartilage was less clearly identified, with a faint labeling. However, there was no label at the tide-mark nor inside the marrow cavities. The cartilage thickness for this patient was 2200–2400 μm on the UA block and 2100–2400 μm on the lanthanide block. Trials with other metal salts reported in the literature gave unsatisfactory results. PTA could label the articular cartilage but staining was less intense (Fig. 2E). IKI labeled the cartilage but the hematopoietic areas were heavily stained while the fat cells did not take iodine (Fig. 2E). Iopamiron faintly stained the upper layers of the articular cartilage (Fig. 2G).

3.2. Condylar cartilage and bone in BTX injected rats

MicroCT measurements are summarized in Table 1. A smaller condylar C.BV/C.TV was observed at the right *vs.* left hemimandible in the BTX group ($p < 0.05$). There was no significant difference between the right side in the BTX group and the values obtained in the CTRL group. There was no significant difference between the left side in the BTX group and both sides in the CTRL group. When trabecular bone was accurately measured on 2D section, a bone loss was clearly seen on the condylar bone at the right side (*i.e.* paralyzed) in the BTX group with a reduced trabecular density and wider marrow cavities. No difference was noted when comparing both sides of the CTRL group. The BTX group had a significantly lower condylar B.Ar/T.Ar (−32%) at the right side compared to the left side ($p < 0.05$). The BTX group had a significantly lower condylar B.Ar/T.Ar (−25%) at the right side compared to the right side of the CTRL group ($p < 0.05$). There were no significant differences between left sides of the BTX group and both sides of the CTRL group.

Table 1
. Quantitative analysis on MicroCT images. Bone morphometric parameters obtained before UA impregnation (absolute bone volume and trabecular bone volume); cartilage thickness determined after UA impregnation.

	CTRL left	CTRL right	BTX left	BTX right
C.BV/C.TV (%)	76.83 ± 1.38	74.35 ± 1.12	80.23 ± 1.02	74.85 ± 1.63[a]
B.Ar/T.Ar (%)	66.98 ± 3.53	63.54 ± 2.59	70.86 ± 1.27	38.96 ± 3.81[a,b]
Cart.Th (μm)	164 ± 25	161 ± 25	168 ± 12	169 ± 12

[a] Significant difference between the right *vs.* the left side.
[b] Significant difference *vs.* CTRL.

After UA impregnation, the whole thickness of the articular cartilage was clearly seen whereas it was not visible before impregnation (Fig. 3A and B). The tide-mark was clearly seen. UA was also deposited in the bone matrix and inside the marrow spaces. In some locations, bands with an increased X-ray density were noticed at the surface of trabecular and endosteal bone. No difference was noted when comparing Cart.Th between the right and left sides in the BTX group and similarly in the CTRL group (Table 1). No difference could be found between the right sides of CTRL and BTX rats. The average cartilage thickness for all rats of the study was 167 ± 8 μm.

3.3. Histological analysis

The human femoral head appears in Fig. 2A. The tide mark was clearly identified and the layer of calcified cartilage appears very thin. In rat mandibular condyles, histological analysis revealed the presence of articular cartilage (Fig. 3C). It had the same appearance as the cartilage seen in 2D sections after MicroCT. The presence of osteoid seams at the surface of trabecular bone around marrow spaces was noted.

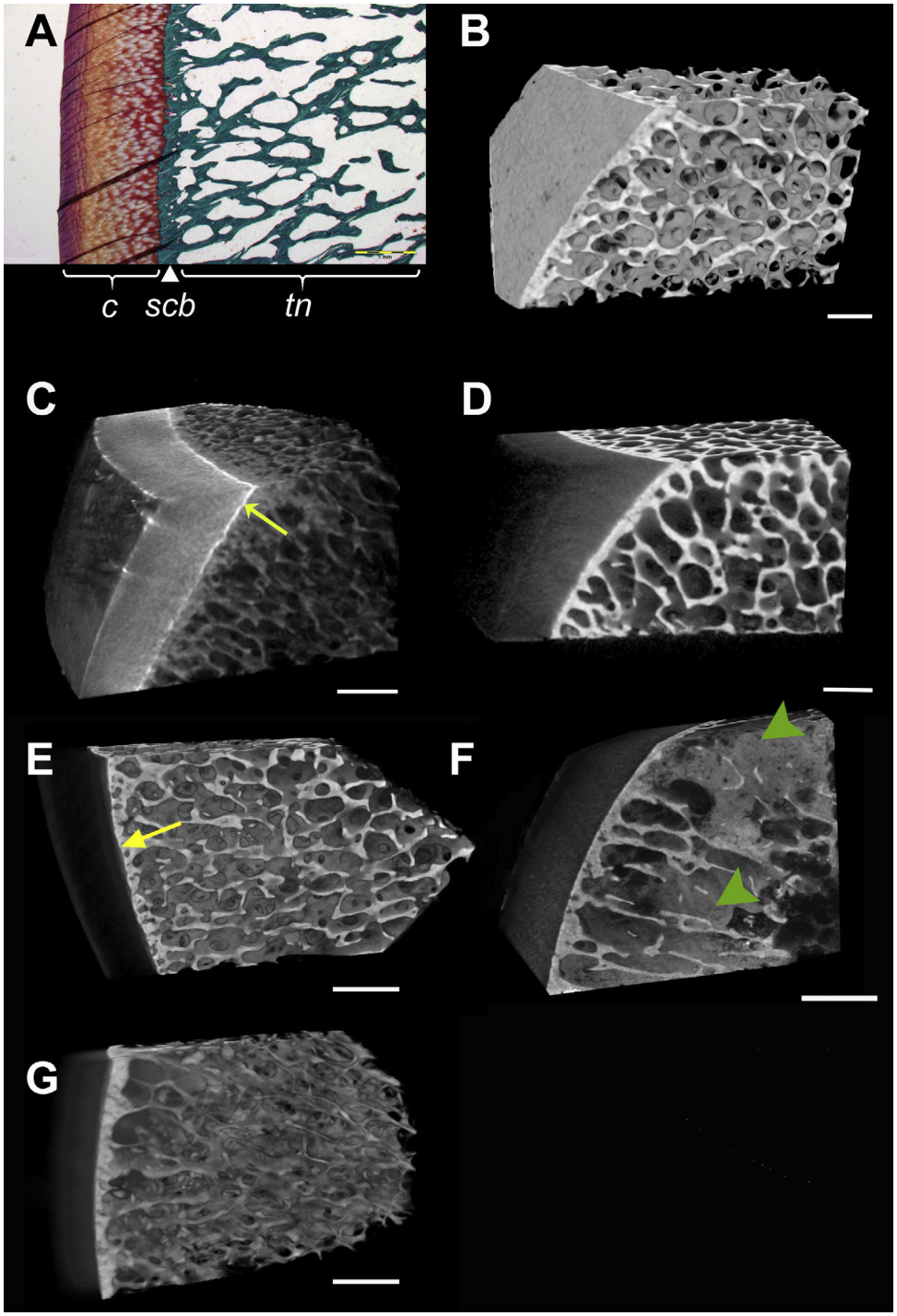


Fig. 2. (A) Histological aspect of a femoral head embedded undecalcified (Goldner's trichrome). C = articular cartilage, scb = subchondral bone, tn = trabecular network. The arrow indicates the tide-mark. (B) MicroCT analysis of a piece of the same femoral head without metallic impregnation; the articular cartilage is not seen. (C) MicroCT analysis of a piece of the same femoral head impregnated with UA, the tide-mark is heavily marked with the metallic salt (arrow). (D) MicroCT analysis of fragment from the same femoral head impregnated with the solution of lanthanides; the articular cartilage is less clearly identified. (E) MicroCT analysis from a piece of another femoral head stained with PTA. The cartilage is faintly stained but the tide-mark is evidenced (arrow). (F) MicroCT analysis from a piece of another femoral head stained with IKI. Areas of marrow cells are heavily stained (arrowheads). (G) MicroCT analysis from a piece of another femoral head stained with Iopamiron 300. The upper layer of the cartilage is ill-defined. In all images the scale bar stands for 1 mm.(For interpretation of the references to color in this legend, the reader is referred to the web version of the article.)

4. Discussion

A significant advance in the bone field arose with the development of microCT around the 2000s. This method is superior to scanning electron microscopy at low magnifications and allows direct 3D measurements of the bone mass, porosity and microarchitecture (Ruegsegger, 1994; Sasov and Van Dyck, 1998). The method is faster than morphometric analysis done on histological sections; moreover new microCTs have a resolution in the 2–3 μm/pixel range. In addition microCT is nondestructive and the samples can be processed for additional histological studies. Unfortunately microCT is only suitable for tissues with high inherent X-ray contrast, such as bone which is a mineralized tissue. Because soft tissues, such as articular cartilage, are non-mineralized, they

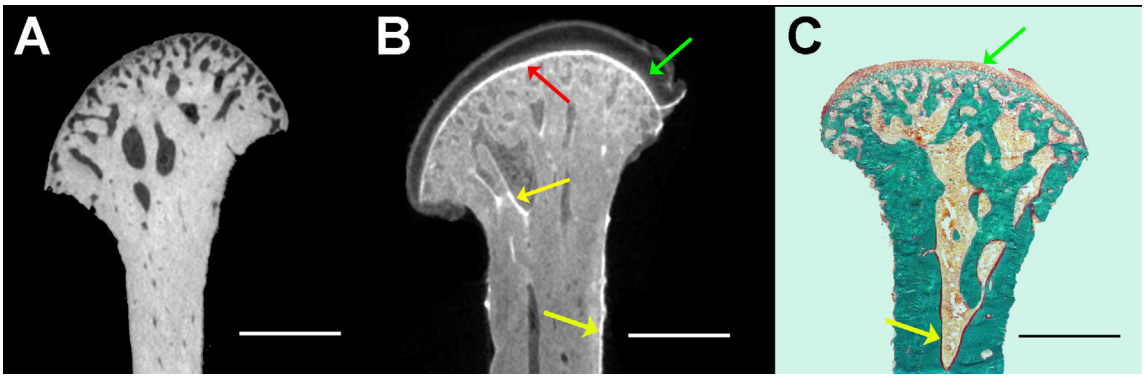


Fig. 3. (A) 2D frontal section of a right condylar process after microCT analysis, showing the aspect without UA impregnation. The articular cartilage is not visible. (B) 2D frontal section of a right condylar process after UA impregnation. Articular cartilage is strongly visible Tendosteum, some trabeculae and the periosteal surface (probably corresponding to osteoid seams) is noted (yellow arrows). (C) Histological aspect of a condylar process embedded undecalcified (Goldner's trichrome) showing articular cartilage (green arrow) and osteoid seams at the endosteum (yellow arrow). In all images the scale bar stand for 500 μm. (For interpretation of the references to color in this legend, the reader is referred to the web version of the article.)

absorb X-ray less intensely, making them not visible with microCT. Therefore, contrast enhancement using a "staining" procedure is a prerequisite for cartilage imaging. Several different procedures have been described in the literature to "stain" soft tissues using ionic or non-ionic contrast agents: ioxaglic acid, osmium tetroxide, IKI, PTA, PMA, gadolinium or iodinated contrasts agents for computed tomography (Cockman et al., 2006; Das Neves Borges et al., 2014; Kerckhofs et al., 2013; Metscher, 2009; Nieminen et al., 2015; Pauwels et al., 2013; Renders et al., 2014; Xie et al., 2009; Yoo et al., 2011). To date none of them is fully satisfactory and a simple, reproducible, non-destructive and high-standard technique for cartilage contrast enhancement, allowing 3D analysis is still lacking. Results from our pre-study show that none of these compounds appeared satisfactory on fixed articular cartilage.

UA can be utilized as a contrast enhancer for soft tissues in transmission electron microscopy, and has been used in this manner for decades. The uranyl ion is known to bind to phosphate groups of nucleic acids and to proteins (especially collagen) (Hayat, 2000). Recent reports have raised that radioactivity generated by UA could be dangerous and lanthanides have been proposed as a surrogate for UA (Hosogi et al., 2015). However, uranium is toxic at a high concentration in human and its harmful effects are more related to direct toxicity than radioactivity (Keith et al., 2007). UA is classified as hazardous substance and dangerous good due to its direct toxicity. Standard precautions must therefore be taken as in every electron microscopy laboratory (use of gloves to handle the solution under a laboratory fume cabinet, waste solutions discarded in specific vials). In living beings, uranium ingestion or inhalation can undergo deposition and accumulation in bone. It was recently found that uranium preferentially accumulates in the calcifying areas of bone (endosteal, periosteal) after a single injection of uranyl nitrate (Bourgeois et al., 2015). In our preliminary trials, we experimented with a number of metallic salts that have been reported to enhance cartilage contrast in micro or nanoCT. Iodine created a heavy staining of marrow cells; shrinkage is also described in the literature for highly hydrated tissues but this was not investigate in this pre-study (Vickerton et al., 2013). PTA gave a pale contrast of the articular cartilage. Gadolinium, proposed for MR imaging did not work properly on fixed tissues (Bashir et al., 1997; Cockman et al., 2006). Iodinated anionic contrast agents recommended for peripheral quantitate computed tomography (pQCT) (Silvast et al., 2009) were also ineffective to provide a sufficient contrast on fixed cartilage, especially on the upper layer of the cartilage. On the contrary, UA was found to provide the best contrast in microCT for the human hip cartilage. Lanthanides enhanced the human articular cartilage faintly by binding to glycosaminoglycanes. Because the thick human hip cartilage was more clearly identified by UA, we selected this procedure to enhance the contrast of the thin cartilage of the mandibular condyles in rat. As described by others, UA tends to localize in the bone matrix by a substitution mechanism with the mineral and an adsorption on some non-collagenous proteins (Bourgeois et al., 2015). This could explain why a heavy labeling of the tide-mark and some areas of the endosteum or trabeculae (probably corresponding to osteoid seams) were noted in addition to a faint marrow fixation. Both PTA and UA are known to be fixed by collagen. A similar labeling of the tide-mark is therefore reported with PTA staining (Das Neves Borges et al., 2014; Nieminen et al., 2015). X-ray attenuation obtained with PTA and PMA staining appears to depend on collagen distribution, *i.e.*, cartilage depth (Nieminen et al., 2015). Cartilage stains less strongly with PTA compared to other tissues (Metscher, 2009). In our hands, PTA provides cartilage 3D imaging of poorer quality than UA (Das Neves Borges et al., 2014).

Histomorphometry is the standard procedure for articular cartilage thickness measurement. Nevertheless, this technique seems unreliable for quantitative measurement since there are difficulties in reproducing the same orientation for each sample, due to section obliquity (Howard and Reed, 2004; Vesterby et al., 1987). Morphometric analysis of cartilage thickness has been done after contrast enhancement with Hexabrix in microCT although the cartilage was less clearly delineated than in the present study (Renders et al., 2014; Xie et al., 2009). A histomorphometric analysis of the cartilage of mandibular condyles in young rabbit was recently presented (Matthys et al., 2015, 2016).

In the present study bone loss was found at the right condyles after BTX injection in the right *M. Masseter* and *M. temporalis* in adult rats. These results fit in well with the literature and confirm our previous findings (Kün-Darbois et al., 2015; Matthys et al., 2015). Mandibular bone loss is due to the BTX-induced disuse of the temporomandibular joint. Whether disuse also affects condylar cartilage is still controversial (Matthys et al., 2016). Condylar cartilage assessment in this model of disuse has become a subject of interest. It is known that articular cartilage can be strongly affected by mechanical status of the joint (Matthys et al., 2015). In young growing rats having received BTX injection in *M. Masseter*, the mandible growth was impaired and the cartilage thickness was significantly reduced (Kim et al., 2008). This was associated with an increase in the number of apoptotic cells (determined by the TUNEL assay) in the proliferation and hypertrophic zones. On the contrary, no change in condylar cartilage thickness was found after a unilateral BTX injection in *M. Masseter* in young rabbits (Matthys et al., 2015, 2016). It should be noted that both papers have used

histological measurements without the stereological requirement of using systematic random sections (Howard and Reed, 2004). Another explanation could be that a reduction in cartilage thickness can be found only in young growing animals but not in adults. In the present study, we were able to have a precise and reproducible localization of the cutting planes in 3D. We could not evidence a reduction in cartilage thickness between the two sides of the same BTX rat nor between the control and BTX animals. In addition, we used adult animals in which growth was complete.

5. Conclusion

In the present study, we aimed at assessing a new method of contrast enhancement by UA using microCT that would permit quantitative analysis of articular cartilage thickness. It allows a simple and non-destructive assessment of articular cartilage morphology, whereas cartilage is normally radiolucent. Other metal salts reported in the literature could also label cartilage but the intensity of staining was lower in microCT images. UA "staining" was found effective in the assessment and quantification of the condylar articular cartilage of the mandible in the BTX rat model of disuse. Although a reduction of bone mass was observed in the condyle, no difference was observed in cartilage thickness one month after a BTX injection.

Conflict of interest

The authors declare that they have no conflicts of interest concerning this article.

Acknowledgments

This work was made possible by grants from the French Ministry of Research. Many thanks to Mrs. Lechat for secretarial assistance. Authors are greatly indebted to the SCAHU (Service commun d'animalerie hospitalo-universitaire) of Angers, especially to P. Legras and J. Roux for their help with the animal care. They also thank Mrs. Nadine Gaborit for her skillful assistance with microCT and histotechnology. JDKD received a scholarship from the ARS (Agence régionale de santé) «Pays de la Loire».

References

Bashir, A., Gray, M.L., Boutin, R.D., Burstein, D., 1997. Glycosaminoglycan in articular cartilage in vivo assessment with delayed Gd(DTPA)(2-)-enhanced MR imaging. Radiology 205, 551–558.

Bourgeois, D., Burt-Pichat, B., Le Goff, X., Garrevoet, J., Tack, P., Falkenberg, G., Van Hoorebeke, L., Vincze, L., Denecke, M.A., Meyer, D., Vidaud, C., Boivin, G., 2015. Micro-distribution of uranium in bone after contamination: new insight into its mechanism of accumulation into bone tissue. Anal. Bioanal. Chem. 407, 6619–6625.

Carson, F., Hladik, C., 2009. Fixation. In: Carson, F., Hladik, C. (Eds.), Histotechnology: A Self-Instructional Text. American Society for Clinical Pathology Press, Chicago, IL, pp. 9–13.

Chappard, D., 2014. Technical aspects: how do we best prepare bone samples for proper histological analysis? In: Heymann, D. (Ed.), Bone Cancer Progression and Therapeutic Approaches. , 2nd ed. Acad. Press/Elsevier Inc., London, pp. 111–120.

Chappard, D., Chennebault, A., Moreau, M., Legrand, E., Audran, M., Baslé, M.F., 2001. Texture analysis of X-ray radiographs is a more reliable descriptor of bone loss than mineral content in a rat model of localized disuse induced by the *Clostridium botulinum* toxin. Bone 28, 72–79.

Cockman, M.D., Blanton, C.A., Chmielewski, P.A., Dong, L., Dufresne, T.E., Hookfin, E.B., Karb, M.J., Liu, S., Wehmeyer, K.R., 2006. Quantitative imaging of proteoglycan in cartilage using a gadolinium probe and microCT. Osteoarthr. Cartil. 14, 210–214.

Das Neves Borges, P., Forte, A.E., Vincent, T.L., Dini, D., Marenzana, M., 2014. Rapid, automated imaging of mouse articular cartilage by microCT for early detection of osteoarthritis and finite element modelling of joint mechanics. Osteoarthr. Cartil. 22, 1419–1428.

Hayat, M.A., 2000. Principles and Techniques of Scanning Electron Microscopy. Biological Applications, 4th ed. Cambridge Univ. Press, Cambridge, NY/Madrid.

Hosogi, N., Nishioka, H., Nakakoshi, M., 2015. Evaluation of lanthanide salts as alternative stains to uranyl acetate. Microscopy (Oxf.) 64, 429–435.

Howard, V., Reed, M., 2004. Unbiased Stereology: Three-Dimensional Measurement in Microscopy. Garland Science.

Keith, L.S., Faroon, O.M., Fowler, B.A., 2007. Uranium. In: Nordberg, G.F., Fowler, B.A., Nordberg, M. (Eds.), Handbook on the Toxicology of Metals. , 3rd ed. Academic Press, San Diego, pp. 881–901.

Kerckhofs, G., Sainz, J., Marechal, M., Wevers, M., Van de Putte, T., Geris, L., Schrooten, J., 2014. Contrast-enhanced nanofocus X-ray computed tomography allows virtual three-dimensional histopathology and morphometric analysis of osteoarthritis in small animal models. Cartilage 5, 55–65.

Kerckhofs, G., Sainz, J., Wevers, M., Van de Putte, T., Schrooten, J., 2013. Contrast-enhanced nanofocus computed tomography images the cartilage subtissue architecture in three dimensions. Eur. Cell Mater. 25, 179–189.

Kim, J.Y., Kim, S.T., Cho, S.W., Jung, H.S., Park, K.T., Son, H.K., 2008. Growth effects of botulinum toxin type A injected into masseter muscle on a developing rat mandible. Oral Dis. 14, 626–632.

Kün-Darbois, J.D., Libouban, H., Chappard, D., 2015. Botulinum toxin in masticatory muscles of the adult rat induces bone loss at the condyle and alveolar regions of the mandible associated with a bone proliferation at a muscle enthesis. Bone 77, 75–82.

Matthys, T., Ho Dang, H.A., Rafferty, K.L., Herring, S.W., 2015. Bone and cartilage changes in rabbit mandibular condyles after 1 injection of botulinum toxin. Am. J. Orthod. Dentofacial Orthop. 148, 999–1009.

Matthys, T., Ho Dang, H.A., Rafferty, K.L., Herring, S.W., 2016. Authors response. Am. J. Orthod. Dentofacial Orthop. 149, 443–445.

Metscher, B.D., 2009. MicroCT for comparative morphology simple staining methods allow high-contrast 3D imaging of diverse non-mineralized animal tissues. BMC Physiol. 9, 11.

Naveh, G.R., Brumfeld, V., Dean, M., Shahar, R., Weiner, S., 2014. Direct microCT imaging of non-mineralized connective tissues at high resolution. Connect. Tissue Res. 55, 52–60.

Nieminen, H.J., Ylitalo, T., Karhula, S., Suuronen, J.P., Kauppinen, S., Serimaa, R., Haeggstrom, E., Pritzker, K.P., Valkealahti, M., Lehenkari, P., Finnila, M., Saarakkala, S., 2015. Determining collagen distribution in articular cartilage using contrast-enhanced micro-computed tomography. Osteoarthr. Cartil. 23, 1613–1621.

Pauwels, E., Van Loo, D., Cornillie, P., Brabant, L., Van Hoorebeke, L., 2013. An exploratory study of contrast agents for soft tissue visualization by means of high resolution X-ray computed tomography imaging. J. Microsc. 250, 21–31.

Renders, G.A., Mulder, L., Lin, A.S., Langenbach, G.E., Koolstra, J.H., Guldberg, R.E., Everts, V., 2014. Contrast-enhanced microCT (EPIC-muCT) ex vivo applied to the mouse and human jaw joint. Dentomaxillofac. Radiol. 43, 20130098.

Ruegsegger, P., 1994. The Use of Peripheral QCT in the Evaluation of Bone Remodelling, 4. The Endocrinology, pp. 167–176.

Sasov, A., Van Dyck, D., 1998. Desktop X-ray microscopy and microtomography. J. Microsc. 191, 151–158.

Silvast, T., Jurvelin, J., Lammi, M., Töyräs, J., 2009. pQCT study on diffusion and equilibrium distribution of iodinated anionic contrast agent in human articular cartilage – associations to matrix composition and integrity. Osteoarthr. Cartil. 17, 26–32.

Sophia Fox, A.J., Bedi, A., Rodeo, S.A., 2009. The basic science of articular cartilage structure composition and function. Sports Health 1, 461–468.

Vesterby, A., Kragstrup, J., Gundersen, H., Melsen, F., 1987. Unbiased stereologic estimation of surface density in bone using vertical sections. Bone 8, 13–17.

Vickerton, P., Jarvis, J., Jeffery, N., 2013. Concentration-dependent specimen shrinkage in iodine-enhanced microCT. J. Anat. 223, 185–193.

Xie, L., Lin, A.S., Guldberg, R.E., Levenston, M.E., 2010. Nondestructive assessment of sGAG content and distribution in normal and degraded rat articular cartilage via EPIC-microCT. Osteoarthr. Cartil. 18, 65–72.

Xie, L., Lin, A.S., Levenston, M.E., Guldberg, R.E., 2009. Quantitative assessment of articular cartilage morphology via EPIC-microCT. Osteoarthr. Cartil. 17, 313–320.

Yoo, H.J., Hong, S.H., Choi, J.Y., Lee, I.J., Kim, S.J., Choi, J.A., Kang, H.S., 2011. Contrast-enhanced CT of articular cartilage experimental study for quantification of glycosaminoglycan content in articular cartilage. Radiology 261, 805–812.

Clin Oral Invest
DOI 10.1007/s00784-017-2080-8

ORIGINAL ARTICLE

Asymmetric bone remodeling in mandibular and maxillary tori

Jean-Daniel Kün-Darbois[1,2] · **Bernard Guillaume**[1,3] · **Daniel Chappard**[1]

Received: 9 June 2016 / Accepted: 9 February 2017
© Springer-Verlag Berlin Heidelberg 2017

Abstract
Objectives Tori are frequent paucisymptomatic bony outgrowths of the oral cavity in three locations: *torus palatinus* (TP), *mandibularis* (TM), and *maxillaris* (TMax). Their usually described histological characteristics are unspecific: normal cortical bone with more or less trabecular bone. The aim of this study was to describe tori's specific morphological and histomorphometric characteristics.
Materials and methods Histological characteristics in a series of 18 tori collected after surgical removal were analyzed. Microcomputed tomography provided a 3D analysis. Mineral apposition rate (MAR) was measured after double tetracycline labeling. Osteoid tissue was identified by Goldner's trichrome and osteoclasts by the tartrate resistant acid phosphatase identification in undecalcified sections. Iron and aluminum were detected by histochemical staining methods. Osteoid thickness and MAR were determined at the outer surface of the torus and in the Haversian canals.
Results Tori appeared made of lamellar Haversian bone in 16/18 cases. Osteoid thickness did not differ between the outer surface and within the canals. An asymmetric bone remodeling was observed in the Haversian canals of 15 tori: osteoid seams were deposited on the side close to the free torus surface, and Howship's lacunae with numerous osteoclasts were observed on the opposite side. A high MAR was found at the surface of the tori and within the canals. There was no iron or aluminum deposit.
Conclusions Tori may be characterized by a specific asymmetric bone remodeling which seems to determine their shape.
Clinical relevance This finding could constitute a specific histological feature allowing to differentiate tori from exostoses.

Keywords Torus · Bone remodeling · Exostoses · Histomorphometry · Aluminum · Iron

Introduction

Tori are frequent and benign bony outgrowths of the oral cavity. They are named after the Latin *torus* that means "lump". They are covered with a thin and poorly vascularized mucosa [1, 2]. They present a slow and progressive growth that may stop spontaneously [1]. A *torus palatinus* (TP) is usually located at the palate, along the longitudinal ridge of the hard palate on either side of the median raphe of the palatine bone. A *torus mandibularis* (TM) is usually located at the mandible (on the lingual side of the horizontal branch above the mylohyoid line at the level of the premolar and/or canine area) [1]. A less common form is *torus maxillaris* (TMax) which is located at the maxilla (on the palatal or vestibular side of the alveolar process of the maxilla) [2]. According to the anatomical location (TP, TM, or TMax),

Electronic supplementary material The online version of this article (doi:10.1007/s00784-017-2080-8) contains supplementary material, which is available to authorized users.

✉ Jean-Daniel Kün-Darbois
daniel.kun-darbois@univ-angers.fr

[1] GEROM Groupe d'Etude Remodelage Osseux et bioMatériaux, Research Group on Bone Remodeling and bioMaterials, LHEA, IRIS-IBS Institut de Biologie en Santé, Université d'Angers, 4 rue Larrey, 49933 Angers Cedex, France

[2] Department of Maxillo-facial surgery, CHU d'Angers, 4 rue Larrey, 49933 Angers Cedex, France

[3] CFI Centre Français d'Implantologie, 6 rue de Rome, 75008 Paris, France

Published online: 23 February 2017

the clinical and epidemiological characteristics are not strictly alike [2]. They are often bilateral but may be unilateral [3]. The general prevalence is about 10 to 30% and varies according to ethnic groups, age, and gender [1, 4, 5]. Tori are more frequent in some ethnic groups (Japanese, Caucasian, Norwegian, Eskimos) [1, 3, 6]. The etiology remains unknown and could be multifactorial. A genetic origin is the most widely accepted theory today, but an autosomal dominant inheritance explains only 30% of the cases [1, 2]. Environmental factors seem to play a role in the incidence of tori. A mechanical origin due to occlusal stress is advocated to explain the occurrence of TM [1, 3, 6]. An interplay between genetic and environmental factors cannot be excluded [7]. Tori are frequently asymptomatic, and their surgical removal is indicated in some cases, mainly, before dental prosthetic rehabilitation, as a source of autogenous bone graft in implant surgery or for patients' desire (esthetic reasons or cancerophobia) [1]. The usually described histological characteristic is not specific: tori are composed of normal cortical bone with more or less trabecular bone according to their size [1, 7, 8]. The aim of the present study was to find tori's specific characteristics by describing morphological and histological bone characteristics in a series of human tori. Microcomputed tomography (microCT), histology, and histochemical were used to characterize the morphological aspect of the tori.

Participants and methods

Participants

Tori were collected in three maxillo-facial surgery departments in Angers, Paris, and Tours (France). All patients undergoing surgical removal of a torus between 2011 and 2015 were included. All participants had given their informed consent before participating to the study. Clinical characteristics are summarized in Table 1. Ten participants, 2 males, and 8 females were included. All participants were Caucasians. The average age was 51.8 ± 5.11 years. Tumors were removed in one piece and fixed in formalin until use. They were then sent to the bone histopathology unit of Angers University Hospital.

A double tetracycline labeling technique was used to measure mineral apposition rate (MAR) by osteoblasts [9]. Demethyl chlortetracycline (Alkonatrem®, Laboratoires Genopharm, Saint-Thibault-des-Vignes, France) was given at the dose of 600 mg, twice a day according to a strict schedule: 2 days on, 10 days off, 4 days on. Surgical removal of the torus was performed between 2 and 7 days after the end of the second label (in order to avoid unspecific label on the eroded surfaces). Samples were fixed immediately in formalin and stored in a fridge until analysis.

This experimental protocol was approved by the local ethical committee of Angers University Hospital and was done in accordance with the institutional guidelines of the French Ethical Committee (protocol number 2016-31) and with the 1964 Helsinki declaration and its later amendments.

Microcomputed tomography

Samples were analyzed by microCT prior to histological embedding. MicroCT allowing a 3D evaluation of these tumors was performed using a Skyscan 1172 X-ray computerized microtomograph (Bruker microCT, Kontich, Belgium) equipped with an X-ray tube working at 70 kV/100 μA. Bone samples were placed in plastic tubes filled with water to prevent desiccation. The tube was fixed on a brass stub with plasticine. Analysis was done with a pixel size corresponding to 8.29 μm; the rotation step was fixed at 0.25° with a 0.5-mm aluminum filter. For each sample, a stack of 2D sections was obtained and reconstructed using NRecon software (Bruker microCT, Kontich, Belgium) and analyzed with CTAn software release 1.13.11.0 (Bruker microCT, Kontich, Belgium). The 3D reconstruction of the specimens was obtained with the ANT and CTVol softwares (Bruker microCT, Kontich, Belgium). The programs allowed reconstruction from the stacks of 2D sections by either surface or volume rendering.

Histology

The size of the tori was determined according to Woo's classification [8, 10]. Bone samples were embedded undecalcified in poly(methyl methacrylate). Sections (7 μm in thickness) were cut dry on a heavy-duty microtome equipped with 50° tungsten carbide knives (Leica Polycut S, Rueil-Malmaison, France). Sections were stained by Goldner's trichrome for the identification of osteoid. Histochemical identification of osteoclasts (bone resorbing cells) was done by the tartrate resistant acid phosphatase (TRAcP) method [11]. The presence of iron (Fe) and aluminum (Al) in tori was searched by histochemical methods. The Perls' Prussian blue and solochrome azurine staining methods were used for the identification of Fe^{3+} and Al^{3+}, respectively [12]. These histochemical reactions were done in cleaned glass vials, and the technicians never used metallic forceps during the staining to avoid contamination. Observations were performed at the cortical (outer) surface of each torus (Ct.) and at the surface of the Haversian canal (Ca.). The osteoid seam thickness was determined at the outer surface of the torus (Ct.O.Th) and at the surface of the Haversian canal (Ca.O.Th). The MARs were determined on unstained 10 μm thick sections, at the outer surface of the torus (Ct. MAR), and at the surface of the Haversian canal (Ca.MAR). It was determined as the average value of the distance between all double labels (four measurements at equidistant locations per label) divided by the number of days between the given

Table 1 Clinical characteristics

Torus	Participant number	Age (years)	Sex	Side	Bone	Length (mm)	Elevation (mm)	Woo's classification	Surgical indication	Shape
1	1	39	M	R	Mandible	12	6	Small	Prosthetic	Round
2	1	39	M	L	Mandible	15	6	Medium	Prosthetic	Elongated
3	2	45	F	R	Mandible	9	6	Small	Esthetic	Round
4	2	45	F	L	Mandible	10	2	Small	Esthetic	Round
5	3	39	F	L	Maxilla	7	3	Small	Esthetic	Round
6	3	39	F	L	Maxilla	2	0.5	Small	Esthetic	Round
7	4	81	M	L	Mandible	1.5	1	Small	Prosthetic	Elongated
8	4	81	M	L	Mandible	1	1	Small	Prosthetic	Round
9	5	65	F	R	Mandible	6	3	Small	Prosthetic	Round
10	5	65	F	L	Mandible	5	2	Small	Prosthetic	Round
11	6	58	F	R	Mandible	22	5.5	Medium	Prosthetic	Elongated
12	6	58	F	L	Mandible	7	2	Small	Prosthetic	Round
13	7	57	F	R	Mandible	23	5	Medium	Prosthetic	Elongated
14	8	62	F	R	Mandible	7	4	Small	Prosthetic	Round
15	8	62	F	L	Mandible	8	5	Small	Prosthetic	Round
16	9	34	F	R	Mandible	18	3	Medium	Esthetic	Elongated
17	9	34	F	R	Mandible	8	3	Small	Esthetic	Round
18	10	30	F	R	Mandible	15	8	Medium	Esthetic	Round

doses of tetracycline. All histomorphometric measurements and the nomenclature used follow the ASBMR (American Society for Bone and Mineral Research) recommendations [13].

Statistical analysis

Statistical analysis was performed using the Systat statistical software release 13.1 (Systat Software Inc., San José, CA). All data were expressed as mean ± standard error of the mean (SEM). Differences among groups were analyzed by a non-parametric ANOVA (Kruskall–Wallis) and between groups by the Mann and Whitney's *U* test. Means were compared using a paired *t* test. Differences were considered significant when $p < 0.05$.

Results

Clinical characteristics

All participants underwent surgical removal of the tori before prosthetic rehabilitation or for esthetical reasons (Table 1). Eighteen tori from 10 participants were analyzed. They were all localized on the internal (lingual) side of the horizontal branch of the mandible, above the mylohyoid line, and at the level of the canine and/or the first premolar except two that were localized at vestibular side of the maxilla in one participant. They all presented a convex shape in the oral cavity (Fig. 1). Five tori presented an elongated shape, and 13 tori presented a round shape. Tori were bilateral in five participants and were situated on the same side in three participants. Tori were unique and unilateral in two participants. No TP were enrolled in the present study.

Microcomputed tomography

The general globular shape of the tori was clearly identified with a smooth free surface, and the implantation surface was well differentiated (Fig. 2a). The software possibility to threshold the internal porosity inside the torus revealed the presence of numerous Haversian canals. The 3D orientation of the canals was often in random directions in contrast to the canalar orientation in the normal mandibular cortice which runs in parallel (Fig. 2b). This aspect can be well identified in the supplementary video.

Histological analysis

According to Woo's classification, there were 13 small and 5 medium tori. The average length of the tori was 9.8 ± 1.54 mm, and the average elevation was 3.66 ± 0.5 mm. Under polarization microscopy, tori appeared made of lamellar bone in 16/18 cases and the structure units were true osteons with a central Haversian canal (Fig. 3a). In 2/18 tori, the bone texture was a mix of woven bone packed with a small amount of lamellar bone. Histological analysis revealed the presence of osteoid seams in two different

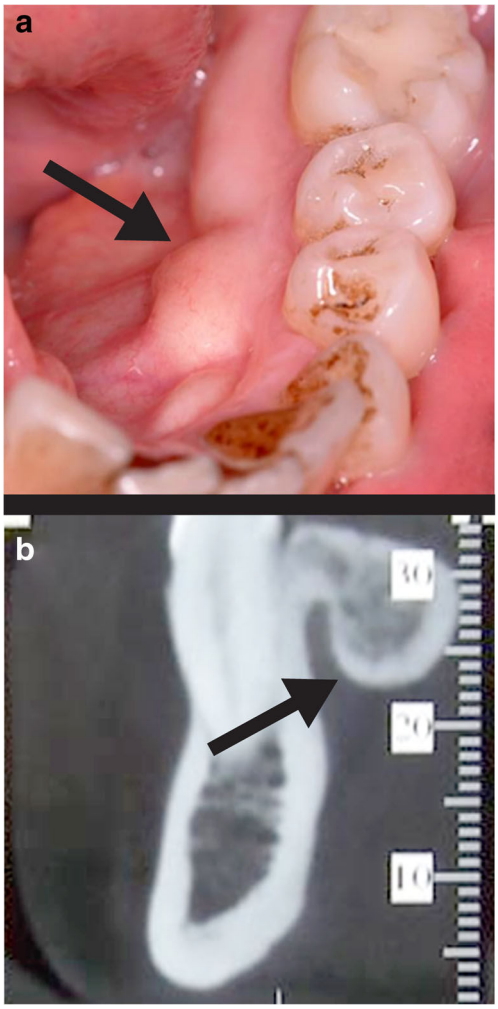


Fig. 1 **a** Intraoral view of a lingual *torus mandibularis* in a female patient (*arrow*). **b** Sagittal CT scan section showing a lingual *torus mandibularis* (*arrow*)

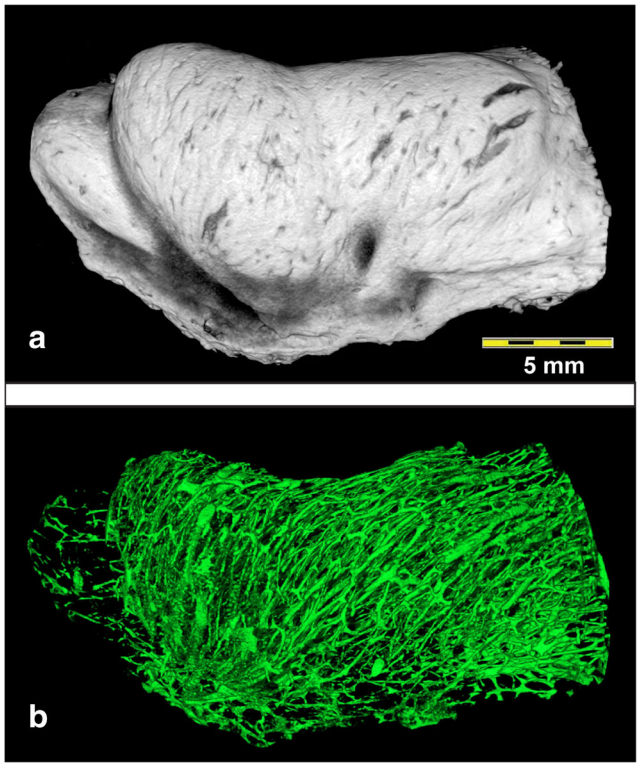


Fig. 2 MicroCT analysis. **a** 3D reconstruction showing the general globular shape of a *torus mandibularis* (*lingual view*). **b** 3D reconstruction showing the orientation of the numerous Haversian canals in random directions in the same tori (*lingual view*)

locations: at the external free surface of the torus and inside the Haversian canals in 17/18 cases. Osteoid thickness was similar at the surface of the tori and inside the canals (Ct.O.Th: 12.0 ± 1.3 μm; Ca.O.Th: 13.6 ± 0.7 μm; p = 0.093) (Table 2). The most intriguing aspect was the asymmetric disposition of the osteoid seams which were laid on the canal surface closest to the free torus surface in 15/18 tori of the study (Fig. 3b). The opposite surface of the canal was frequently occupied by Howship's lacunae (Fig. 3b). TRAcP-stained sections evidenced numerous true osteoclasts in this location in 11/18 tori (Fig. 3c). This corresponds to an active and asymmetric bone remodeling observed in almost every tori of the study.

In the six participants having received a double tetracycline labeling, the mineralization rate was not statistically different at the surface of the tori and inside the canals (Ct.MAR: 0.66 ± 0.12 μm/day; Ca.MAR: 0.92 ± 0.09 μm/day; p = 0.121) (Fig. 3d). The Ca.MAR determined here was higher (p = 0.0001) than the normal MAR (0.72 ± 0.12 μm/day) [14]. There was no difference between Ct.MAR and normal MAR (p = 0.2289) (Table 2). It attests high mineralization rates in tori of the present study.

Fe^{3+} and Al^{3+} were not identified in the bone matrix of any torus of the present study.

Discussion

In the literature, the most frequent indication for torus removal is a prosthetic treatment or an interference with dental prosthesis; it was the same in the present study [1, 15]. Tori are also frequently removed as a source of autogenous bone graft in implant surgery [1, 15–19]. Other causes of excision are disturbances of phonation, limitation of masticatory mechanics, sensitivity due to a thin mucosa layer, inflammation, ulcer of traumatic origin, retention of food remains, and patients' desire (esthetic reasons or cancerophobia) [1]. Other possible complications due to the presence of tori are submandibular calculi, bisphosphonate-related osteonecrosis, osteitis, osteomyelitis, and intubation difficulties [3, 20–26]. However, tori remain frequently asymptomatic, and their removal is rarely indicated [1, 27]. The indication for a surgical removal of tori must be carefully established, since complications may occur: infections, fractures, or hemorrhages. Specific complications

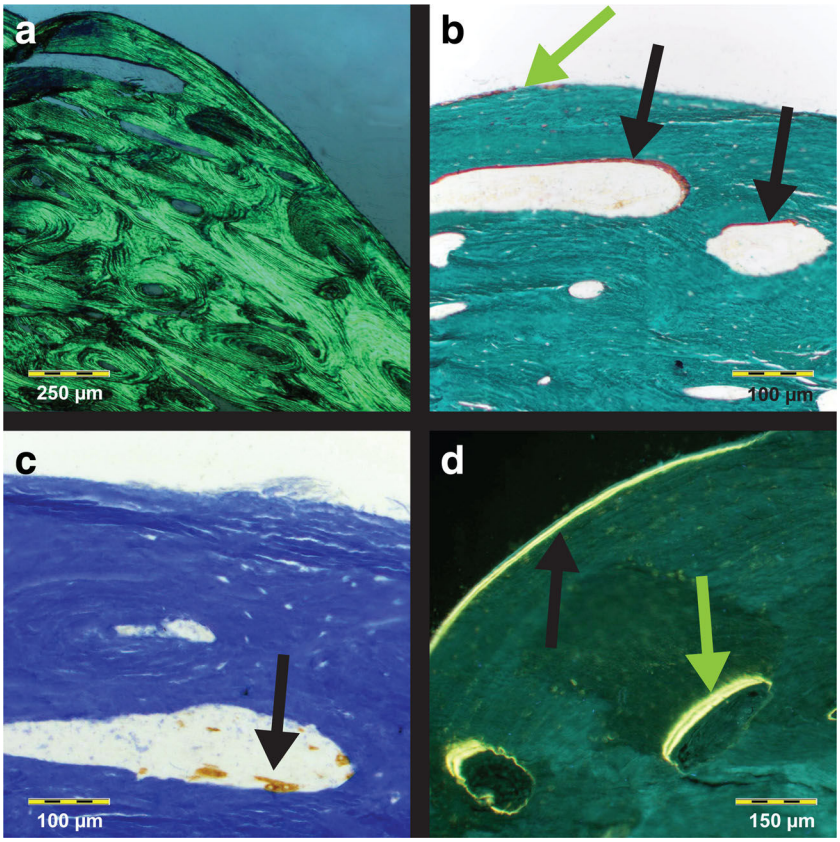


Fig. 3 Histological analysis. **a** Torus section seen in polarized microscopy showing normal cortical bone made of lamellar bone with true osteons and a central Haversian canal. **b** Torus section stained by Goldner's trichrome showing the presence of osteoid seams in two different locations: at the external free surface of the torus (*green arrow*) and inside the Haversian canals (*black arrows*). Note the asymmetric disposition of the osteoid seams which are laid on the canal surface closest to the free torus surface. The opposite surface of the canal is occupied by Howship's lacunae. **c** TRAcP-stained section showing asymmetric disposition of osteoclasts (*arrow*) which are laid on the canal surface furthest to the free torus surface. **d** Torus section showing double tetracycline labeling in the same locations as osteoid seams: at the external free surface of the torus (*white arrow*) and on the Haversian canals surface closest to the free torus surface (*green arrow*)

may also occur: neighboring teeth devitalization, palatine or lingual nerves injuries, and salivary ducts injuries [1, 28]. Surgery is usually performed under local anesthesia, and a general anesthesia is frequently required for TP excision [2]. The sub-periosteal detachment must provide a large operating field. The lesion can be removed in one piece or not, using osteotomes, burrs, and/or high speed turbines [1].

The overall prevalence of tori is variable and can reach 10 to 30% in some papers; it varies according to ethnic groups and gender [1, 2, 4–6, 29–41]. Tori are more frequent in some ethnic groups (Japanese, Caucasian, Norwegian, Indian, and Eskimo) [1–3, 6]. The prevalence also increases with age [2, 6]. TP seem to be more often present in females and TM in males [1, 4]. According to the anatomic location, the overall prevalence is about 20% for TP, 17% for TM, and 6% for TMax in the general population [2]. They are frequently bilateral in 80% of the cases [2]. TMax localized on the palatal side are sometimes classified as TP by some authors [2].

Table 2 Comparison of histomorphometric measures

	Normal	Ca	Ct
O.Th (μm)	<15	13.6 ± 0.7	12.0 ± 1.3
MAR (μm/day)	0.72 ± 0.12	0.92 ± 0.09[a]	0.66 ± 0.12

[a] Indicates a significant difference vs. normal MAR

The etiology remains unknown and could be multifactorial. An embryological theory has been proposed to explain the origin of TM with the existence of an alteration at the protruding medial lamina and the bending Meckel's cartilage formed during the development of the mandible [42]. A genetic origin, with autosomal dominant inheritance, is the most widely accepted theory today for TM, TP, and TMax [1–3]. However, a strictly genetic inheritance is found only in 30% of the cases [1]. Furthermore, a link between the occurrence of tori and genetic bone diseases has been shown [43]. Mutations in the low-density lipoprotein receptor-related protein 5 *(LRP5)* gene can result in osteosclerosis and may lead to a thickened or an elongated mandible with the occurrence of tori [44, 45]. Tori are also a characteristic of the Gardner's syndrome, an autosomal dominant

disease characterized by the development of gastrointestinal polyps and malignant transformation [46, 47].

On the other hand, mechanical factors related to the occlusal stress during mastication are advocated by many authors for TM [1–3, 6]. The occlusal force was found significantly higher in patients with TM by using a pressure sensitive sheet [6]. A significant correlation between the incidence of tori and the presence of abraded teeth due to bruxism has also been shown [7, 40]. In an animal model with paralysis of the masticatory muscles (*M. masseter* and *M. temporalis*) by the *Botulinum* toxin, the occurrence of a hypertrophic bone metaplasia at the enthesis of *M. Digastricus* was found [48]. It is well-known that an increased muscle activity can stimulate bone remodeling and increases bone apposition [49]. This fact supports the etiological hypothesis of mechanical causes related to a disequilibrium of occlusal forces due to an increased muscle activity. However, since tori have no topographical relation with muscle attachments, this pathological sequence cannot be extrapolated to human tori. So, an interplay between genetic and environmental factors cannot be excluded [7]. The cause of tori can therefore be explained by the conjunction of different factors: a torus is primarily a genetic trait, and environmental factors such as mechanical stress could be necessary for its development [4].

Few articles in the literature describe the histology of tori, and they often report histological organization similar to normal bone [1]. Tori are usually described made of lamellar cortical bone with the central presence of a cancellous network, sometimes made of woven bone, only when a large size is attained [1, 7, 8]. The presence of "lacunae" (Haversian canals), normal osteocytes, and scattered areas of connective tissue containing dilated blood vessels is also reported [2, 7]. The nature, texture, and structure of the bone constituting the tori correspond to a bone quality encountered in normal bone cell activity [50]. This explains that good clinical results are observed when tori are used for bone grafting [1, 15–19]. In the present study, an asymmetric active bone remodeling is reported for the first time. It leads to a unidirectional bone growth toward the oral cavity that explains the usual convex shape of tori and an escape to the mechanical stimuli related to occlusal forces. The use of undecalcified bone sections allowed the identification of osteoid tissue together with a histodynamic analysis after tetracycline labeling. These findings cannot be obtained using conventional histopathologic methods after decalcification and paraffin embedding. It is also the first time that microCT is used to characterize the external and internal microarchitecture of these tumors. This technique offers a unique possibility to evidence the 3D network of Haversian canals distribution in cortical bone [51]. This facility was used here to evidence the complex 3D distribution of Haversian canals in the tori.

The osteoid seam thicknesses determined in the present study were found normal (<15 μm) indicating the absence of osteomalacia. The Ca.MAR determined here was higher than normal MAR. This attests a high osteoblastic activity at the outer surface of the Haversian canals. The presence of woven bone reflects an active remodeling in 2/18 tori of the study. This might concern tori at an early stage before being completely remodeled in lamellar bone. Unfortunately, these two participants did not receive the double tetracycline labeling.

Tori are not similar to bone exostosis developing at the metaphysis of long bones in children and teenagers. Exostosis is a frequent benign cartilage-capped bony tumor. They may occur as solitary tumors (due to a possible dysregulation of osteoprogenitor cells) or as multiple tumors in the case of an autosomal genetic disorder (the multiple hereditary exostoses-MHE). A study found the pathologic presence of Al in exostosis in two thirds of the patients and the presence of Fe in half of the patients [12, 52]. In the present study, Fe and Al were never observed in the tori. This may seem surprising since tori develop inside the oral cavity, and ingesta are known to be a major source for Al to enter in the body [12].

Conclusion

Tori are a specific entity that develops on bones built by intramembranous ossification, and their shape seems to be determined by a specific asymmetric bone remodeling. This finding constitutes a specific histological feature allowing pathologists to differentiate tori from exostoses.

Acknowledgments Authors are greatly indebted to all surgeons who addressed bone samples to the laboratory and especially Pr. D. Goga and Dr. S. Badja. Authors also thank Mrs. Nadine Gaborit for her skillful assistance with microCT and histotechnology.

Compliance with ethical standards

Conflict of interest The authors declare that they have no conflict of interest.

Funding No financial disclosure.

Ethical approval All procedures performed in the present study were in accordance with the ethical standards of the institutional and national research committee and with the 1964 Helsinki declaration and its later amendments. This experimental protocol was approved by the local ethical committee of Angers University Hospital (France) and was done in accordance with the institutional guidelines of the French Ethical Committee (protocol number 2016-31).

Informed consent Informed consent was obtained from all individual participants included in the study.

Financial disclosure None.

References

1. Garcia-Garcia AS, Martinez-Gonzalez JM, Gomez-Font R, Soto-Rivadeneira A, Oviedo-Roldan L (2010) Current status of the torus palatinus and torus mandibularis. Med Oral Patol Oral Cir Bucal 15:e353–e360
2. Loukas M, Hulsberg P, Tubbs RS, Kapos T, Wartmann CT, Shaffer K, Moxham BJ (2013) The tori of the mouth and ear: a review. Clin Anat 26:953–960
3. Chossegros C, Foletti JM, Graillon N, Guyot L (2016) Oral torus or tori, why? Rev Stomatol Chir Maxillofac Chir Oral 117:59–61
4. Ihunwo AO, Phukubye P (2006) The frequency and anatomical features of torus mandibularis in a Black South African population. Homo 57:253–262
5. Yoshinaka M, Ikebe K, Furuya-Yoshinaka M, Hazeyama T, Maeda Y (2010) Prevalence of torus palatinus among a group of Japanese elderly. J Oral Rehabil 37:848–853
6. Yoshinaka M, Ikebe K, Furuya-Yoshinaka M, Maeda Y (2014) Prevalence of torus mandibularis among a group of elderly Japanese and its relationship with occlusal force. Gerodontology 31:117–122
7. Antoniades DZ, Belazi M, Papanayiotou P (1998) Concurrence of torus palatinus with palatal and buccal exostoses: case report and review of the literature. Oral Surg Oral Med Oral Pathol Oral Radiol Endod 85:552–557
8. Seah YH (1995) Torus palatinus and torus mandibularis: a review of the literature. Aust Dent J 40:318–321
9. Melsen F, Mosekilde L (1978) Tetracycline double-labeling of iliac trabecular bone in 41 normal adults. Calcif Tissue Res 26:99–102
10. Woo JK (1950) Torus palatinus. Am J Phys Anthropol 8:81–111
11. Chappard D (2014) Technical aspects: how do we best prepare bone samples for proper histological analysis? In Heymann D (ed) bone cancer: progression and therapeutic approaches, 2nd edn. Acad. Press; Elsevier Inc., London, pp 111–120
12. Chappard D, Bizot P, Mabilleau G, Hubert L (2016) Aluminum and bone: review of new clinical circumstances associated with Al(3+) deposition in the calcified matrix of bone. Morphologie 100:95–105
13. Dempster DW, Compston JE, Drezner MK, Glorieux FH, Kanis JA, Malluche H, Meunier PJ, Ott SM, Recker RR, Parfitt AM (2013) Standardized nomenclature, symbols, and units for bone histomorphometry: a 2012 update of the report of the ASBMR Histomorphometry Nomenclature Committee. J Bone Miner Res 28:2–17
14. Meunier PJ, Chavassieux P (1985) L'histomorphométrie moyen d'évaluation de la masse osseuse. Rev Rhum Malad Osteo-Art 52:669–673
15. Ephros H, Klein R, Sallustio A (2015) Preprosthetic surgery. Oral Maxillofac Surg Clin North Am 27:459–472
16. Wang CJ, Huang CB, Grossman SH, Pourati J (2016) Vertical ridge augmentation with mandibular lingual torus block graft : a case letter. J Oral Implantol 42:369–372
17. Moraes EF Jr, Damante CA, Araujo SR (2010) Torus palatinus: a graft option for alveolar ridge reconstruction. Int J Periodont Rest Dent 30:283–289
18. Hassan KS, Al-Agal A, Abdel-Hady AI, Swelam WM, Elgazzar RF (2015) Mandibular tori as bone grafts: an alternative treatment for periodontal osseous defects-clinical, radiographic and histologic morphology evaluation. J Contemp Dent Pract 16:192–200
19. Santhanakrishnan M, Rangarao S (2014) Mandibular Tori: a source of autogenous bone graft. J Ind Soc Periodontol 18:767–771
20. Kaneko K, Takahashi H (2014) Bisphosphonate-related osteonecrosis of the palatal torus. ORL J Otorhinolaryngol Relat Spec 76:353–356
21. Godinho M, Barbosa F, Andrade F, Cuzzi T, Ramos ESM (2013) Torus palatinus osteonecrosis related to bisphosphonate: a case report. Case Rep Dermatol 5:120–125
22. Durrani MA, Barwise JA (2000) Difficult endotracheal intubation associated with torus mandibularis. Anesth Analg 90:757–759
23. Manganaro AM, Faulk-Eggleston J, Schanzer RB, Dagostino M (1997) Osteitis in a torus mandibularis secondary to trauma. Gen Dent 45:74–77
24. Pasqual HN, Pasqual RJ (1968) Osteomyelitis of torus palatinus: report of a case. Oral Surg Oral Med Oral Pathol 25:532–533
25. Smith HW (1963) Osteitis of the torus palatinus with sequestration. Review of the literature and report of two cases. Arch Otolaryngol 78:811–815
26. Best SR, Kobler JB, Friedman AD, Barbu AM, Zeitels SM, Burns JA (2014) Effect of mandibular tori on glottic exposure during simulated suspension microlaryngoscopy. Ann Otol Rhinol Laryngol 123:188–194
27. MacInnis EL, Hardie J, Baig M, al-Sanea RA (1998) Gigantiform torus palatinus: review of the literature and report of a case. Int Dent J 48:40–43
28. Kun-Darbois JD, Pare A, Chemli H, Daher G, Breheret R (2014) Cervical crepitus after dental extraction. Rev Stomatol Chir Maxillofac Chir Orale 115:e17–e18
29. Romanos GE, Sarmiento HL, Yunker M, Malmstrom H (2013) Prevalence of torus mandibularis in Rochester, New York, region. N Y State Dent J 79:25–27
30. Sathya K, Kanneppady SK, Arishiya T (2012) Prevalence and clinical characteristics of oral tori among outpatients in Northern Malaysia. J Oral Biol Craniofac Res 2:15–19
31. Choi Y, Park H, Lee JS, Park JC, Kim CS, Choi SH, Cho KS, Chai JK, Jung UW (2012) Prevalence and anatomic topography of mandibular tori: computed tomographic analysis. J Oral Maxillofac Surg 70:1286–1291
32. Hiremath VK, Husein A, Mishra N (2011) Prevalence of torus palatinus and torus mandibularis among Malay population. J Int Soc Prev Community Dent 1:60–64
33. Sisman Y, Ertas ET, Gokce C, Akgunlu F (2008) Prevalence of torus palatinus in cappadocia region population of Turkey. Eur J Dent 2:269–275
34. Jainkittivong A, Apinhasmit W, Swasdison S (2007) Prevalence and clinical characteristics of oral tori in 1,520 Chulalongkorn University Dental School patients. Surg Radiol Anat 29:125–131
35. Yildiz E, Deniz M, Ceyhan O (2005) Prevalence of torus palatinus in Turkish schoolchildren. Surg Radiol Anat 27:368–371
36. Bruce I, Ndanu TA, Addo ME (2004) Epidemiological aspects of oral tori in a Ghanaian community. Int Dent J 54:78–82
37. Al-Bayaty HF, Murti PR, Matthews R, Gupta PC (2001) An epidemiological study of tori among 667 dental outpatients in Trinidad & Tobago, West Indies. Int Dent J 51:300–304
38. Gorsky M, Raviv M, Kfir E, Moskona D (1996) Prevalence of torus palatinus in a population of young and adult Israelis. Arch Oral Biol 41:623–625
39. Shah DS, Sanghavi SJ, Chawda JD, Shah RM (1992) Prevalence of torus palatinus and torus mandibularis in 1000 patients. Ind J Dent Res 3:107–110
40. Reichart PA, Neuhaus F, Sookasem M (1988) Prevalence of torus palatinus and torus mandibularis in Germans and Thai. Community Dent Oral Epidemiol 16:61–64
41. Ohno N, Sakai T, Mizutani T (1988) Prevalence of torus palatinus and torus mandibularis in five Asian populations. Aichi Gakuin Dent Sci 1:1–8
42. Rodriguez-Vazquez JF, Sakiyama K, Verdugo-Lopez S, Amano O, Murakami G, Abe S (2013) Origin of the torus mandibularis: an embryological hypothesis. Clin Anat 26:944–952

43. Hosoi T, Yoda T, Yamaguchi M, Amano H, Orimo H (2003) Elderly women with oral exostoses had higher bone mineral density. J Bone Miner Metab 21:120–122
44. Wang C, Zhang BH, Zhang H et al (2013) The A242T mutation in the low-density lipoprotein receptor-related protein 5 gene in one Chinese family with osteosclerosis. Intern Med 52:187–192
45. Boyden LM, Mao J, Belsky J, Mitzner L, Farhi A, Mitnick MA, Wu D, Insogna K, Lifton RP (2002) High bone density due to a mutation in LDL-receptor-related protein 5. N Engl J Med 346:1513–1521
46. Agrawal D, Newaskar V, Shrivastava S, Nayak PA (2014) External manifestations of Gardner's syndrome as the presenting clinical entity. BMJ Case Rep DOI. doi:10.1136/bcr-2013-200293
47. Bilkay U, Erdem O, Ozek C, Helvaci E, Kilic K, Ertan Y, Gurler T (2004) Benign osteoma with Gardner syndrome: review of the literature and report of a case. J Craniofac Surg 15:506–509
48. Kun-Darbois JD, Libouban H, Chappard D (2015) Botulinum toxin in masticatory muscles of the adult rat induces bone loss at the condyle and alveolar regions of the mandible associated with a bone proliferation at a muscle enthesis. Bone 77:75–82
49. Sugiyama T, Meakin LB, Browne WJ, Galea GL, Price JS, Lanyon LE (2012) Bones' adaptive response to mechanical loading is essentially linear between the low strains associated with disuse and the high strains associated with the lamellar/woven bone transition. J Bone Miner Res 27:1784–1793
50. Chappard D, Baslé MF, Legrand E, Audran M (2011) New laboratory tools in the assessment of bone quality. Osteoporos Int 22: 2225–2240
51. Cooper D, Turinsky A, Sensen C, Hallgrimsson B (2003) Quantitative 3D analysis of the canal network in cortical bone by micro-computed tomography. Anat Rec B 274:169–179
52. Chappard D, Mabilleau G, Moukoko D, Henric N, Steiger V, Le Nay P, Frin JM, De Bodman C (2015) Aluminum and iron can be deposited in the calcified matrix of bone exostoses. J Inorg Biochem 152:174–179

Clinical Oral Investigations

Bone mineralization and vascularization in bisphosphonate related osteonecrosis of the jaw: an experimental study in the rat

--Manuscript Draft--

Manuscript Number:	CLOI-D-17-00415R1
Full Title:	Bone mineralization and vascularization in bisphosphonate related osteonecrosis of the jaw: an experimental study in the rat
Article Type:	Original Article
Corresponding Author:	Daniel Chappard, MD, PhD faculty of Medicine Angers, france FRANCE
Corresponding Author Secondary Information:	
Corresponding Author's Institution:	faculty of Medicine
Corresponding Author's Secondary Institution:	
First Author:	Jean-Daniel KÜN-DARBOIS, MD
First Author Secondary Information:	
Order of Authors:	Jean-Daniel KÜN-DARBOIS, MD
	Hélène Libouban, Ph.D
	Guillaume Mabilleau, Ph.D
	Florence Pascaretti, HT
	Daniel Chappard, MD, PhD
Order of Authors Secondary Information:	
Funding Information:	French Minister of Research (Not applicable) — Not applicable
Abstract:	Objectives Pathogenesis of bisphosphonate-related osteonecrosis of the jaws (BRONJ) is not fully explained. An antiangiogenic effect of bisphosphonates (BPs) or an altered bone quality have been advocated. The aims of the present study were to analyze alveolar mandibular vascularization and bone quality in rats with BRONJ. Materials and Methods 38 Sprague-Dawley rats were randomized into 2 groups: zoledronic acid (ZA), n=27 and control (CTRL) n=11. The ZA group received a weekly IV injection of ZA (100µg/kg) during 10w. The CTRL group received saline. After 6w, extraction of the right mandibular molars was performed. Rats were sacrificed after 14w. Microtomography characterized bone lesions and vascularization after injection of a radio-opaque material. Raman microspectroscopy evaluated bone mineralization. Results 55 % of ZA rats presented bone exposure and signs of BRONJ. None sign was found at the left hemimandible in the ZA group and in the CTRL group. Vascular density appeared significantly increased in the right hemimandibles of the CTRL group compared to the left hemimandibles. Vascularization was reduced in the ZA group. A significantly increased of the mineral-to-amide ratio was found in the alveolar bone of ZA rats. Conclusions In a rat model of BRONJ, microtomography evidenced osteonecrosis in BRONJ. Raman spectroscopy showed an increased mineralization. Vascularization after tooth extraction was impaired by ZA. Clinical Relevance Prolonged BP administration caused an increase in the mineralization and a quantitative reduction of the vascularization in the alveolar bone; both factors might be

	involved concomitantly in the BRONJ pathophysiology.
Response to Reviewers:	see attached cover letter

Authors
Click here to download Authors' Response to Reviewers' Comments Cover_letter_Response_to_reviewers _CLOI-D-17-

université angers FACULTÉ DE MÉDECINE

GEROM Groupe d'Etudes "Remodelage Osseux et bioMatériaux"
LHEA : Laboratoire d'Histologie – Embryologie

▶ Pr. D. Chappard
Pr M. Audran
Dr B. Guillaume
Pr. E. Legrand
Pr. Ph. Mercier
H. Libouban

Angers, le 03/10/2017

To the Editor-in-chief:
Prof. Matthias Hanning
Clinical Oral Investigations

Dear Prof. Matthias Hanning,

We would like you to consider the revised research paper **# CLOI-D-17-00415** entitled:
"Bone mineralization and vascularization in bisphosphonate related osteonecrosis of the jaw: an experimental study in the rat"
for publication in Clinical Oral Investigations as an original paper.

Revisions have been made following the requests made by the reviewers and yourself. You will find a detailed response to the reviewers below. Revised text is highlighted in yellow in the revised version of the manuscript.

Reply to reviewer # 1

1. **Concern of the reviewer:** The study focusses on the role of bone remodeling in BRONJ, that do not fully explain the mechanisms of the etiopathogenesis of this disease. Some more aspects of other hypotheses could have been discussed.
Our response: An additional section has been added in the discussion to discuss the etiopathogenesis of BRONJ and other hypotheses.
Revised text: "In the present study, an impaired jaw bone vascularization due to an in vivo antiangiogenic effect of BPs was evidenced. The hypothesis of an inhibition of angiogenesis due to BPs in the pathophysiology of BRONJ is thus reinforced. Moreover, a significant increase of mineralization was found in the alveolar bone of ZA rats. This fact is in line with the pathophysiological hypothesis of altered bone quality with an increased stiffness of the bone matrix, due to a uniformity of the mineralization degree. The precise role of other pathophysiological hypotheses is still to be studied: direct toxicity of BPs for epithelial cells [31], reduced microcirculation of the gingiva, influence of BPs on immune cells leading to specific infections (Actynomyces) or osteomyelitis [22, 32]. A recent review summarizes all the currently advocated hypotheses [24]."

2. **Concern of the reviewer:** The animal model is worth to be reported but there are some more models producing reliable BRONJ lesions in rodents.
Our response: As mentionned in our first version, this is discussed in the first section of the discussion. Other animal models of BRONJ found in the literature are mentioned; they are all different and various rates of BRONJ are reported (from 0% to 100%). A recent review by Mitsimponas on the animal models of BRONJ is now added.
Revised text: „A recent review by Mitsimponas summarizes all animal models of BRONJ that have been developed (51)."

3. **Concern of the reviewer:** Figures 2 and 4 can be omitted.
Our response: As requested, figures 2 and 4 (and related text and legends) were removed from the manuscript. Other figures have been consequently renamed. There are now 6 figures instead of 8.
Revised text: not applicable

GEROM Groupe d'Etudes "Remodelage Osseux et bioMatériaux" UPRES EA 4658 LHEA- Laboratoire d'Histologie - Embryologie
IRIS- IBS Institut de Biologie en Santé, CHU d'Angers, 49933 Angers Cedex - France
Tel: 02 44 68 83 49 from abroad Tel: (33) 244 68 83 49
Fax : 02 44 68 83 50 Web site: http://www.gerom-angers.fr/>

4. **Concern of the reviewer:** In Figure 8 the selection of statistical significant correlations is unclear. In 4 groups the corresponding groups or the intra-animal groups should be correlated.
Our response: Figure 8 has been renamed figure 6. This figure has been completely recomputed to highlight the results. The bar graph is now substituted by a dot-and-whiskers plot and the non-significant values are in grey while the significant values remain in black. The figure caption has been rewritten.
Revised text: see figure 6. Caption: "○: CRTL rats, ●: ZA rats. Significant and non-significant differences appear between each group. "

5. **Concern of the reviewer:** Abbreviations should be explained when used the first time (even in the abstract)
Our response: A few abbreviations that were not previously explained at the first use are now explained adequately in the revised text, we apologize.
Revised text: "bisphosphonates (BPs)", "zoledronic acid (ZA)", "control (CTRL)"

We hope these revisions will suit the Editorial Board and yourself and thank you in advance.

Yours sincerely,

sProf. D. CHAPPARD

manuscript
Click here to download Manuscript
article_ZA_manuscript_CLOI-D-17-00415_revised.docx
Click here to view linked References

CLOI-D-17-00415 – Revised version

Bone mineralization and vascularization in bisphosphonate related osteonecrosis of the jaw: an experimental study in the rat

Jean-Daniel KÜN-DARBOIS, MD [a,b]; Hélène LIBOUBAN, PhD, [a]; Guillaume MABILLEAU, PhD, [a,c]; Florence PASCARETTI-GRIZON, HT, [a]; Daniel Chappard, MD, PhD, [a, c] *

[a] GEROM Groupe d'Etude Remodelage Osseux et bioMatériaux, LHEA, IRIS-IBS Institut de Biologie en Santé, Université d'Angers, CHU d'Angers, 4, rue Larrey, 49933 ANGERS Cedex - FRANCE.

[b] Service de chirurgie maxillo-faciale et stomatologie, CHU d'Angers, 4, rue Larrey, 49933 Angers Cedex - FRANCE.

[c] SCIAM Service Commun d'Imagerie et Analyses Microscopiques, IRIS-IBS Institut de Biologie en Santé, Université d'Angers, CHU d'Angers, 4, rue Larrey, 49933 ANGERS Cedex - FRANCE.

* Please send all correspondence to:

Daniel CHAPPARD, M.D., Ph.D.	**Tel :** (+33) 244 68 83 43
GEROM – LHEA, IRIS - IBS	**Fax :** (+33) 244 68 84 51
CHU d'Angers	**e-mail :** daniel.chappard@univ-angers.fr
49933 ANGERS Cedex - FRANCE	

ABSTRACT

Objectives

Pathogenesis of bisphosphonate-related osteonecrosis of the jaws (BRONJ) is not fully explained. An antiangiogenic effect of bisphosphonates (BPs) or an altered bone quality have been advocated. The aims of the present study were to analyze alveolar mandibular vascularization and bone quality in rats with BRONJ.

Materials and Methods

38 Sprague-Dawley rats were randomized into 2 groups: zoledronic acid (ZA), n=27 and control (CTRL) n=11. The ZA group received a weekly IV injection of ZA (100µg/kg) during 10w. The CTRL group received saline. After 6w, extraction of the right mandibular molars was performed. Rats were sacrificed after 14w. Microtomography characterized bone lesions and vascularization after injection of a radio-opaque material. Raman microspectroscopy evaluated bone mineralization.

Results

55 % of ZA rats presented bone exposure and signs of BRONJ. None sign was found at the left hemimandible in the ZA group and in the CTRL group. Vascular density appeared significantly increased in the right hemimandibles of the CTRL group compared to the left hemimandibles. Vascularization was reduced in the ZA group. A significantly increased of the mineral-to-amide ratio was found in the alveolar bone of ZA rats.

Conclusions

In a rat model of BRONJ, microtomography evidenced osteonecrosis in BRONJ. Raman spectroscopy showed an increased mineralization. Vascularization after tooth extraction was impaired by ZA.

Clinical Relevance

Prolonged BP administration caused an increase in the mineralization and a quantitative reduction of the vascularization in the alveolar bone; both factors might be involved concomitantly in the BRONJ pathophysiology.

244 words

Keywords

Bisphosphonate; BRONJ; rat model; osteonecrosis; vascularization; Raman; microtomography.

Running title: Mineralization and vascularization in BRONJ

Introduction

Bisphosphonates (BPs) are structural analogs of inorganic pyrophosphate and they are resistant to enzymatic hydrolysis. They have a strong affinity for the hydroxyapatite crystal and can remain several years in bone. They inhibit bone resorption by interfering with the mevalonate pathway in the osteoclast [1]. A large number of studies has confirmed their interest in reducing the incidence of osteoporosis-related fractures by increasing bone mineral density (BMD) [2, 3]. In human, intravenous amino-BPs injections are used in several indications such as osteoporosis, bone metastases, multiple myeloma or hypercalcemia associated with an increased osteoclast number [4, 5].

Antiresorptive drug related osteonecrosis of the jaw (ARONJ) is a major adverse event due to antiresorptive treatments and was first described with BP [6-9]. It is clinically defined as an area of exposed bone of the jaws that do not heal within eight weeks after identification in a patient with an antiresorptive drug history and without irradiation therapy to the craniofacial region [10, 11]. The incidence of bisphosphonate related osteonecrosis of the jaw (BRONJ) ranges between 1% to 10% in patients undergoing IV BP therapy [12, 13]. The highest risk is in patients with multiple myeloma receiving iv zoledronic acid (ZA) treatment [14]. BRONJ is more often located at the mandible (70%) than at the maxilla (30%) [15]. A triggering factor with bone exposure (mainly consisting in tooth extractions) is found in the majority of cases [10, 15-18]. A BP therapy is often considered as a contraindication to dental implant treatment [19-21].

The pathogenesis of BRONJ seems multifactorial but is not fully explained yet [22-24]. An explanation could be an impairment of jaw bone vascularization due to an antiangiogenic effect of BPs [25-29]. The role of bone quality with an increased stiffness of the bone matrix, due to an uniformity of the mineralization degree, has also been advocated [30]. Another explanation could be a direct toxicity of BPs for epithelial cells combined with a reduced microcirculation of the gingiva [22, 31]. The development of chronic osteomyelitis due to a contamination with *Actynomyces* is reported [22, 32].

An animal model mimicking the clinical features of BRONJ may help to understand the pathophysiological mechanisms of BRONJ and evaluate new treatments. Several models have been described in laboratory animals but none of them reproduce strictly the clinical characteristics observed in the human disease [33-36].

The aims of the present study were to provoke BRONJ in the rat and to analyze the mandibular vascularization after intravascular injection of a radio-opaque material. The quality of the bone material was also assessed by Raman microspectrometry and quantitative backscattered electron imaging (qBEI) to evaluate the mineralization degree of the bone matrix.

Material and methods

Animals and experimental procedure

Animal care and experimental protocols were approved by the French Ministry of Research and were done in accordance with the institutional guidelines of the French Ethical Committee (protocol agreement number 01857.01), the European Communities Council Directive of 24 November 1986 (86/609/EEC) and under the supervision of authorized investigators. The flow chart of the study appears in (Fig. 1). Fifteen weeks-old male Sprague-Dawley rats (n=38), weighing 486.3 ± 10.8 g, were used for the study (Janvier-Labs, Le Genest-Saint-Isle, France). They were acclimated for two weeks to the local vivarium conditions (24 °C and 12 h/12 h light dark cycle) where they were given standard laboratory food (UAR, Villemoison-sur-Orge, France) and water *ad libitum*. Rats were randomized into 2 groups: a control group (CTRL, n=11) and a zoledronic acid group (ZA, n=27). Rats from the ZA group were anesthetized with isoflurane and injected intravenously with ZA (Zometa®, Novartis Pharma GmbH, Nuremberg, Germany) at a dose of 100 µg/kg, once a week, during 10 weeks. Injections were performed in a tail vein. Each animal of the ZA group received a total dose of ZA of 1000 µg/kg at the end of the protocol. Rats of the CTRL group were similarly injected with equivalent volume of saline solution. At sixth week, extractions of the 3 right mandibular molars were performed in rats of both group (see below). Rats were weighted weekly and sacrificed 14 weeks after the first injection by CO_2 inhalation. Visual examination of mandibular molar regions was performed in order to look for exposed bone. Rats were then randomized in two subgroups: subgroup A and subgroup B. $CTRL_A$ and ZA_A groups were used for microCT, Raman microspectrometry and qBEI analysis; $CTRL_B$ and ZA_B groups were injected with barium sulfate for vascularization analysis. Hemimandibles were then dissected, defleshed and fixed in formalin during 24 hours and transferred in absolute acetone.

Tooth extractions

Extraction of the molars was done as follows. General anesthesia was induced by intraperitoneal injection of 100 mg/kg ketamine (Renaudin, Aïnhoa, France) and 10 mg/kg xylazine (Rompun® 2%, Bayer, Leverkusen, Germany). Analgesia was obtained using subcutaneous injections of buprenorphine (Vetergesic®, Sogeval, Laval, France) at a dose of 0.03 mg/kg, half an hour before surgical procedure and postoperatively if needed. Tooth extraction was performed using rodent specific instrumentation (Coveto, Montaigu, France). Adequate exposure was obtained using a mouth gag and rodent cheek dilator with lingual traction. Each tooth was removed progressively using a Crossley molar luxator and a molar extractor. The first molar was separated into two halves with the luxator before removing. If needed, hemostasis was obtained with simple compression and no suture was done. No additional drug and no antibiotic was given. Rats were closely monitored until awakening.

Microcomputed tomography (microCT)

MicroCT of the right and left hemimandibles was performed using a Skyscan 1172 X-ray computerized microtomograph (Bruker microCT, Kontich, Belgium) equipped with an X-ray tube working at 70 kV/ 100 µA. Bones were placed in Eppendorf's tubes filled with water to prevent desiccation. The tubes were fixed on a brass stub with plasticine. Analysis was done with a pixel size corresponding to 10.5 µm; the rotation step was fixed at 0.25° and exposure was done with a 0.5 mm aluminum filter. For each hemimandible, a stack of 2D-sections was obtained and reconstructed using NRecon software (Bruker) and analyzed with CTan software (Skyscan, release 1.13.11.0). Frontal, axial and sagittal sections of alveolar regions were then obtained from 3D models using a surface-rendering program (Ant, release 2.0.5, Skyscan, Belgium). Three dimensional reconstructions were obtained using CTVox software (Skyscan, release 2.5).

Raman microspectroscopic analysis

The left hemimandibles were used to evaluate bone quality at the alveolar bone where no tooth extraction had been done. Bone samples were immersed in sodium hypochlorite (50% in water) to remove organic tissues, rinsed 4 times in ultrapure water and dried at room temperature. They were then polished on a grinding machine (Struers, Copenhagen, Denmark) using ascending grads of polishing paper (1200, 2000, and 4000) during 2 min each to expose the alveolar bone

and the teeth roots. Bones were affixed onto glass slides with a hand press to obtain a horizontal surface parallel to the slide. Raman analyses were performed on a Senterra microscope with the OPUS 5.5 software (Bruker optic, Ettlingen, Germany). The excitation laser wavelength was 785 nm with an excitation power of 50mw and 8-12 cm^{-1} spectral resolution to avoid the autofluorescence of the collagen. For each sample the final spectrum was obtained by averaging twenty scans of 40 seconds. Average Raman spectra were obtained for control alveolar bone, ZA impregnated alveolar bone and dehydrated ZA from all rats from group A. An automatic baseline was applied and four physicochemical parameters were determined from spectra [37]:

- Mineralization (mineral to matrix ratio) is the intensity ratio between the ν_1PO_4 (960 cm^{-1}) peak to the matrix bands (amide I 1667 cm^{-1} or amide III 1243 cm^{-1}).
- Carbonate substitution is the intensity ratio between B-type CO_3^{2-} (1071cm^{-1}) band and the ν_1PO_4 (960cm^{-1}) band.
- Relative proteoglycan (PG) content is the ratio of GAG/CH_3 (1365-1390 cm^{-1}) to the amide III band.
- Crystallinity is the inverse of the full width at half maximum intensity of the ν_1PO_4 band (960 cm^{-1}).

ZA spectrum was obtained from a sample of dehydrated ZA using the same procedure.

Quantitative backscattered electron imaging (qBEI) and energy-dispersive X-ray spectroscopy (EDS)

Quantitative backscattered electron imaging was employed to determine the bone mineral density distribution (BMDD) in the same regions of alveolar bone as Raman analysis as previously reported. This methodology has been described in full details elsewhere [38, 39]. Bone samples were embedded undecalcified in poly (methylmethacrylate) and the blocks were polished to a 0.5-µm finish with diamond particles, carbon-coated and observed with a scanning electron microscope (EVO LS10, Carl Zeiss Ltd, Nanterre, France) equipped with a five quadrants semi-conductor backscattered electron detector. The microscope was operated at 20 keV with a probe current of 250 pA and a working distance of 15 mm. The alveolar bone area located and imaged at a 100X nominal magnification, corresponding to a pixel size of 1.1 µm per pixel. Four images per samples were taken and the gray levels distribution of each image was analyzed with a lab-made routine in ImageJ. Three variables were obtained from the bone mineral density distribution: Ca_{peak} as the most frequently observed calcium concentration,

Ca_{mean} as the average calcium concentration and Ca_{width} as the width of the histogram at half maximum of the peak.

Furthermore, the elemental atomic bone composition was determined by energy-dispersive X-ray spectroscopy (EDS) with a 20mm² X-max detector (Oxford Instruments, Abingdon, UK) fitted in the SEM and the Inca software. The Ca/P ratio was computerized as the atomic ratio between calcium and phosphorus percent.

Analysis of bone vascularization

Catheterism of the right common carotid artery was done using a 24G catheter (Introcan Safety®, BBraun, Melsungen, Germany) under a binocular microscope (Leica, Weitzlar, Germany) with microsurgical specific instrumentation. Ligature of the catheter was done with an 8/0 suture thread. Venotomy of the right internal jugular vein was done to ensure blood drainage. First, a vascular rinse was performed using 5 ml of heparinized saline (Héparine sodique, Panpharma, Fougères, France). A solution composed of 5% of gelatin and 95% of a commercial barium sulfate solution used for digestive X-ray analysis (Micropaque®, Guerbet, Roissy, France) was prepared by heating at 37°C. Then, 4 ml of this warmed solution were injected through the catheter. Ligature of the right and left common carotid arteries and the right and left internal jugular veins were done so that the solution remains in the injected vessels. The injected animals were placed in a cold room (4°C) for 24 hours to allow hardening of the vascular injection fluid. Hemimandibles were then dissected, defleshed and fixed in formalin until use.

MicroCT examination was done as described for microvascular analysis [40]. Briefly, a first microCT acquisition was done as described above. Samples were then decalcified using a mixture composed of 4 % of formic acid, 10 % of formalin in distilled water, changed twice a day, during 6 days. Decalcified samples were then rinsed in tap water to remove acid remnants and kept in formalin until use. A second microCT was then performed with the same procedure except for the rotation step which was fixed at 0.10° to allow better detail identification. So, for each hemimandible, two stacks of 2D-sections were obtained (undecalcified and decalcified samples) and reconstructed using NRecon software (Bruker). 3D vascular reconstructions were obtained using VG Studio MAX 2.1 software (Volume Graphics GmbH, Heidelberg, Germany). 3D vascular volume of the alveolar bone (VV/TV_{ALV}, in %) was measured using CTAn software (Bruker). The reference volume of alveolar bone tissue TV_{ALV} was selected by a routine facility of the software after overimposing the 3D model obtained on the 1st scan prior

to decalcification to the 2nd scan of the decalcified mandible. Technical details have been described previously [40].

Statistical analysis

Statistical analysis was performed using the Systat statistical software release 13.0 (Systat Software Inc., San José, CA). All data were expressed as mean ± standard error of the mean (SEM). Differences between groups were analyzed by a non-parametric test (Kruskall-Wallis). Differences were considered significant when $p<0.05$.

Results

Animal loss and body weight

Eight rats died before sacrifice: 3 in the CTRL group and 5 in the ZA group. One rat died after an intravenous injection of ZA, seven rats died during the surgical procedure. In each group, the remaining rats were randomized in two subgroups: subgroup A and subgroup B (Fig. 1).
All rats gained weight during all time period of the study. Weight gain was 9.8 ± 0.7 g per week (12.5 ± 1.6 g for the CTRL group and 8.7 ± 0.7 g for the ZA group). A weight loss occurred during the two weeks following the tooth extraction procedure. The average weight loss was -12.6 ± 2.2 g (i.e. -2.16% of pre-extraction weight) with -19.7 ± 5.8 g for the CTRL group and -10.1 ± 1.8 g for the ZA group. No statistical difference was found between groups for any of these parameters at any time.

Macroscopic examination

Fifty-five percent of ZA treated rats had an impaired healing with BRONJ lesions, consisting in mucosal ulcerations with large bone exposures, at the teeth extraction site (Fig. 2). No exposed mandibular bone was found in other locations. Normal wound healing with intact overlying mucosa and no bone exposure was observed in all rats of the CTRL group.

MicroCT analysis

MicroCT analysis revealed typical signs of BRONJ: cortical osteolysis (n=9), periosteal reaction (n=4) and bone sequestration (n=2) at the right molar area in rats of the ZA_A group (n=11). 2D sections were obtained by a virtual cutting plane passing through the socket of the first molar or horizontally to identify periosteal reaction and bone sequestration (Fig. 3). No signs of BRONJ were found on the left hemimandibles of the ZA_A group nor on the right and left hemimandibles of the CTRL group. Tooth root remnants were noticed in the extraction sockets.

Raman analysis

The averaged Raman spectra of control alveolar bone, ZA impregnated alveolar bone and ZA are shown in Fig. 4. No difference between the spectra of control bone and ZA impregnated bone could be evidenced. The imidazole ring characteristic of ZA was undetectable in ZA impregnated bone. Mineralization ratio was found significantly increased in the ZA_A group (Table 1). Other parameters derived from Raman spectra did not significantly differ between ZA_A and $CTRL_A$ animals.

SEM-qBEI and EDS analysis

No significant differences were found for any of the qBEI parameters (Ca_{mean}, Ca_{peak} and Ca_{width}) between ZA_A and $CTRL_A$ animals (Table 2). The Ca/P ratio did not significantly differ between the ZA_A and $CTRL_A$ groups.

Vascularization analysis

3D reconstructions of micro vessels of alveolar bone were obtained (Fig. 5). The pedicle of the *nervus alveolaris inferior* was well seen and could be easily followed, the technique was also able to characterize the very thin capillaries in the alveolar region. On the 3D reconstructions, the vascular density seemed increased in the right hemimandible of $CTRL_B$ group after the tooth extraction. The vascular density also appeared reduced in the right hemimandibles of the ZA_B group but no difference was noticed at naked eye on the 3D reconstructions between the density of the vascular bed on the left side of the CTRL and ZA animals. When VV/TV_{ALV} was measured, a significant difference was evidenced between the left and right side of the CTRL

group (Fig. 6). A significant reduction of the vascular bed was also evidenced when comparing the right side of the ZA_R and the $CTRL_R$ group.

Discussion

Clinically exposed bone is the main element of the clinical diagnosis of BRONJ in human. Our animal model's characteristics are close to those found in the literature [33, 35, 41-44]. The rat is the most used animal model for the development of bisphosphonates osteonecrosis of the jaw [33]. ZA doses used in the present study were very high (400 µg / kg per month) and are equivalent to those used in clinical practice for the treatment of myeloma in human [27, 45]. The use of high doses and long lasting treatment are known to significantly increase the chance to develop BRONJ lesions [46]. We chose to use IV injection because it has the highest success rates in models of the literature and because it is similar to human clinic [42, 45, 47]. Tooth extraction was selected here as a triggering factor since BRONJ occurs after a tooth extraction in 60% of patients [15]. Similarly, we performed mandibular rather than maxillary tooth extraction, despite its difficulty, because BRONJ occurs more frequently at the mandible in 70% of the patients [48, 49]. Selected animals were free of diseases for which zoledronic acid is administered in human (e.g. osteoporosis, myeloma, bone metastasis) and of other conditions, cofactors, co-existing systemic diseases and concomitant medications. The aim was to avoid confounding factors and to demonstrate that BRONJ induction was only due to BPs. No additional drugs, such as dexamethasone and antibiotics were given to animals. Additional drugs do not seem to give better results in BRONJ induction [33]. Macroscopic observations showed a bone exposure in 55% of the ZA treated animals and none in the control animals in the present study. Animal models aim at getting a high incidence of BRONJ: in the literature, varying rates of exposed bone are found in treated animals (0%, 14%, 33%, 67% and 100%) and none in controls [33, 42, 45, 47, 50]. A recent review by Mitsimponas summarizes all animal models of BRONJ that have been developed [51]. However, bone exposure may be difficult to evidence because of its limited size and it should not be the only element to consider in assessing the quality of a BRONJ model. There was no significant weight difference between the 2 groups in the study. Only three comparable models in the literature report a statistical analysis of weight [41, 44, 52]. Weight is a parameter reflecting the animal welfare. Our results show that our model with tooth extraction and ZA has no negative impact on the animal.

In addition to clinical examination, microCT is used to assess the diagnosis of BRONJ in the rat since it provides three-dimensional images, two-dimensional re-slicing in different planes. Numerous images of periosteal apposition and cortical erosion were found in ZA treated rats. This has previously been reported in animal models of BRONJ [42, 53, 54]. Images of bone sequestration were also found in the present study as in human BRONJ [53].

Raman aimed at investigating the presence of ZA in the bone matrix and to see the influence of this bisphosphonate on the mineral crystallinity. ZA was undetectable in the impregnated bone of ZA rats because the tissue concentration are very low [55]. In human bone sequesters from BRONJ patients, the characteristic bands of ZA could not be evidenced and an increase in the mineral to organic ratio was observed [56]. In another study, a decrease of crystallinity, determined with a 632 nm laser, was found in the newly-formed bone in a calvaria defect in ZA treated rats [57]. No change in crystallinity was found in the present study but the wavelength of our laser (785 nm) was different and another study reporting the Raman spectrum of ZA at 514 nm also show differences [58]. A SEM study with qBEI analysis found an increase in the calcium content of the bone matrix in animals treated during three years [59]. In the present study, this technique failed to identify similar changes, probably due to the shorter duration of the experiment. In a microCT experiment in ZA-treated rats treated up to 6 months, bone mineral density was found increased at the jaw [60]. Bone quality in rats treated with alendronate (another amino bisphosphonate) was found altered with an increased bone mineral density [61].

Analysis of the micro-vascularization showed that tooth extraction in CTRL animals increased vascularization in the mandibular alveolar bone. An increased capillary ingrowth is a normal reaction following tooth extraction [62]. ZA administration impaired this reactional increased vascular volume on the right side of ZA_A rats. In vitro antiangiogenic effects of BP have been reported in several publications [26, 63, 64]. Some animal or human studies have found that BPs decrease the micro-vessel density and circulating endothelial cells and angiogenesis [25, 27-29, 47, 65-67]. This is the first study that analyzed bone micro-vascular bed in an animal model of BRONJ by vascular opacification and microCT.

In the present study, an impaired jaw bone vascularization due to an *in vivo* antiangiogenic effect of BPs was evidenced. The hypothesis of an inhibition of angiogenesis due to BPs in the

pathophysiology of BRONJ is thus reinforced. Moreover, a significant increase of mineralization was found in the alveolar bone of ZA rats. This fact is in line with the pathophysiological hypothesis of altered bone quality with an increased stiffness of the bone matrix, due to a uniformity of the mineralization degree. The precise role of other pathophysiological hypotheses is still to be studied: direct toxicity of BPs for epithelial cells [31], reduced microcirculation of the gingiva, influence of BPs on immune cells leading to specific infections (*Actynomyces*) or osteomyelitis [22, 32]. A recent review summarizes all the currently advocated hypotheses [24].

In the present study we aimed at provoking BRONJ in a rat model with mandibular tooth extraction. Clinical examination and MicroCT evidenced numerous signs of BRONJ. Our animal model of BRONJ has therefore some limitations. Mandibular molars extraction is not easy to perform since root remnants were observed. However, this created mandible osteonecrosis, a condition that reflects the human disease which is more frequently observed at the mandible. The clinical and radiographic success rates obtained were lower than expected but fitted in well with similar studies reported in the literature.

Conclusion

The animal model described in the present study includes many elements of microCT diagnosis of BRONJ that are similar to what is found in computed tomography in human BRONJ [68]. Raman spectroscopy evidenced an increased mineral to matrix ratio in the alveolar bone after a prolonged treatment with ZA. SEM-qBEI evidenced no increase in the calcium content of the bone matrix in treated rats. Vascularization was increased after tooth extraction in the alveolar bone of control animals but was impaired by zoledronic acid in the same location in treated rats.

Table 1

Comparison between averages of spectroscopic parameters for each group after Raman analysis.

	ZA	CTRL	*p*
Mineral/amide I	38.94 ± 1.40	32.94 ± 1.91	0.03
Mineral/amide III	72.10 ± 4.94	52.05 ± 4.70	0.02
Carbonate substitution	0.133 ± 0.002	0.131 ± 0.005	NS
Crystallinity	111×10^{-6}	111×10^{-6}	NS
PG content	0.198 ± 0.071	0.173 ± 0.043	NS

The gray boxes highlight a significant difference between ZA *vs*. CTRL

Table 2

qBEI and EDS parameters measured on the alveolar bone of the left hemimandibles

	ZA	CTRL	*p*
Ca_{peak} (%Ca)	18.57 ± 0.22	18.79 ± 0.34	NS
Ca_{mean} (%Ca)	18.1 ± 0.19	18.33 ± 0.3	NS
Ca_{width} (%Ca)	3.3 ± 0.13	3.32 ± 0.17	NS
Ca/P	1.423 ± 0.008	1.420 ± 0.018	NS

Author contributions

Jean-Daniel KÜN-DARBOIS performed animal handling, zoledronic acid injections, teeth extractions and wrote the paper. Hélène LIBOUBAN performed animal handling and zoledronic acid injections, Guillaume MABILLEAU performed the SEM-qBEI analysis, Florence PASCARETTI performed Raman analysis, Daniel CHAPPARD designed the study, performed microCT analysis and wrote parts of the manuscript.

Compliance with Ethical Standards

Conflicts of interest

The authors declare that they have no conflicts of interest concerning this article.

Funding

No financial disclosure.

Ethical approval

All procedures performed in the present study were in accordance with the ethical standards of the institutional and national research committee and with the 1964 Helsinki declaration and its later amendments. This experimental protocol was approved by the local ethical committee of Angers University Hospital (France) and was done in accordance with the institutional guidelines of the French Ethical Committee (protocol number 2016-31).

Acknowledgments

The authors thank Mrs. N. Retailleau and S. Lemière for microCT. This work was made possible by funding from the French Minister of Research. Authors are greatly indebted to the SCAHU (Service commun d'animalerie hospitalo-universitaire) of Angers, especially to P. Legras and J. Roux for their help with the animal care.

LEGENDS OF FIGURES

Fig. 1. Flow chart of the study showing animal repartitions in control group (CTRL) and Zoledronic acid group (ZA) and in subgroup A ($CTRL_A$ and ZA_A) and subgroup B ($CTRL_B$ and ZA_B).

Fig. 2. Macroscopic aspects of extraction sites after sacrifice showing bone exposure in a ZA treated rat (A) and normal wound healing with no bone exposure in a CTRL rat (B). The scale bars stand for 2 mm.

Fig. 3. MicroCT analysis of alveolar bone modifications. 2D frontal sections of the right (A) and left (B) hemimandible of a rat of the ZA group. (C) 2D axial section of a right hemimandible of a rat of the ZA group showing periosteal reaction on the lingual side (black arrows) and bone sequestration (arrowhead) on the vestibular side. Tooth root remnants can be noticed in the extraction sockets.

Fig. 4. Raman spectra of control alveolar bone (A), ZA impregnated alveolar bone (B) and dehydrated ZA (C). ZA spectrum is undetectable in the ZA impregnated bone.

Fig. 5. (A) 3D MicroCT of the vascular bed in the molar areas of a left side of a CTRL rat (B) right side of a CTRL rat having had a molar extraction showing and increase in vessel density; (C) right side of a ZA_A rat with a decreased vascular bed on the right side. White arrows show the alveolar areas. Green arrows show the vascular pedicle of the *nervus alveolaris inferior*. In all images, the scale bar stands for 4 mm.

Fig. 6. 3D vascular volume of the alveolar bone (VV/TV_{ALV}) for each group. ○: CRTL rats, ●: ZA rats. Significant and non-significant differences appear between each group.

REFERENCES

1. Russell RGG (2011) Bisphosphonates: the first 40 years. Bone 49:2-19
2. Harrington JT, Ste-Marie LG, Brandi ML, Civitelli R, Fardellone P, Grauer A, Barton I, Boonen S (2004) Risedronate rapidly reduces the risk for nonvertebral fractures in women with postmenopausal osteoporosis. Calcif Tissue Int 74:129-135
3. Pols HA, Felsenberg D, Hanley DA, et al. (1999) Multinational, placebo-controlled, randomized trial of the effects of alendronate on bone density and fracture risk in postmenopausal women with low bone mass: results of the FOSIT study. Fosamax International Trial Study Group. Osteoporos Int 9:461-468
4. Terpos E (2012) Bisphosphonate anticancer activity in multiple myeloma. Anti-cancer agents in medicinal chemistry 12:123-128
5. Musto P, Petrucci MT, Bringhen S, et al. (2008) A multicenter, randomized clinical trial comparing zoledronic acid versus observation in patients with asymptomatic myeloma. Cancer 113:1588-1595
6. Wang J, Goodger NM, Pogrel MA (2003) Osteonecrosis of the jaws associated with cancer chemotherapy. J Oral Maxillofac Surg 61:1104-1107
7. Marx RE (2003) Pamidronate (Aredia) and zoledronate (Zometa) induced avascular necrosis of the jaws: a growing epidemic. J Oral Maxillofac Surg 61:1115-1117
8. Rachner TD, Platzbecker U, Felsenberg D, Hofbauer LC (2013) Osteonecrosis of the jaw after osteoporosis therapy with denosumab following long-term bisphosphonate therapy. Mayo Clin Proc 88:418-419
9. Ruggiero S (2014) Osteonecrosis of the jaw: BRONJ and ARONJ. Fac Dent J 5:90-93
10. Ruggiero SL, Dodson TB, Assael LA, Landesberg R, Marx RE, Mehrotra B, Task Force on Bisphosphonate-Related Osteonecrosis of the Jaws AAoOMS (2009) American Association of Oral and Maxillofacial Surgeons position paper on bisphosphonate-related osteonecrosis of the jaw - 2009 update. Aust Endodont J 35:119-130
11. Ruggiero SL, Mehrotra B (2009) Bisphosphonate-related osteonecrosis of the jaw: diagnosis, prevention, and management. Annu Rev Med 60:85-96
12. Vahtsevanos K, Kyrgidis A, Verrou E, et al. (2009) Longitudinal cohort study of risk factors in cancer patients of bisphosphonate-related osteonecrosis of the jaw. J Clin Oncol 27:5356-5362
13. Walter C, Al-Nawas B, Frickhofen N, Gamm H, Beck J, Reinsch L, Blum C, Grotz KA, Wagner W (2010) Prevalence of bisphosphonate associated osteonecrosis of the jaws in multiple myeloma patients. Head Face Med 6:11
14. Migliorati CA, Woo SB, Hewson I, Barasch A, Elting LS, Spijkervet FK, Brennan MT (2010) A systematic review of bisphosphonate osteonecrosis (BON) in cancer. Supp Care Cancer 18:1099-1106
15. Woo SB, Hellstein JW, Kalmar JR (2006) Narrative [corrected] review: bisphosphonates and osteonecrosis of the jaws. Ann Intern Med 144:753-761
16. Marx RE, Cillo JE, Jr., Ulloa JJ (2007) Oral bisphosphonate-induced osteonecrosis: risk factors, prediction of risk using serum CTX testing, prevention, and treatment. J Oral Maxillofac Surg 65:2397-2410
17. Marx RE, Sawatari Y, Fortin M, Broumand V (2005) Bisphosphonate-induced exposed bone (osteonecrosis/osteopetrosis) of the jaws: risk factors, recognition, prevention, and treatment. J Oral Maxillofac Surg 63:1567-1575

18. Boonyapakorn T, Schirmer I, Reichart PA, Sturm I, Massenkeil G (2008) Bisphosphonate-induced osteonecrosis of the jaws: prospective study of 80 patients with multiple myeloma and other malignancies. Oral oncology 44:857-869
19. Diz P, Scully C, Sanz M (2013) Dental implants in the medically compromised patient. J Dent 41:195-206
20. Kwon T-G, Lee C-O, Park J-W, Choi S-Y, Rijal G, Shin H-I (2014) Osteonecrosis associated with dental implants in patients undergoing bisphosphonate treatment. Clin Oral Implants Res 25:632-640
21. Ata-Ali J, Ata-Ali F, Peñarrocha-Oltra D, Galindo-Moreno P (2016) What is the impact of bisphosphonate therapy upon dental implant survival? A systematic review and meta-analysis. Clin Oral Implants Res 27:e38-e46
22. Rasmusson L, Abtahi J (2014) Bisphosphonate associated osteonecrosis of the jaw: an update on pathophysiology, risk factors, and treatment. Int J Dent 2014:471035
23. Cardemil C, Thomsen P, Larsson Wexell C (2015) Jaw Bone Samples From Bisphosphonate-Treated Patients: A Pilot Cohort Study. Clin Implant Dent Relat Res 17 Suppl 2:e679-691
24. Voss PJ, Poxleitner P, Schmelzeisen R, Stricker A, Semper-Hogg W (2017) Update MRONJ and perspectives of its treatment. J Stomatol Oral Maxillofac Surg 118:232-235
25. Pabst AM, Ziebart T, Ackermann M, Konerding MA, Walter C (2014) Bisphosphonates' antiangiogenic potency in the development of bisphosphonate-associated osteonecrosis of the jaws: influence on microvessel sprouting in an in vivo 3D Matrigel assay. Clin Oral Invest 18:1015-1022
26. Petcu EB, Ivanovski S, Wright RG, Slevin M, Miroiu RI, Brinzaniuc K (2012) Bisphosphonate-related osteonecrosis of jaw (BRONJ): an anti-angiogenic side-effect? Diagn Pathol 7:78
27. Sharma D, Ivanovski S, Slevin M, Hamlet S, Pop TS, Brinzaniuc K, Petcu EB, Miroiu RI (2013) Bisphosphonate-related osteonecrosis of jaw (BRONJ): diagnostic criteria and possible pathogenic mechanisms of an unexpected anti-angiogenic side effect. Vascular cell 5:1
28. Wehrhan F, Stockmann P, Nkenke E, Schlegel KA, Guentsch A, Wehrhan T, Neukam FW, Amann K (2011) Differential impairment of vascularization and angiogenesis in bisphosphonate-associated osteonecrosis of the jaw-related mucoperiosteal tissue. Oral Surg Oral Med Oral Pathol Oral Radiol Endod 112:216-221
29. Stresing V, Fournier PG, Bellahcene A, Benzaid I, Monkkonen H, Colombel M, Ebetino FH, Castronovo V, Clezardin P (2011) Nitrogen-containing bisphosphonates can inhibit angiogenesis in vivo without the involvement of farnesyl pyrophosphate synthase. Bone 48:259-266
30. Im G-I, Jeong S-H (2015) Pathogenesis, management and prevention of atypical femoral fractures. J Bone Metab 22:1-8
31. Reid IR, Bolland MJ, Grey AB (2007) Is bisphosphonate-associated osteonecrosis of the jaw caused by soft tissue toxicity? Bone 41:318-320
32. Russmueller G, Seemann R, Weiss K, Stadler V, Speiss M, Perisanidis C, Fuereder T, Willinger B, Sulzbacher I, Steininger C (2016) The association of medication-related osteonecrosis of the jaw with Actinomyces spp. infection. Sci Rep 6:31604
33. Sharma D, Hamlet S, Petcu E, Ivanovski S (2013) Animal models for bisphosphonate-related osteonecrosis of the jaws--an appraisal. Oral Dis 19:747-754
34. Sarkarat F, Kalantar Motamedi MH, Jahanbani J, Sepehri D, Kahali R, Nematollahi Z (2014) Platelet-Rich Plasma in Treatment of Zoledronic Acid-Induced Bisphosphonate-related Osteonecrosis of the Jaws. Trauma monthly 19:e17196

35. Tsurushima H, Kokuryo S, Sakaguchi O, Tanaka J, Tominaga K (2013) Bacterial promotion of bisphosphonate-induced osteonecrosis in Wistar rats. Int J Oral Maxillofac Surg 42:1481-1487
36. Li CL, Lu WW, Seneviratne CJ, Leung WK, Zwahlen RA, Zheng LW (2014) Role of periodontal disease in bisphosphonate-related osteonecrosis of the jaws in ovariectomized rats. Clin Oral Implants Res
37. Akkus O, Polyakova-Akkus A, Adar F, Schaffler MB (2003) Aging of microstructural compartments in human compact bone. J Bone Miner Res 18:1012-1019
38. Roschger P, Fratzl P, Eschberger J, Klaushofer K (1998) Validation of quantitative backscattered electron imaging for the measurement of mineral density distribution in human bone biopsies. Bone 23:319-326
39. Mabilleau G, Mieczkowska A, Libouban H, Simon Y, Audran M, Chappard D (2015) Comparison between quantitative X-ray imaging, dual energy X-ray absorptiometry and microCT in the assessment of bone mineral density in disuse-induced bone loss. J Musculoskel Neuronal Interact 15:42-52
40. Nyangoga H, Mercier P, Libouban H, Basle MF, Chappard D (2011) Three-dimensional characterization of the vascular bed in bone metastasis of the rat by microcomputed tomography (MicroCT). PLoSOne 6:e17336
41. Abtahi J, Agholme F, Aspenberg P (2013) Prevention of osteonecrosis of the jaw by mucoperiosteal coverage in a rat model. Int J Oral Maxillofac Surg 42:632-636
42. Pautke C, Kreutzer K, Weitz J, Knodler M, Munzel D, Wexel G, Otto S, Hapfelmeier A, Sturzenbaum S, Tischer T (2012) Bisphosphonate related osteonecrosis of the jaw: A minipig large animal model. Bone 51:592-599
43. Marino KL, Zakhary I, Abdelsayed RA, Carter JA, O'Neill JC, Khashaba RM, Elsalanty M, Stevens MR, Borke JL (2012) Development of a rat model of bisphosphonate-related osteonecrosis of the jaw (BRONJ). J Oral Implantol 38 Spec No:511-518
44. Abtahi J, Agholme F, Sandberg O, Aspenberg P (2012) Bisphosphonate-induced osteonecrosis of the jaw in a rat model arises first after the bone has become exposed. No primary necrosis in unexposed bone. J Oral Pathol Med 41:494-499
45. Biasotto M, Chiandussi S, Zacchigna S, et al. (2010) A novel animal model to study non-spontaneous bisphosphonates osteonecrosis of jaw. J Oral Pathol Med 39:390-396
46. Hoff AO, Toth BB, Altundag K, et al. (2008) Frequency and risk factors associated with osteonecrosis of the jaw in cancer patients treated with intravenous bisphosphonates. J Bone Miner Res 23:826-836
47. Aguirre JI, Akhter MP, Kimmel DB, Pingel JE, Williams A, Jorgensen M, Kesavalu L, Wronski TJ (2012) Oncologic doses of zoledronic acid induce osteonecrosis of the jaw-like lesions in rice rats (Oryzomys palustris) with periodontitis. J Bone Miner Res 27:2130-2143
48. Mavrokokki T, Cheng A, Stein B, Goss A (2007) Nature and frequency of bisphosphonate-associated osteonecrosis of the jaws in Australia. J Oral Maxillofac Surg 65:415-423
49. Bamias A, Kastritis E, Bamia C, et al. (2005) Osteonecrosis of the jaw in cancer after treatment with bisphosphonates: incidence and risk factors. J Clin Oncol 23:8580-8587
50. Hokugo A, Christensen R, Chung EM, Sung EC, Felsenfeld AL, Sayre JW, Garrett N, Adams JS, Nishimura I (2010) Increased prevalence of bisphosphonate-related osteonecrosis of the jaw with vitamin D deficiency in rats. J Bone Miner Res 25:1337-1349
51. Mitsimponas K, Moest T, Iliopoulos C, Rueger T, Mueller C, Lutz R, Shakib K, Neukam F, Schlegel K (2016) Search for a reliable model for bisphosphonate-related osteonecrosis

of the jaw: establishment of a model in pigs and description of its histomorphometric characteristics. Br J Oral Maxillofac Surg 54:883-888

52. Ersan N, van Ruijven LJ, Bronckers AL, Olgac V, Ilguy D, Everts V (2013) Teriparatide and the treatment of bisphosphonate-related osteonecrosis of the jaw: a rat model. Dentomaxillofac Radiol 43:20130144
53. Aghaloo TL, Kang B, Sung EC, Shoff M, Ronconi M, Gotcher JE, Bezouglaia O, Dry SM, Tetradis S (2011) Periodontal disease and bisphosphonates induce osteonecrosis of the jaws in the rat. J Bone Miner Res 26:1871-1882
54. Pacheco VN, Langie R, Etges A, Ponzoni D, Puricelli E (2015) Nitrogen-containing bisphosphonate therapy: assessment of the alveolar bone structure in rats - a blind randomized controlled trial. Int J Exp Pathol 96:255-260
55. Russell RGG, Watts NB, Ebetino FH, Rogers MJ (2008) Mechanisms of action of bisphosphonates: similarities and differences and their potential influence on clinical efficacy. Osteoporos Int 19:733-759
56. Juillard A, Falgayrac G, Cortet B, Vieillard M-H, Azaroual N, Hornez J-C, Penel G (2010) Molecular interactions between zoledronic acid and bone: An in vitro Raman microspectroscopic study. Bone 47:895-904
57. Olejnik C, Falgayrac G, During A, Cortet B, Penel G (2016) Doses effects of zoledronic acid on mineral apatite and collagen quality of newly-formed bone in the rat's calvaria defect. Bone 89:32-39
58. Boanini E, Gazzano M, Bigi A (2012) Time course of zoledronate interaction with hydroxyapatite nanocrystals. J Phys Chem C 116:15812-15818
59. Misof BM, Roschger P, Gabriel D, Paschalis EP, Eriksen EF, Recker RR, Gasser JA, Klaushofer K (2013) Annual intravenous zoledronic acid for three years increased cancellous bone matrix mineralization beyond normal values in the HORIZON biopsy cohort. J Bone Miner Res 28:442-448
60. Vermeer J, Renders G, Duin M, Jansen I, Bakker L, Kroon S, Vries T, Everts V (2017) Bone-site-specific responses to zoledronic acid. Oral Dis 23:126-133
61. Verzola MHA, Frizzera F, de Oliveira GJPL, Pereira RMR, Rodrigues-Filho UP, Nonaka KO, Orrico SRP (2015) Effects of the long-term administration of alendronate on the mechanical properties of the basal bone and on osseointegration. Clin Oral Implants Res 26:1466-1475
62. Huebsch RF, Coleman RD, Frandsen AM, Becks H (1952) The healing process following molar extraction. I. Normal male rats (long-evans strain). Oral Surg Oral Med Oral Pathol 5:864-876
63. Fournier P, Boissier S, Filleur S, Guglielmi J, Cabon F, Colombel M, Clezardin P (2002) Bisphosphonates inhibit angiogenesis in vitro and testosterone-stimulated vascular regrowth in the ventral prostate in castrated rats. Cancer Res 62:6538-6544
64. Tang X, Zhang Q, Shi S, Yen Y, Li X, Zhang Y, Zhou K, Le AD (2010) Bisphosphonates suppress insulin-like growth factor 1-induced angiogenesis via the HIF-1alpha/VEGF signaling pathways in human breast cancer cells. Int J Cancer 126:90-103
65. Allegra A, Alonci A, Penna G, et al. (2010) Bisphosphonates induce apoptosis of circulating endothelial cells in multiple myeloma patients and in subjects with bisphosphonate-induced osteonecrosis of the jaws. Acta Haematol 124:79-85
66. Allegra A, Oteri G, Nastro E, et al. (2007) Patients with bisphosphonates-associated osteonecrosis of the jaw have reduced circulating endothelial cells. Hematol Oncol 25:164-169
67. Bi Y, Gao Y, Ehirchiou D, Cao C, Kikuiri T, Le A, Shi S, Zhang L (2010) Bisphosphonates cause osteonecrosis of the jaw-like disease in mice. Am J Pathol 177:280-290

68. Sigua-Rodriguez EA, da Costa Ribeiro R, de Brito AC, Alvarez-Pinzon N, de Albergaria-Barbosa JR (2014) Bisphosphonate-related osteonecrosis of the jaw: a review of the literature. Int J Dent 2014:192320

Figure 1

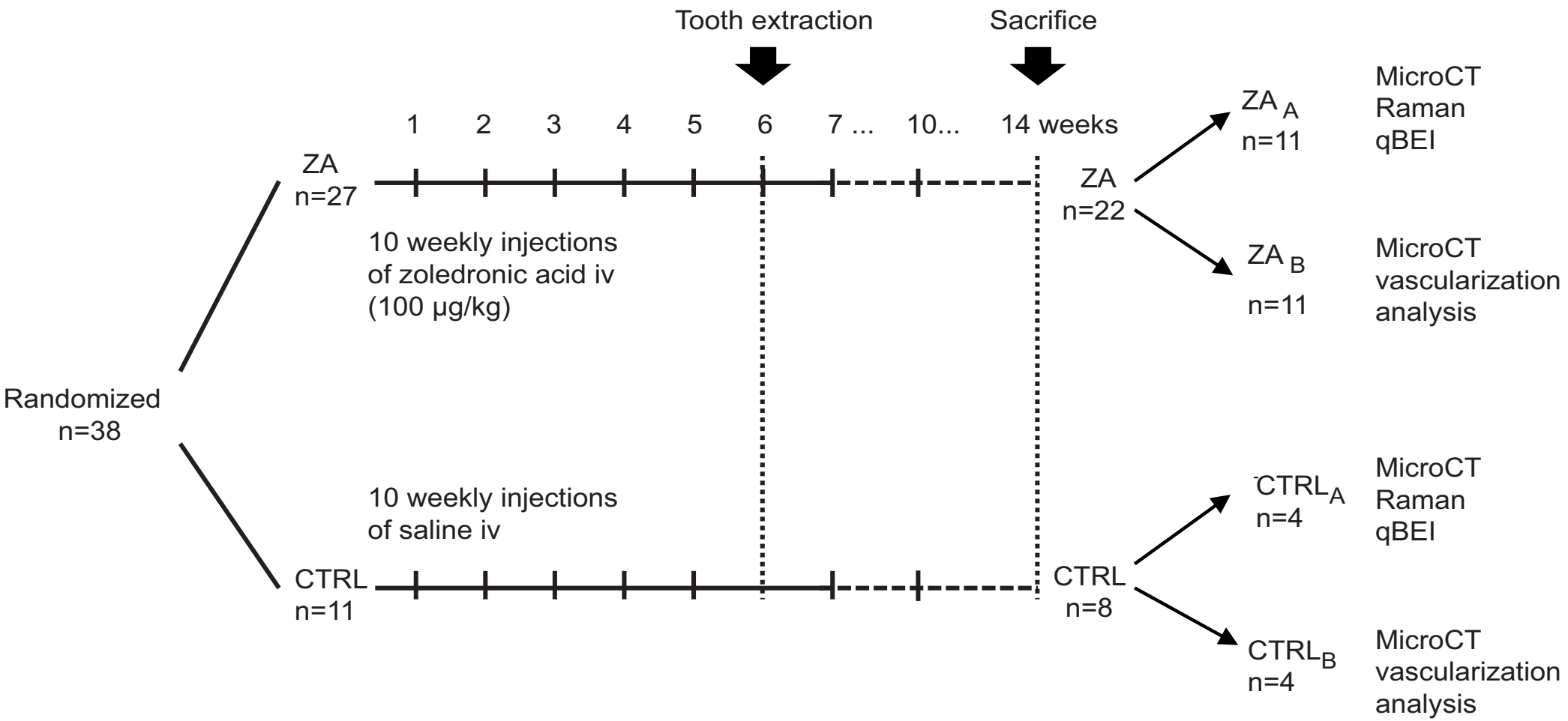

Tooth extraction
Sacrifice
1
2
3
4
5
6
7 ...
10...
14 weeks
Randomized
n=38
ZA
n=27
10 weekly injections
of zoledronic acid iv
(100 µg/kg)
CTRL
n=11
10 weekly injections
of saline iv
ZA
n=22
ZA A
n=11
MicroCT
Raman
qBEI
ZA B
n=11
MicroCT
vascularization
analysis
CTRL
n=8
CTRL A
n=4
MicroCT
Raman
qBEI
CTRL B
n=4
MicroCT
vascularization
analysis

Figure 2

Click here to download Figure fig_2_macroscopicalaspects.tif

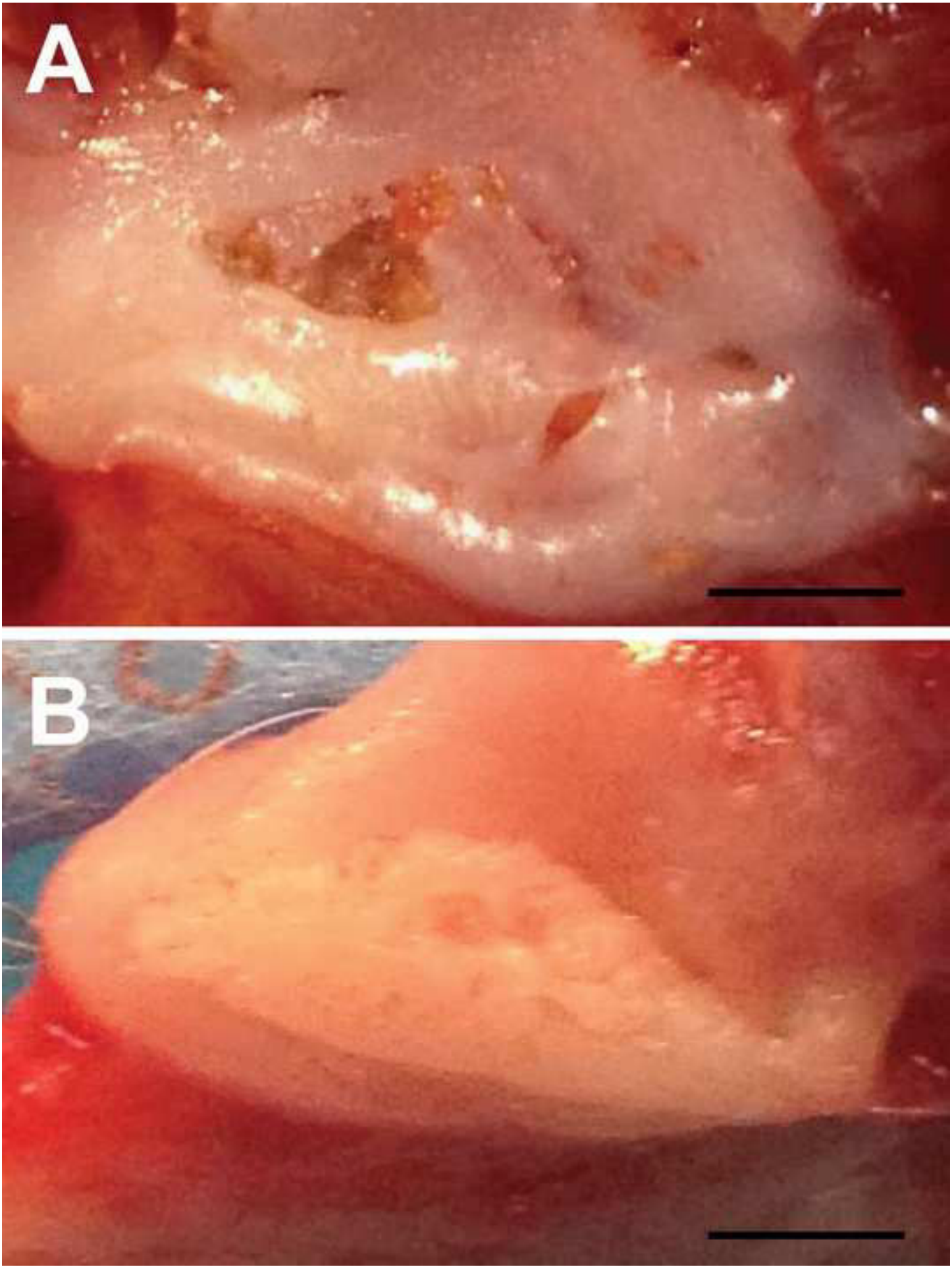


Figure 3

Click here to download Figure fig_3_MicroCT_2D.tif

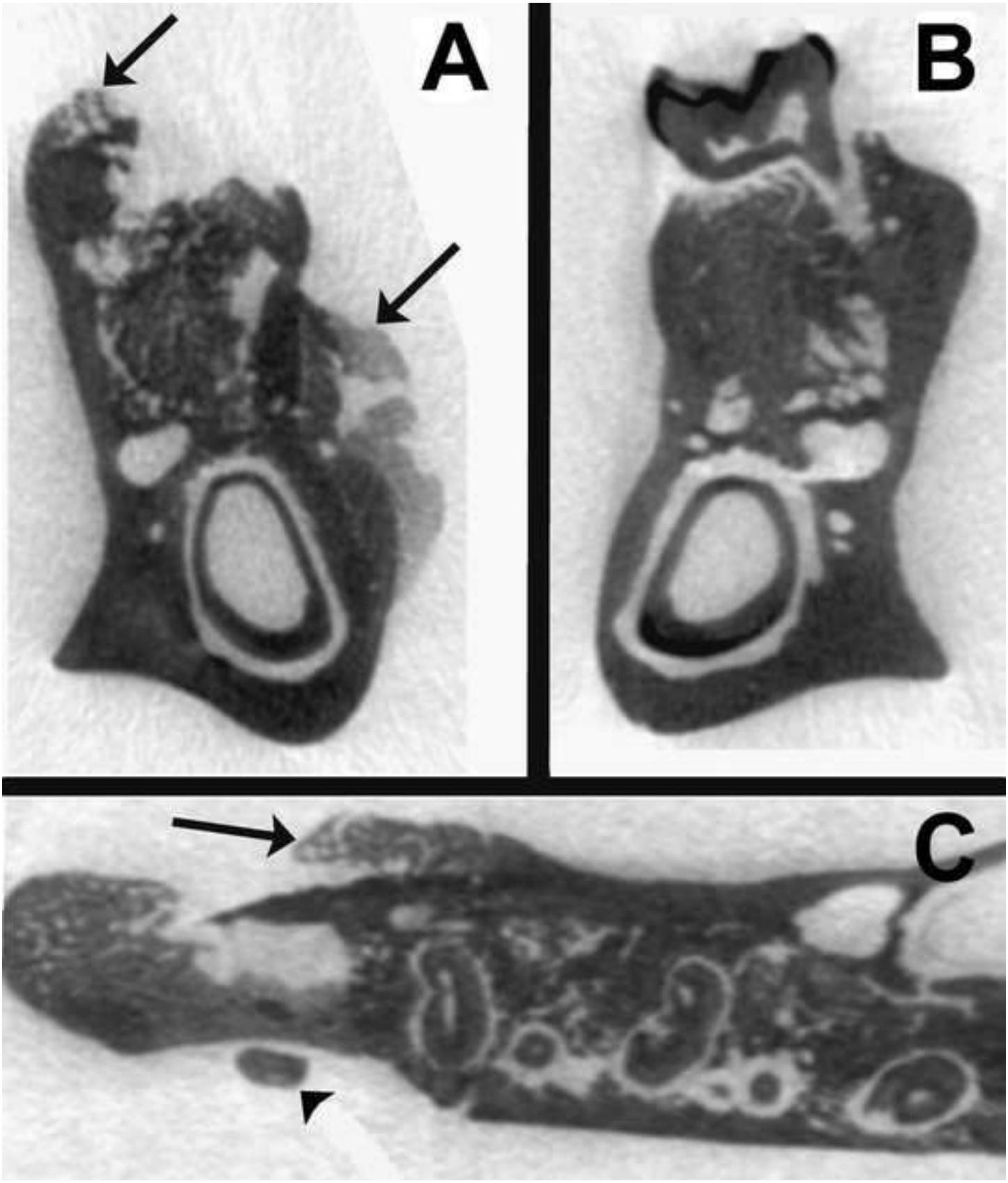


Figure 4

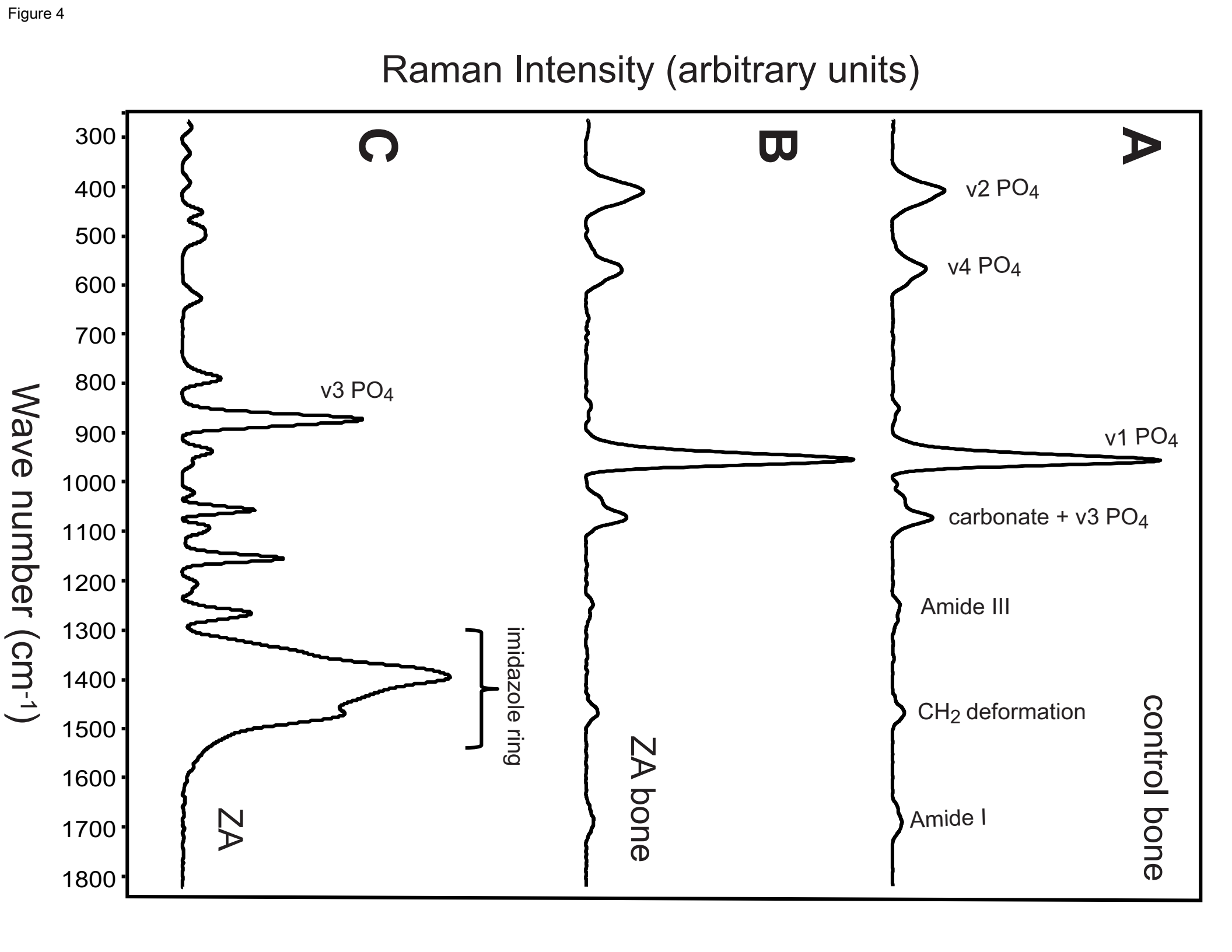

Raman Intensity (arbitrary units)
Wave number (cm-1)
300
400
500
600
700
800
900
1000
1100
1200
1300
1400
1500
1600
1700
1800
A
v2 PO4
v4 PO4
v1 PO4
carbonate + v3 PO4
Amide III
CH2 deformation
Amide I
control bone
B
ZA bone
C
v3 PO4
imidazole ring
ZA

Figure 5

Click here to download Figure fig_5_MicroCT_Vascularization.tif

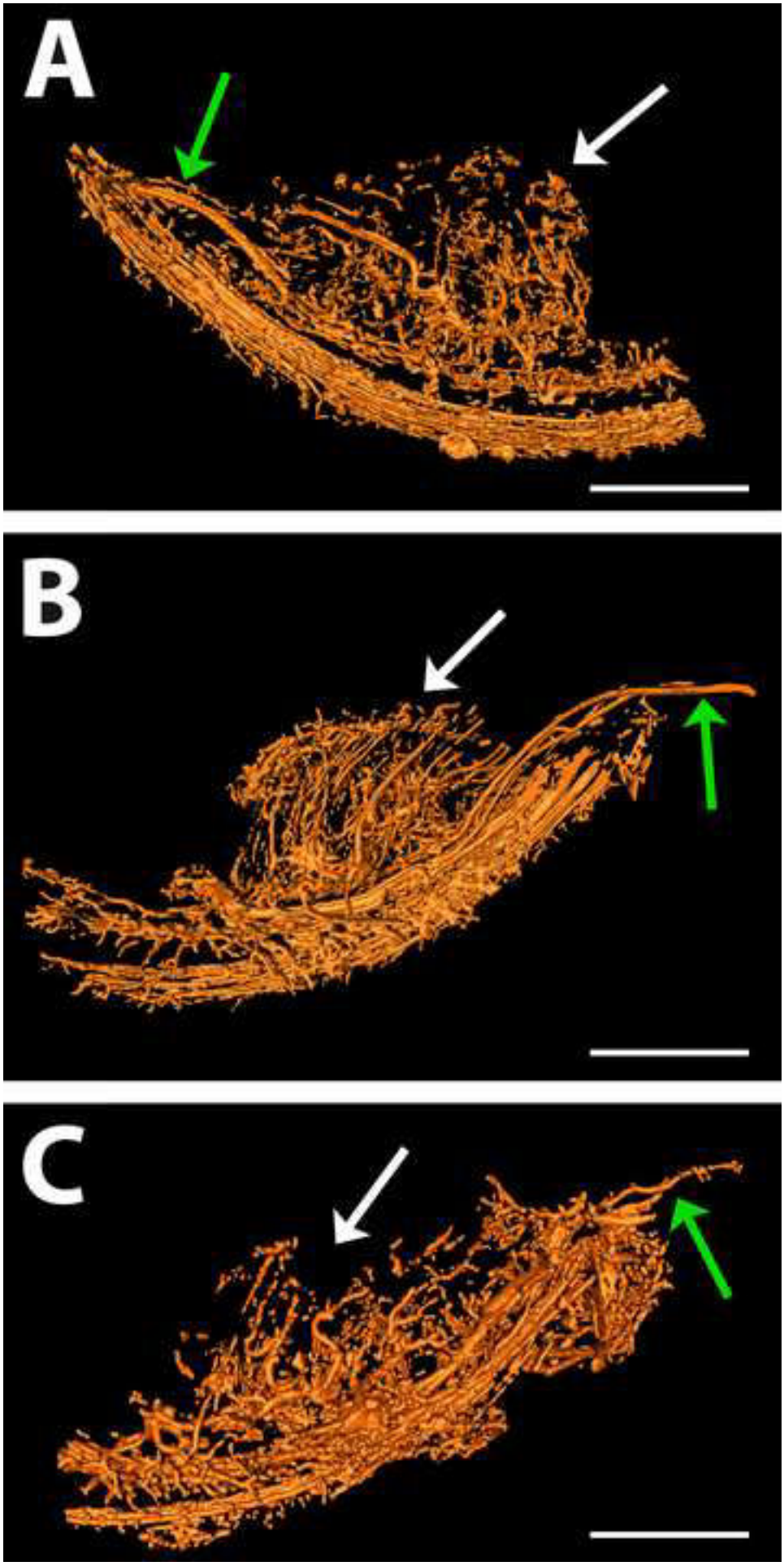


Figure 6

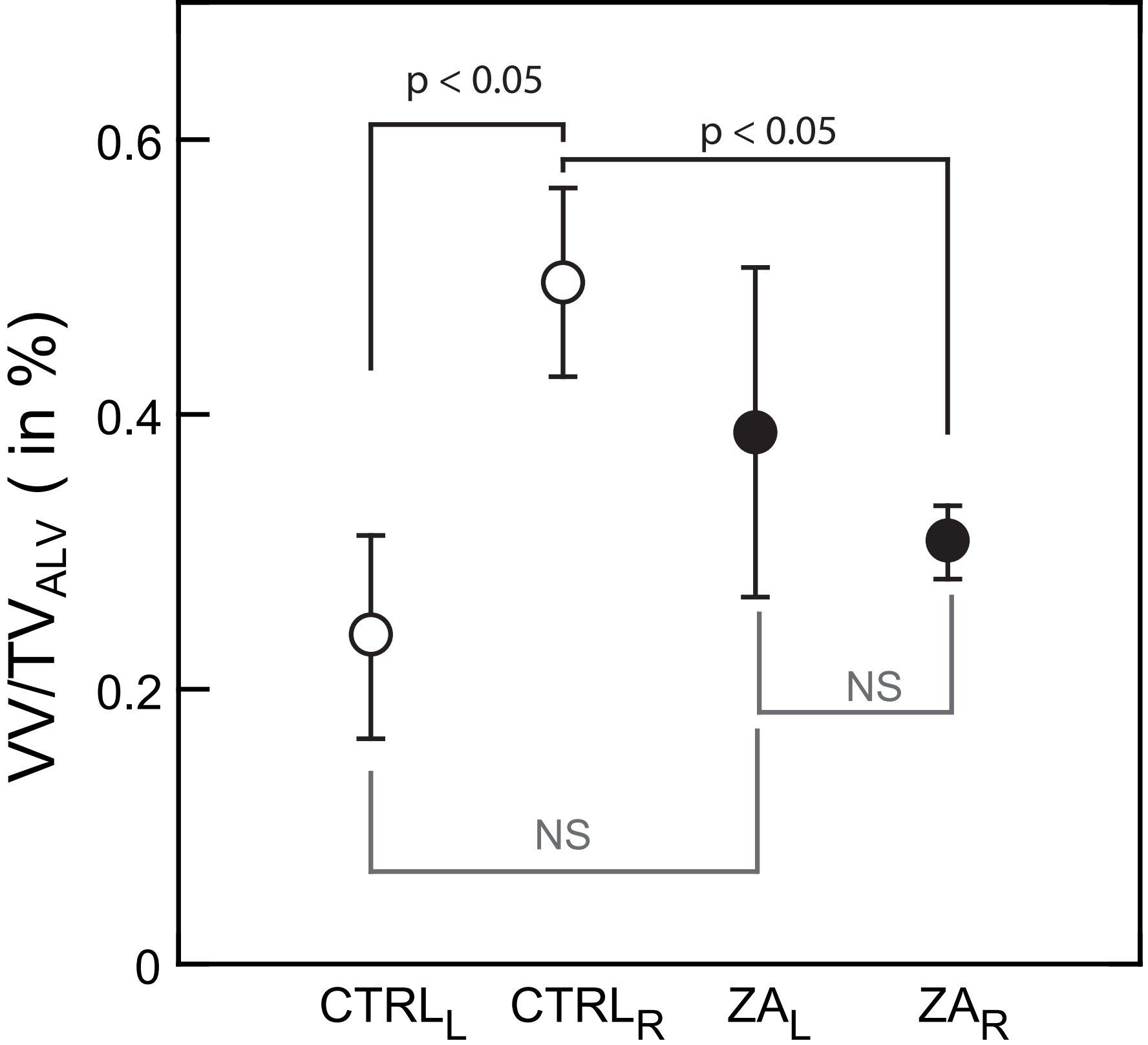


Table 1: Comparison between averages of spectroscopic parameters for each group after Raman analysis.

	ZA	CTRL	*p*
Mineral/amide I	38.94 ± 1.40	32.94 ± 1.91	0.03
Mineral/amide III	72.10 ± 4.94	52.05 ± 4.70	0.02
Carbonate substitution	0.133 ± 0.002	0.131 ± 0.005	NS
Crystallinity	111×10^{-6}	111×10^{-6}	NS
PG content	0.198 ± 0.071	0.173 ± 0.043	NS

The gray boxes highlight a significant difference between ZA *vs*. CTRL

Table 2: qBEI and EDS parameters measured on the alveolar bone of the left hemimandibles

	ZA	**CTRL**	***p***
Ca_{peak} (%Ca)	18.57 ± 0.22	18.79 ± 0.34	NS
Ca_{mean} (%Ca)	18.1 ± 0.19	18.33 ± 0.3	NS
Ca_{width} (%Ca)	3.3 ± 0.13	3.32 ± 0.17	NS
Ca/P	1.423 ± 0.008	1.420 ± 0.018	NS

UNIVERSITE BRETAGNE LOIRE

université angers

Thèse de Doctorat

Daniel KÜN-DARBOIS

Remodelage osseux et pathologies oro-faciales

Bone remodeling and oro-facial pathologies

Résumé

Un 1er travail a étudié les effets osseux mandibulaires de l'injection unilatérale dans les muscles masticateurs de toxine botulique (BTX) chez le rat adulte. Ceci entraine une perte osseuse mandibulaire condylienne et alvéolaire homolatérale importante. Une hypertrophie osseuse de l'enthèse d'insertion mandibulaire du muscle digastrique a été observée et pourrait correspondre à une étiologie pour les tori.
Les effets de la BTX sur le cartilage articulaire condylien mandibulaire dans le même modèle animal ont été recherchés par analyse microtomographique du cartilage articulaire après augmentation de contraste à l'acétate d'uranyle. Aucune différence d'épaisseur cartilagineuse n'a été mise en évidence entre les groupes contrôles et BTX.
Le 3ème travail a consisté en l'étude histologique et microtomographique des tori mandibulaires chez l'homme. Les tori sont différents des exostoses des os longs par plusieurs caractéristiques (dont l'absence de Fe et Al dans la matrice osseuse) et une asymétrie du remodelage osseux a été mise en évidence.
La 4ème partie a consisté en l'étude de la qualité osseuse et de la microvascularisation alvéolaire dans un modèle animal d'ostéonécrose mandibulaire (ONM) aux bisphosphonates (BP). Des signes cliniques et microtomographiques d'ONM ont été observés dans la majorité des cas. La minéralisation osseuse était plus élevée après imprégnation en BP. La microvascularisation osseuse alvéolaire apparaissait augmentée après avulsion dentaire chez les animaux contrôles mais pas chez les animaux ayant reçu des BP témoignant ainsi d'un effet antiangiogénique in vivo des BP qui pourrait jouer un rôle dans la physiopathologie de l'ONM.

Mots clés
Remodelage osseux, Toxine botulique, Torus mandibularis, Remodelage asymétrique, Microtomographie, Bisphosphonates, Ostéonécrose, Microvascularisation.

Abstract

First, bone changes at the mandible were studied after a unilateral botulinum toxin (BTX) injection in masticatory muscles in adult rats. A major alveolar and condylar bone loss was evidenced. The occurrence of a hypertrophic bone metaplasia at the digastric muscle enthesis was evidenced as well. This could constitute an etiological factor for tori.
Then, condylar articular cartilage changes at the mandible were studied in the same BTX animal model, using microtomography after contrast enhancement of cartilage with uranyl acetate. Cartilage thickness measurement showed no difference when comparing control and BTX groups.
A third work studied mandibular tori in human using histologic and microtomographic techniques. Tori appeared different from long bone exostoses by several characteristics (absence of Fe and Al in the bone matrix) and a specific asymmetric bone remodeling was evidenced.
The fourth part consisted in the study of alveolar mandibular vascularization and quality of the bone matrix in an animal model of osteonecrosis of the jaws (ONJ) after bisphosphonates (BP) injections. Clinical and microtomographic signs of ONJ were found in most of the cases. An increased mineralization of the alveolar bone was observed after BP impregnation. Microvascularization was increased after tooth extraction in the alveolar bone of control animals but it was impaired in ZA treated rats. Such an in vivo antiangiogenic effect of BPs could play a role in the pathophysiology of ONJ.

Key Words
Bone remodeling, Botulinum toxin, Torus mandibularis, Asymmetric bone remodeling, Microtomography, Bisphosphonates, Osteonecrosis, Microvascularization